UCLouvain

École polytechnique de Louvain

Evaluation of Water Repellency of Fabrics Using Droplet Impact Dynamics and Machine Learning

Author : **Patrick James CRUZ**
Supervisors : **Alain JONAS**, **Gian-Marco RIGNANESE**
Readers : **Pierre-Paul DE BREUCK, Arnaud DELCORTE**, **Karine GLINEL**
Academic year 2020–2021
Master [120] in Chemical and Materials Engineering

Abstract

The principles of droplet impact are the foundation of the design of water-repellent solid surfaces. Although it has been known that textiles must also possess water repellency to resist the impacting raindrops during outdoor use, their water-repellent behavior based on droplet impact dynamics is still not well-understood. Here we investigated the dynamic behavior of droplet on rough woven fabrics coated with hydrophobic formulations through droplet impact test. We have also successfully integrated machine learning in this work to predict the spreading and rebound behavior of droplet, as well as to describe its overall dynamics. It was found that the droplet spreading characteristics do not provide any information on water repellency of the woven fabrics, even though the observed rebound characteristics show a wide range of water-repellent behavior among these fabrics. In addition, though high water repellency can be achieved by using fabrics with high roughness, fabric roughness is not the only factor to consider: the precise texture of the fabric surface plays a crucial role too. Our analysis revealed that the dynamic behavior of droplet during impact test was in fact strongly linked to the roll-off tendency of droplet during roll-off test.

Keywords: Water repellency, woven fabrics, roughness, hydrophobic coatings, droplet impact dynamics, rebound, roll-off, machine learning

Acknowledgments

Now that the end of my master's program is near, I would like to express my deepest gratitude to everyone who has helped me finish this incredible challenging journey.

First, I wanted to thank my committee for giving me guidance to understand the different parts of my research and help me put them together. I am extremely grateful to my supervisors Prof. Jonas and Prof. Gian-Marco for accepting me as their master's student and making this collaborative work possible. From answering several questions in emails and in person, up to constantly checking on me all throughout the year, I am really thankful to both of you. I would like to thank Prof. Glinel too for providing me immediate assistance and advice whenever I needed it, particularly on the experimental work of the project. I am also grateful to Pierre-Paul for all the information and helpful tips, in whichever aspect of machine learning. I also wanted to thank Prof. Delcorte in advance for accepting my request for him to be part of my jury. To everyone in my committee, thank you for staying with me throughout this research journey.

I would also like to thank: Dr. Sallem for providing me a really solid foundation on using the goniometer, especially when making measurements and recording movies; Ms. D'Haese for training me on the preparation of coated fabrics; Ms. Magnin for training me in using microscope; Ms. Bouchat for providing all the materials that I needed in this work, including the (unforgettable) chocolates. I also wanted to thank everyone in the Boltzmann A2 laboratory for the wonderful conversations and advice— especially in the middle of a pandemic.

Finally, I am dedicating this work to my family, friends, acquaintances and my bestfriend who is now in heaven, Bibble. Without them, I would have not been able to see this research through until the end.

To everyone who believed in me and supported me, my heart goes to all of you.

Table of Contents

List of Tables and Figures 3

List of Abbreviations and Symbols 5

1 Introduction and Overview 6
1.1 Droplet Impact Dynamics 6
1.2 Water Repellency of Textiles 7
1.3 Machine Learning in Droplet Impact Dynamics and Textile Design 8
1.4 Primary Goals and Scope of Research 9

2 Theoretical Framework 11
2.1 Wettability as Surface Phenomenon 11
2.2 Wettability of Textiles 12
2.3 Droplet Impact Dynamics 14
2.3.1. Fundamental Principles 14
2.3.2. Splashing Dynamics 15
2.3.3. Spreading Dynamics 16
2.3.4. Rebound Dynamics 17
2.4 Machine Learning 19
2.4.1. Artificial Neural Network 19
2.4.2. Random Forest 21
2.4.3. Principal Component Analysis 22

3 Experimental 23
3.1 Preparation of Coated Fabrics 23
3.2 Physical Characteristics of the Fabrics 24
3.3 Contact and Roll-Off Angle Measurements 24
3.4 Droplet Impact Dynamics Studies 25
3.5 Analysis of Videos and Extraction of Relevant Parameters 25
3.6 Machine Learning 27
3.7 Experimental Limitations of the Study 28

4 Results and Discussion 30
4.1 Contact Angle and Roll-Off Angle of Coated Fabrics 30
4.2 Splashing Behavior of Droplet on Coated Fabrics. 31
4.3 Spreading Behavior of Droplet on Coated Fabrics. 34
4.4 Rebound Behavior of Droplet on Coated Fabrics 39
4.5 Water Repellency of Coated Fabrics 44
4.6 Application of Machine Learning 47
4.7 Global Perspective 51

5 Summary, Conclusions and Future Work 55

References 56

Supplementary 58

List of Tables and Figures

Introduction

(F) 1.1 Image sequence of a droplet impacting on a surface 6

Theoretical Framework

(F) 2.1 The evolution of static contact angle θ with the hydrophobicity of a smooth solid substrate (top); The two (non)-wetting states of a droplet on a rough solid substrate (bottom) 11

(F) 2.2 Comparison of two different woven fabrics 12

(F) 2.3 Different outcomes of the interaction of an impacting droplet with a solid surface 14

(F) 2.4 Difference between S_{max} and ξ_{max} of a droplet at maximum spreading state 17

(F) 2.5 Millisecond image sequences showing partial rebound of water droplet 18

(F) 2.6 A typical *ANN* multi-layer perceptron architecture 20

(F) 2.7 Calculation inside an artificial neuron 20

(F) 2.8 A typical decision tree architecture 21

Experimental

(T) 3.1 Characteristics of commercial hydrophobic coatings 23

(T) 3.2 Physical characteristics of fabric samples 24

(F) 3.1 Experimental setup of droplet impact dynamics studies 25

(T) 3.3 Relevant video output parameters for droplet impact dynamics studies 26

(T) 3.4 Input features and target parameters for *ANN* and *RF* models 27

Results and Discussion

(T) 4.1 Contact angle for different coated fabrics 30

(T) 4.2 Roll-off angle for different coated fabrics 30

(F) 4.1 Contact angle and roll-off angle values as function of fabric roughness and coating type 31

(F) 4.2 Comparison between a droplet exhibiting (1) non-splashing and (2) splashing behavior 32

(F) 4.3 Splashing behavior of droplet on different fabrics over a range of Weber number *We* 34

(F) 4.4 Comparison of maximum contact width D_{max} of the droplet between two *PhobRSH*-coated fabrics of different roughness at different Weber number *We* 35

(F) 4.5 Global variation of dimensionless maximum contact width ξ_{max} with Weber number *We* 35

(F) 4.6 Variation of dimensionless maximum contact width ξ_{max} with Weber number *We*, highlighting different fabrics 36

(F) 4.7 Variation of dimensionless maximum contact width ξ_{max} with Weber number *We*, highlighting different coatings 37

(F) 4.8 Evolution of droplet contact width with time for different *PhobRSH*-coated fabric samples 38

(F) 4.9 Comparison between a droplet not rebounding and rebounding off completely the surface for two *PhobRSH*-coated fabrics of different roughness at *low We* 39

(F) 4.10 Comparison between a droplet exhibiting partial rebound and jetting off the surface of *PhobRSH*-coated fabric at *low We* 40

(F) 4.11 Complete pinning of droplet on *PhobRSH*-coated fabric at *high We* 41

(F) 4.12 Variation of restitution coefficient R_C with Weber number *We,* highlighting different fabrics 42

(F) 4.13 Variation of restitution coefficient R_C with Weber number *We,* highlighting different coatings 42
(F) 4.14 Average restitution coefficient R_C for different coated fabrics for a specific Weber number *We* range 43
(F) 4.15 In-depth comparison of restitution coefficient R_C of the fabric samples for a small Weber number *We* range 45
(T) 4.3 Physical characteristics of fabric samples 46
(F) 4.16 Prediction of dimensionless maximum contact width ξ_{max} of the droplet based on Artificial Neural Network *(ANN)* 48
(F) 4.17 Ranking of relevance of each feature in the prediction of dimensionless maximum contact width ξ_{max} using *permutation importance* 49
(F) 4.18 Prediction of restitution coefficient R_C of the droplet based on Random Forest (*RF*) 49
(F) 4.19 Ranking of relevance of each feature in the prediction of restitution coefficient R_C using *permutation importance* 50
(F) 4.20 Visual representation of droplet dynamic behavior in different fabrics at low *We* based on the first two principal components of *PCA* 50
(T) 4.4 Influence of different physical parameters on droplet dynamic behavior 52
(F) 4.21 In-depth comparison of maximum receding rate in different fabrics for a small *We* range 53

Supplementary

(F) S.3.1 Optical microscope images of the fabric samples 58
(F) S.3.2 Impact speed as a function of dropping height of the droplet 60
(F) S.3.3 Rebound height as a function of square of non-contact time 60
(F) S.3.4 Mean squared error *(MSE*) as a function of maximum tree depth 61
(F) S.4.1 Contact angle and roll-off angle values for different coated fabrics (with error bars) 61
(T) S.4.1 Comparison of the effect of frame rate using two different fabrics 62
(F) S.4.2 Visual representation of droplet dynamic behavior in different fabrics at low *We* based on the first two principal components of *PCA*, using *We* as colormap 62
(F) S.4.3 In-depth comparison of equilibrium contact width in different fabrics for a small *We* range 63

List of Abbreviations and Symbols

Adam	Adaptive moment estimation
ANN	Artificial Neural Network
ML	Machine Learning
MSE	Mean squared error
PCA	Principal Component Analysis
ReLU	Rectified Linear Unit
RF	Random Forest
D_o	Initial droplet diameter
D_{max}	Maximum diameter of the droplet directly in contact with the surface
$\langle d_f \rangle$	Mean fiber diameter
$K = We(Re)^{0.5}$	Splashing parameter
$Oh = We^{0.5}/Re$	Ohnesorge number
r (Experimental)	Fabric roughness
r ≥ 1 (Wenzel)	Effective surface (contact) area divided by the projected area of a flat surface
R_C	Restitution coefficient
$\langle R_C \rangle_{We}$	R_c averaged over relevant *We* range
$Re = \rho V D_o / \mu$	Reynold's number
S_{max}	Ratio of the droplet's maximum spreading diameter to its initial diameter
t_{ms}	Maximum spreading time
V or V_{Bl}	(Initial) droplet speed before impacting the surface
V_{Al}	Droplet speed after impacting the surface
V_{stick}	Critical impact speed for droplet sticking
$We = \rho V^2 D_o / \sigma$	Weber number
ξ_{max}	Dimensionless maximum contact width
ρ	Liquid density
σ	Liquid surface tension
μ	Liquid viscosity
θ	Static (apparent) contact angle
θ_A	Advancing angle
θ_R	Receding angle
$\Delta\theta$	Contact angle hysteresis
θ_{CB}	Cassie-Baxter contact angle
θ_{RO}	Roll-off angle
θ_W	Wenzel contact angle
θ_Y	Young's contact angle
γ_{SL}	Surface energy at solid/liquid interface
γ_{LV}	Surface energy at liquid/vapor interface
γ_{SV}	Surface energy at solid/vapor interface
$\Phi_s \leq 1$ *(Cassie-Baxter)*	Actual solid-liquid contact area divided by apparent contact area

Introduction and Overview

1.1 *Droplet Impact Dynamics*

One can see even in the most mundane activities of our everyday life how liquid droplets impact on different solid surfaces— whether from a dripping faucet in a kitchen sink, or as raindrops from the sky. Despite appearing trivial, *droplet impact dynamics* has a huge significance in the industry. The most relevant principles in this field are heavily applied in the areas of coating, spray cooling, inkjet printing and anti-icing of crucial aircraft components, among others. [1] [2] [3] This subject is central to the design of self-cleaning surfaces, for instance, where they must strongly repel water droplets. [4]

Given that droplet impact occurs in a fraction of second, the exact dynamic behavior cannot be observed fully by the human eye. Nonetheless, this dynamics can still be described: one example is given in **Figure 1.1,** which is a chronological series of five different stages. (1) First, the spherical droplet impacts the surface, which creates a solid-liquid interface and forms a lamella. (2) Then, the droplet *may* deform and spread in an outward radial motion. (3) Next, the droplet *may* recede inward radially, pulling itself due to a strong interfacial tension with the surface, as well as the inherent surface tension of the liquid. (4) *In some cases*, the droplet regains enough energy as it retracts, allowing it to bounce off eventually— reaching a maximum height and then falling back to the surface. (5) Finally, the droplet achieves an equilibrium state after a series of oscillations. In addition, the droplet may also splash depending on the exact impact conditions, by forming smaller secondary droplets during any of the stages described above.

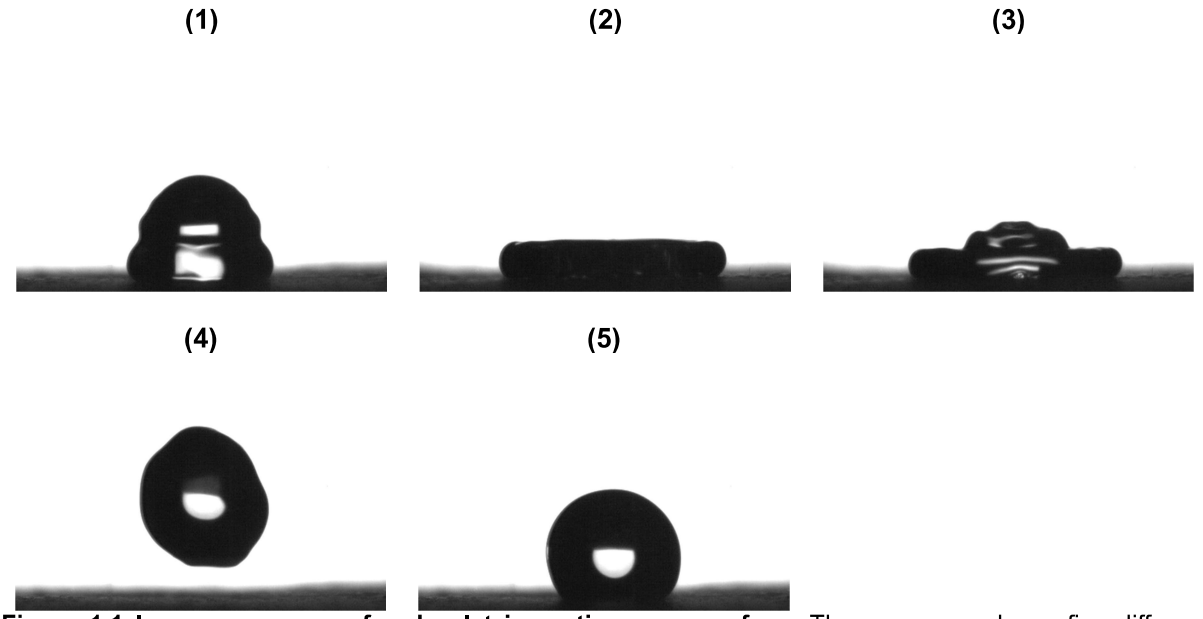

Figure 1.1 Image sequence of a droplet impacting on a surface. The sequence shows five different stages of the dynamic behavior of a droplet: (1) initial impact; (2) spreading; (3) retraction; (4) potential rebound; and (5) equilibrium.

Although the scenario described above gives an illustration of the potential behavior of the droplet upon impact, its actual dynamics still depends on several factors— such as the exact properties of the fluid (mainly its density ρ, surface tension σ and viscosity μ) and the droplet (its actual size and speed) being studied. For the latter case, the initial diameter D_o and impact speed V of the droplet together make up its kinetic energy, which is represented in a dimensionless parameter known as

Weber number We. Weber number accounts for the balance between the kinetic energy and surface energy of the droplet, and is given by the following expression: $We = \rho V^2 D_o / \sigma$. [1] A large *We* can be obtained by increasing the dropping height of the droplet, given that its potential energy is converted to kinetic energy as it falls.

Aside from the characteristics of the fluid and the droplet, the wettability of the surface influences the droplet dynamic behavior too. One way is through the chemical composition of the surface itself. Whereas a surface with *hydrophilic* coating favors a *wetting* state of a water droplet, a surface with *hydrophobic* coating favors its *non-wetting* state— mainly due to the difference between their respective surface energies. On one hand, the favorable interaction between a hydrophilic substrate and a water droplet makes the latter remain *deposited* on the surface. On the other hand, the unfavorable interaction of a water droplet with a hydrophobic substrate makes it retract and gain enough kinetic energy to *rebound* off the surface. Besides its chemistry, the degree of roughness of a surface can also modify its wettability, thereby influencing the droplet behavior as well. Introducing roughness creates (micro)cavities which may trap air pockets and allow a *static* droplet to float on top of roughness structures (at least in a *Cassie-Baxter* state)— thus preventing it from wetting the surface. [5] [6] In addition, a rough surface can generate a wide range of behavior for an *impacting* droplet, such as bouncing, splashing or pinning. [1] [7]

Because of the widely-observed influence of surface characteristics on droplet dynamics, the design of water-repellent surfaces becomes an active field of research. Several researchers have characterized the *water repellency* of hydrophobic surfaces through the rebound behavior of impacting droplets, using a parameter called *restitution coefficient* R_C. Restitution coefficient simply represents the ratio of an object's final velocity after collision to its initial velocity before collision. In the context of droplet dynamics, the square of restitution coefficient R_C^2 thus reveals how much of the initial translational kinetic energy of the droplet is conserved after its impact. With its definition, R_C can be expressed in this work as: $R_C = V_{Af} / V_{Bf}$, where V_{Af} and V_{Bf} are the droplet speed *after* and *before* impacting the surface, respectively (Its exact operating definition will be given in **Experimental**). A high R_C is characterized by a droplet rebounding to a height close to its dropping height, which typically occurs when the surfaces are superhydrophobic. [8] [9] As an example of magnitude, Richard et al. found that a water droplet can exhibit full rebound behavior on a superhydrophobic surface and obtain R_C up to 0.9. [10] This strong rebound behavior is highly desirable for surfaces of objects in which wetting can be a strong issue, such as our personal clothing.

1.2 *Water Repellency of Textiles*

In textile industry, it is highly wanted that the fabrics exhibit high water repellency to be suitable for outdoor use. Fabrics typically absorb the liquid droplets by wicking mechanism when left untreated, however. [11] While this is conventionally addressed by coating the fabrics with hydrophobic formulations, some research studies have also already shown that surface roughness could improve this water repellency behavior. For woven fabrics, the roughness is inherently created by the weave pattern and fiber packing in the yarns, where the latter parameter appears to be a stronger contributor. [12]

However, despite the growing number of research on water repellency of fabrics, a majority of these studies simply focus on their *static* wettability with water droplets, even though the *dynamic* wettability seems more relevant in the context of their use (e.g. when raining). Moreover, while

there are certainly recent studies of droplet impact dynamics on textiles, their focus however is not particularly on water repellency in terms of droplet rebound behavior. For example, a recent study by Zhang et al. has indeed investigated the impact dynamics of water droplets on coated hydrophobic and non-coated hydrophilic textiles. However, they concentrated on understanding the parameters influencing the penetration of water droplets on these fabrics, given that their samples have pore sizes in the range of hundreds of micrometers. [2] Unfortunately, the study of droplet dynamic behavior on textiles— especially focusing on the *rebound* behavior of droplet and using *rough fabrics* as primary subject— has not received enough attention yet. Furthermore, apart from the difficulty raised by studying textiles as subject, droplet impact dynamics is already complex by itself— owing to the interplay of several factors (i.e. fluid properties, droplet properties and surface characteristics) mentioned earlier. It is precisely because of this large number of parameters at play in this field of research that some researchers have turned to the use of *machine learning.*

1.3 *Machine Learning in Droplet Impact Dynamics and Textile Design*

With the ceaseless increase of available data and computational power, Machine Learning (*ML*) has quickly become a popular field over the past decade. (There are different review articles available, such as [13].) *ML* allows extraction of specific relationships and complex patterns in huge datasets, making it extremely useful for a wide range of applications— such as for prediction and optimization, or for design and automation. Majority of the *ML* algorithms being used are either based on *supervised learning* or *unsupervised learning.* On one hand, supervised learning involves prediction of an output from labeled data. It has two main stages: (1) *training phase,* which requires developing a model by analyzing the input data and identifying the relationships between the input parameters (also known as *features* or *predictors*) and a specific *target* parameter; and (2) *test phase,* which requires predicting an output based on a given set of features using the generated model. In addition to these two, a *validation phase* might be implemented in between the training and test phases to evaluate the initial model: validation enables tuning of specific hyperparameters necessary to improve the model accuracy. The simplest example of supervised learning is a (linear) *regression* between two *continuous* parameters, although a *classification* task involving a *categorical* target parameter also falls under this technique. On the other hand, unsupervised learning works with unlabelled data where there is no target parameter. A common example is *clustering*, in which the purpose is to possibly identify subsets sharing specific similar features from the initial set of data.

Given its versatility, *ML* has found its way through several fields— ranging from familiar concepts such as price prediction and risk assessment, up to the more technical ones such as medical prognosis and oceanographic forecasting. For our specific interest, recent efforts have also already been made in applying *ML* on *either* droplet impact dynamics *or* textile design. First, the use of *ML* on drop impact studies showed quite some success. The most relevant example is the work of Yancheshme et al. last 2020, which investigated the behavior of droplet on superhydrophobic surfaces. They positively integrated machine learning in their experimental work to classify the droplet impact behavior— mainly whether splashing, deposition or rebound— based on surface wetting characteristics, fluid properties and kinematic parameters. [14] Another study was successful on using machine learning to evaluate water droplet behavior in terms of ice repellency of concrete samples. They initially quantified this icephobic behavior through the restitution coefficient of bouncing water droplets at freezing temperature, and eventually used those results to predict the performance of concrete samples based on their chemical composition and the exact testing conditions. [15]

Secondly, the application of *ML* in the textile industry is also growing. There are new research interests on identifying the complex relationships among fiber properties, processing parameters and final fabric properties. Some specific examples are: (1) prediction of sewing thread consumption from production parameters; (2) determination of the effect of fabric softener amount on mechanical properties of textiles; (3) automation of detecting clothing defects by classifying fabric images; and (4) prediction of specific functional properties of fabrics, such as heat transfer rate and gas permeability. [14] The last example is the most interesting topic in an engineering perspective, as it gives an opportunity to achieve specific properties with the fabrics by controlling some of their physical parameters. It must be noted however that, to accomplish such task, it is highly crucial to obtain a large dataset of textiles having vastly different properties. [16]

Currently, there are several kinds of *ML* algorithms used to work with textile data, ranging from classification techniques (such as *Support Vector Machines*) up to clustering techniques (such as *K-Means).* [16] In this specific work, three specific *ML* algorithms were used. Two are based on supervised learning, (1) *Artificial Neural Network* (*ANN)* and (2) *Random Forest (RF)*— which will be used to predict an output from several input features. The third algorithm is based on unsupervised learning, (3) *Principal Component Analysis* (*PCA*)— which will be used to identify subsets of samples sharing specific features. The key details of each algorithm will be outlined in **Theoretical Framework**.

1.4 *Primary Goals and Scope of Research*

As mentioned previously, the amount of scientific literature available on water-repellent textiles is still limited despite the incentive of producing technical textiles in this industry. There are no studies at present which aim to understand the *dynamic* water repellency of *rough* textiles to the best of our knowledge. Unfortunately, this also extends to the limited number of research work on the use of machine learning in the field of droplet impact dynamics, particularly in understanding textile properties. Therefore, there is a need to fill such knowledge gap— especially that it could have some ramifications on appropriate textile design for the manufacturers. This matter served as the cornerstone of this work.

The main objectives of this study are: (1) to elucidate the influence of droplet physical properties and fabric surface roughness on three main behaviors (*splashing, spreading* and *rebound*) of a droplet impacting on textiles; (2) to evaluate the *water repellency* of textiles solely based on the *observed rebound behavior* of the droplet, while also providing a global perspective on this subject; and finally, (3) to develop models which can predict and/or describe the dynamic behavior of droplet based on specific machine learning algorithms. With regard to understanding of the influence of droplet physical properties, its impact speed will largely be given more attention and only a few remarks on the effect of droplet volume will be provided. The analysis of the influence of the composition of coatings used for these fabrics, i.e. surface wettability due to chemical contribution, will also only be of secondary importance. In addition, studying the effects of the characteristics of liquid and surrounding gas on the droplet dynamic behavior is already outside the scope of this work.

Similar to previous studies, water repellency is defined in this specific work as the magnitude of rebound of a water droplet impacting on a fabric surface, as quantified in the parameter restitution coefficient R_C. A more water-repellent fabric is thus the one which makes the droplet rebound higher (high R_C) (1) up to a larger dropping height and (2) for a large range of height on average.

This rebound behavior of fabrics will then be predicted using machine learning based on fabric physical characteristics (roughness, unit cell size, fiber diameter and defect count) and droplet properties (diameter and impact speed). Even though the phenomena of pinning (between roughness elements) and penetration (through pores) of droplet were not included in the three main behaviors considered, both events result in the decrease (if not complete loss) of rebound behavior of the droplet due to its strong interaction with the fabric surface. As such, they were thus indirectly accounted for in the experimental design, and the scope of R_C in this work covers these two possibilities in evaluating the water repellency of the fabrics. These two concepts— i.e. droplet pinning and penetration— will be discussed more in detail when establishing a global perspective on water repellency.

This account is divided in five chapters. After this **Introduction**, the theoretical framework will be established by mainly introducing the key principles of droplet impact dynamics in **Chapter 2**. The most relevant concepts in surface science and machine learning will be covered as well in this chapter. Then, the experimental work and some of its limitations will be outlined in **Chapter 3**. Next, the results of this work will be discussed in **Chapter 4**, beginning with the investigation of the influence of different parameters on splashing, spreading and rebound behavior of the droplet. Towards the end of this chapter, the developed machine learning models will be presented— alongside a global perspective on both the water repellency of textiles and droplet dynamic behavior on these substrates. Finally, the most significant work and results of this study will be summarized in **Chapter 5**, ending with some possible directions of this research in the future.

Finally, it is important to emphasize that all the key findings of this research are situated within the context of using rough woven polyester fabrics coated with commercial *hydrophobic* formulations and fixed on solid glass substrates. Thus, caution must be taken when attempting to extend the results for cases involving textiles left with hydrophilic surfaces and/or placed in tension mid-air.

Theoretical Framework

Before discussing the relevant experimental methods and results, it is essential to develop first a more complete theoretical framework to gain a better understanding of the underlying principles in this work. First, the fundamental concepts related to surface wettability will be reviewed in this chapter, which will shortly be narrowed down to the complex case of *rough* textiles. While current methods for assessing their static wettability will be covered briefly, the concepts behind droplet impact dynamics will be given more focus— as the latter appears to be more appropriate for evaluating the water repellency of textiles. Each of the three main droplet behaviors (splashing, spreading and rebound) will be provided with a separate thorough account, after the general context of this subject has been established. Finally, a brief discussion of the principles of the three machine learning algorithms used in this work— Artificial Neural Network (*ANN)*, Random Forest *(RF)* and Principal Component Analysis (*PCA)*— will complete this chapter.

2.1 *Wettability as Surface Phenomenon*

Surface wettability, as its name suggests, refers to the capability of the surface to be wetted by the liquid droplet. [3] It is characterized using a parameter called static contact angle *θ,* which is the angle formed by the part of the droplet directly in contact with the surface. *θ* varies depending on the degree of hydrophobicity of the substrate, as shown in the top figure of **Figure 2.1**. Such tuning of surface wettability is commonly achieved by coating the surface, which would modify its chemistry and thus its corresponding surface energy.

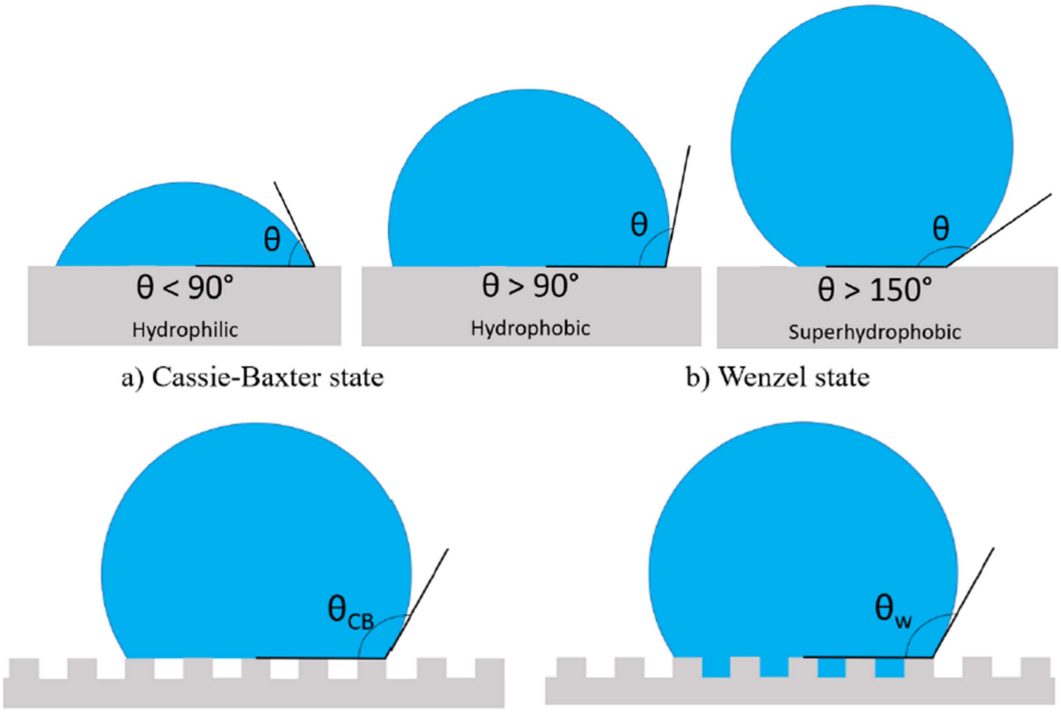

Figure 2.1. The evolution of static contact angle *θ* with the hydrophobicity of a smooth solid substrate (top). The surface hydrophobicity increases from left to right. A hydrophilic surface is characterized by a *θ* below 90˚ by keeping the droplet well-deposited, thereby forming a spherical cap. On the other hand, a hydrophobic surface is characterized by a *θ* above 90˚, with the superhydrophobic one even reaching *θ* above 150˚. In the latter case, it is possible to keep the spherical shape of the droplet, given

that the surface holds a huge fraction of the droplet on top. **The two (non)-wetting states of a droplet on a rough solid substrate (bottom).** The droplet floats on top of roughness microstructure posts of the surface, creating air pockets, in a Cassie-Baxter state (left). In contrast, the droplet fills the cavities and sticks to the actual surface in a Wenzel state (right). Figure taken from [3].

The static contact angle θ is controlled by a balance of interfacial energies, which reflects the overall wetting state of the surface. More precisely, the *Young's contact angle* θ_Y of a droplet on a *flat smooth* surface is described using the famous *Young's equation*:

$$\cos\theta_Y = (\gamma_{SV} - \gamma_{SL}) / \gamma_{LV} \qquad \textbf{Equation 2.1}$$

where γ_{SV}, γ_{SL} and γ_{LV} are the surface energies close to the triple line at solid/vapor, solid/liquid and liquid/vapor interfaces, respectively. Due to the unfavorable (weaker) adhesion of the droplet with the surface compared to the cohesion within the droplet, a more hydrophobic surface generates a larger θ. By convention, surfaces are typically classified as *non-wetting* when they lead to θ greater than 90°. [3]

As shown in **Introduction**, the wettability of a surface can also be tuned by introducing roughness. Two regimes— known as *Cassie-Baxter* state and *Wenzel* state— may describe the interaction of the droplet base with the rough surface, as illustrated in the bottom figure of **Figure 2.1**. Whereas the droplet ignores the roughness structural elements in Cassie-Baxter state, it fills the voids between these elements and adapts to the complete surface in Wenzel state. [3] In both cases, it is assumed that the scale of roughness is much smaller with respect to the droplet size.

While Young's equation works well in solid flat surfaces, caution must be taken when using it for complex surfaces with a certain degree of roughness, as described by the latter two models. This includes objects such as textiles.

2.2 Wettability of Textiles

Textiles are produced by weaving with weft and warp threads, which can be single thick fibers or multifilament yarns of thin fibers. Woven fabrics can be classified as *plain* or *twill* depending on the weave pattern, as depicted in **Figure 2.2**. The fiber acts as the textile building unit, which can either be natural or man-made. [17]

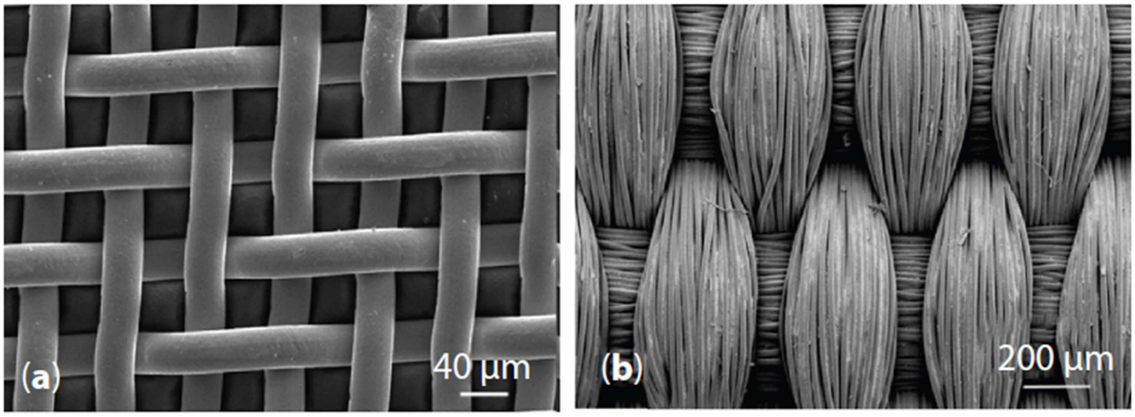

Figure 2.2. Comparison of two different woven fabrics. (a) A twill-woven fabric composed of monofilament yarns (single thick fibers). (b) A plain-woven fabric composed of multifilament yarns. [17]

In contrast with solid planar surfaces, understanding the static and dynamic wetting behavior of textiles is more complicated— as this behavior is typically affected by their geometry, fiber

properties, texture and porosity. For example, one study found that, in order to attain a static contact angle near 170° (i.e. exhibiting a superhydrophobic behavior), a silicone-coated polyester-based textile must possess a precise optimum geometry. [17]

Depending on the textile parameters, as well as the droplet properties, either a Cassie-Baxter or Wenzel state can be observed. As seen previously, a droplet is in contact with air pockets in Cassie-Baxter state, whereas it is in complete contact with the surface in Wenzel state. In Cassie-Baxter state, the apparent Cassie-Baxter contact angle θ_{CB} on rough surface is related to the Young's contact angle θ_Y by the equation:

$$\cos\theta_{CB} = -1 + \Phi_s(1 + \cos\theta_Y) \qquad \textbf{Equation 2.2}$$

where Φ_s represents the ratio of the actual solid-liquid contact area to the total apparent contact area ($\Phi_s \leq 1$).

On the other hand, in Wenzel state, the apparent Wenzel contact angle θ_W can be described as:

$$\cos\theta_W = r\cos\theta_Y \qquad \textbf{Equation 2.3}$$

where r is the roughness factor describing the surface topography. More specifically, r is the ratio of the effective surface (contact) area to the projected area of a flat surface ($r \geq 1$). It is important to stress that the Cassie-Baxter state is particularly useful for modeling rough textiles only when: (1) they demonstrate strong hydrophobic behavior; and (2) they follow the previous assumption of having a roughness scale smaller than droplet size. The latter requirement can be understood more intuitively by considering the effect of varying the density of roughness microstructure posts. On one hand, when the density of posts decreases, the droplet will be in contact with a larger fraction of air and the contact angle increases, assuming a Cassie-Baxter state (see **Equation 2.2** for the effect of Φ_s on θ_{CB}). On the other hand, if the density of posts becomes too low, the droplet may simply place itself in between such posts. Here, the contact angle decreases as the droplet simply fills the bottom surface, similar to the scenario of simply using a flat surface. [10] Finally, there are two recent approaches in describing the texture of textiles and relating it to its apparent contact angle: one involves fractal geometry, while another uses a dimensionless parameter from spatial frequency spectrum of surface profile. [17] Given their complexity, both approaches are already outside the scope of this discussion however.

Aside from the apparent contact angle θ, the wettability of a textile can also be evaluated through a parameter called *roll-off angle* θ_{RO}. When the substrate is sufficiently hydrophobic, the water droplet can easily roll off from a surface when tilted at an angle θ_{RO}. That is, fabrics with lower wettability result in smaller θ_{RO} of the droplet. This parameter can be related to the contact angle hysteresis $\Delta\theta$ of the droplet on the given surface, which is the difference between its advancing angle θ_A (maximum θ) and its receding angle θ_R (minimum θ). Physically, $\Delta\theta$ can be regarded as the friction to be overcome by gravitational work during tilting— which is necessary to move the contact width of the droplet and allow it to roll. In a roll-off test, as the surface is progressively tilted, the droplet will start to deform but keep its initial contact area. Here, θ_A is found in the "downhill" side (larger θ), while θ_R is found in the "uphill" side (smaller θ). [17]

Indeed, both contact angle θ and roll-off angle θ_{RO} provide a measure of wettability of textiles: high θ and low θ_{RO} are characteristics of water-repellent surfaces. However, these tests do not reflect well the actual scenarios of textile becoming exposed to *dynamic* wetting, such as during rain or while washing. These cases can be simulated better in the laboratory by allowing the droplets to impact textiles from a specific dropping height, which is the subject of droplet impact dynamics.

2.3 *Droplet Impact Dynamics*

As covered in **Introduction**, there are typically five stages of droplet dynamic behavior: (1) initial impact; (2) spreading; (3) retraction; (4) rebound; and (5) equilibrium. However, this only represents the *ideal* scenario when using a (super)hydrophobic substrate; several things can actually occur when a droplet hits and interacts with a surface, making the subject extremely complicated. From the illustration in **Figure 2.3**, the impact of a droplet might also lead to its (a) deposition, (b) prompt or corona splash, (c) receding break-up or even (d) partial rebound on the surface.

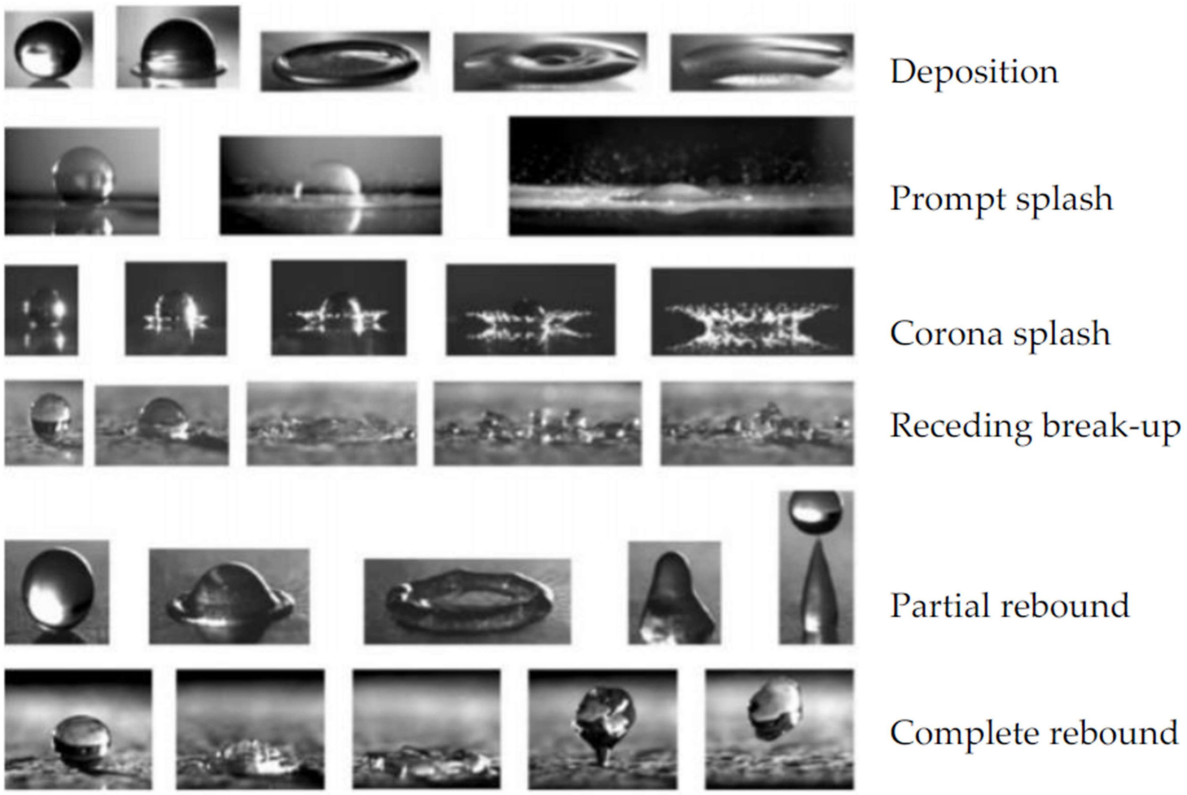

Figure 2.3. Different outcomes of the interaction of an impacting droplet with a solid surface. It must be given emphasis that not all events are mutually-exclusive (e.g. partial rebound can still be observed for a droplet which has already exhibited prompt splashing). Figure taken from [3].

This work will simply focus on three of the general behaviors: (1) splashing (particularly prompt splash and receding break-up), (2) spreading and (3) rebound (whether partial or complete). Before reviewing the related literature specific to each of these three behaviors, it is necessary to have a complete understanding first of the general principles of droplet impact dynamics, focusing on solid surfaces.

2.3.1 Fundamental Principles of Droplet Impact Dynamics

There are several factors which influence the dynamics of impact behavior of the droplet on surfaces, such as: (1) the properties of the fluid (density, viscosity and surface tension); (2) the physical properties of the droplet (diameter and impact speed); and (3) specific characteristics of the surface (chemical wettability, roughness and geometry). The interplay of parameters in the first two properties is encapsulated in specific *dimensionless numbers*, which represent the balance of driving and resistive forces for the droplet's behavior. [3] [14]

An example of these dimensionless parameters is *Weber number We,* which was already seen in **Introduction**. As a reminder, *We* represents the balance between the kinetic and surface energy of the droplet. Another parameter is *Reynold's number Re* which, in contrast, measures the relative magnitude of inertial force to viscous force. It is given by the expression: $Re = \rho V D_o / \mu$, where again, ρ and μ are the fluid density and dynamic viscosity, while D_o and V are the initial droplet diameter and impact speed, respectively. To represent the relative contribution of *We* and *Re* of a droplet, another parameter called *Ohnesorge number Oh* was created, which takes the expression: $Oh = We^{0.5}/Re$.

The balance of these several forces exists at all stages of droplet impact dynamics. First, the conversion of potential energy to kinetic energy during the droplet's fall simply means that the latter energy is at its highest at the moment of impact. With enough kinetic energy, the droplet may deform or eventually spread over the surface upon impact, where a transfer of momentum from vertical to radial direction occurs. [3] The simulation of Eggers et al. found that the driving force for such re-direction of fluid is the relaxation of the high pressure exerted on the base of the droplet; through lateral spreading, the momentary compression of the droplet base is relieved. [31] During spreading, the kinetic energy of the droplet is converted into surface energy through the increase of both the total surface area of the fluid and its contact area with the substrate. However, a fraction of this kinetic energy may also be lost through viscous dissipation, which increases its internal energy through heat. [5] [6] At maximum spreading, the surface energy of the droplet is at its highest, while its kinetic energy is at its lowest (the latter is approximated to be zero in simplistic treatments).

Afterwards, the droplet may retract or not depending on the corresponding surface energy at solid-liquid interface. [3] It is ultimately through this available surface energy that the droplet can regain enough kinetic energy for rebound to occur. However, a droplet may only rebound once a critical value of impact speed is reached, which occurs when the kinetic energy of the droplet exceeds its *initial* surface energy (i.e. when *We* exceeds a specific threshold). As will be seen shortly, the surface area of the droplet increases with *We.* The physical intuition behind the existence of critical impact speed is thus that the droplet must achieve a specific proportion of surface area relative to its volume at maximum spreading in order to gain enough stored energy— which *may* allow it to bounce. Using the expression of *We,* it can be found that this critical speed must be larger than the *order* of $(\sigma/\rho D_o)^{1/2}$, which typically corresponds to a dropping height less than 1 cm. The expression of critical speed reveals too that a large droplet will tend to rebound at a smaller dropping height compared to a small droplet in this low kinetic-energy regime (given the link of impact speed with kinetic energy and dropping height with potential energy). [10]

Finally, the droplet will exhibit several oscillations due to inter-conversion of kinetic and surface energy after receding and/or rebounding. The amplitude of such oscillation, however, is dampened by viscosity over time, until the droplet eventually reaches its equilibrium state. [4] It is worth-mentioning that the droplet may also simply remain deposited and completely wet the surface without exhibiting these oscillations.

2.3.2 Splashing Droplet Dynamics

Splashing refers to the disintegration of a droplet to form smaller secondary droplets. In this work, the two types of splashing observed are (see **Figure 2.3** if necessary): (1) prompt splashing, where the secondary droplets are formed immediately after the main droplet impacts the surface; and (2)

finger splashing or receding break-up, where cylindrical edges (called *fingers*) of the droplet are detached during its retraction.

In several research work involving both experiments and simulations, splashing is observed to occur only when Weber number *We* is sufficiently large, i.e. when the droplet has high impact speed. [6] [18] [19] The primary intuition behind such observation is that sufficient amount of kinetic energy is required to overcome the cohesive energy from surface tension and eventually form new permanent additional surfaces by fragmentation of smaller droplets. Moreover, as will be seen later, the maximum diameter of the droplet directly in contact with the surface increases with *We*. Thus, there is a larger interfacial area for droplet-surface interaction at high *We*, and this more prevalent interaction can also lead to splashing by receding break-up. As a final remark and for the sake of completeness, it was found too that a larger droplet is more likely to exhibit splashing.

To formally establish the threshold for splashing of the droplet, a term known as *splashing parameter K* was conceptualized. Mundo et al. developed this parameter by accounting for the interplay of kinetic energy, surface tension and viscous stress in the fluid, resulting in the following relation: $K = We(Re)^{0.5}$. As a rule-of-thumb, splashing becomes more probable when *K* exceeds 3000. [20] In 2019, Santiago et al. developed a more complete analysis to separate splashing from non-splashing behavior of droplets. By surveying solid surfaces of different characteristics (roughness and chemical wettability), they demonstrated that the splashing threshold depends on the fluid and droplet properties through *K,* as well as the properties of the surface. They observed splashing in rough surfaces, but not in smooth ones, for the same droplet impacting conditions and surface wettability (for superhydrophobic solid glass surfaces). It was then concluded in this study that: micrometer-scale roughness increases the likelihood of splashing by influencing the *dynamic* contact angle of the droplet. [1] Similar previous studies reported this same conclusion that droplet splashing is promoted by surfaces with higher roughness. [3] [19] [20] Finally, it must be recognized that establishing such threshold for splashing will only work if there is a high consistency of surface roughness among local areas, with respect to the droplet size. [20]

2.3.3 Spreading Droplet Dynamics

After impact, the droplet moves outward radially until it reaches its maximum spreading. This state is characterized by a parameter called S_{max}— which is the ratio of the droplet's maximum spreading diameter to its initial diameter. From previous studies, two regimes have been identified based on droplet impact speed *V* concerning the evolution of its maximum spreading behavior*:* (1) *capillary regime* at *low V*; and (2) *viscous regime* at *high V*. [8]

Capillary regime: When *V* is sufficiently low, the maximum spreading of droplet is influenced mainly by the balance between kinetic energy and capillary forces— with minimal contribution from viscous dissipation. [20] If the viscous forces are completely negligible, only a conversion of kinetic energy to surface energy occurs; maximum spreading is thus treated as a simple case where the surface energy is at maximum when the kinetic energy is at minimum. Past studies found that S_{max} can be expressed as a simple function of Weber number *We* in this regime, according to a power law: $S_{max} \propto We^{\beta}$, where β is a value typically ranging from 0.2 to 0.5. [2] Clanet et al. specifically established that $S_{max} \propto We^{0.25}$ using an analytical model based on motion equation and mass conservation. They have confirmed this result through experiments on smooth solid surfaces for both hydrophobic and hydrophilic cases. [8] This dependence of S_{max} has been verified too by other research groups on different surfaces for a wide range of wettability. [9] [21] It is worth-noting that, based on this dependence, only the kinetic energy of the droplet largely governs its maximum

spreading and the wettability of the surface does not seem to play a role. In contrast with this finding, other groups found that a lower maximum spreading will be obtained when the chemical wettability of the surface is decreased. Because of that, more sophisticated models have been developed— such as by accounting for surface wettability using the droplet's apparent contact angle θ. [3] Nevertheless, the proposed scaling law $S_{max} \propto We^{0.25}$ by Clanet et al. is still being widely used as it agrees well with most experimental data on this subject.

Viscous regime: When V is sufficiently high, the maximum spreading of droplet is dictated mainly by the balance between inertial and viscous forces. A huge fraction of the droplet's kinetic energy is thus dissipated by the viscosity of the fluid. In this regime, ξ_{max} varies primarily with Reynold's number Re, through the following relation: $S_{max} \propto Re^{0.2}$. [8] [20]

The observed dependence of S_{max} on either We or Re has physical implications. By increasing its impact speed V, the surface area of the droplet at maximum spreading also increases, albeit at a slower rate due to the fractional scaling factor. In both cases, spreading is driven by the kinetic energy of the droplet and opposed by either its surface tension or its viscosity.

Interestingly, surface roughness appears to play a minor role on the spreading behavior of the droplet too, though with a few contrasting results. For instance, Tang et al. investigated the influence of using rough surfaces on droplet impact dynamics, and found that increasing the roughness decreases both S_{max} and the time required for the droplet to reach this maximum spreading state. [22] However, further studies demonstrated that the roughness only has a significant effect on the spreading behavior when the surfaces are hydrophilic, compared to when they are hydrophobic. [23] [24] Bobinski et al. found a dependence similar with the previous studies ($S_{max} \propto We^{0.25}$) for the maximum spreading of droplet on hydrophobic silicon surfaces with different microstructures (i.e., spacing, length and height of roughness posts). [21] The recent study of Santiago et al. also arrived at the same conclusion— that the spreading behavior on (super)hydrophobic surfaces is not influenced by the micrometer-scale roughness at all. [1]

In this work, the parameter which will characterize droplet spreading is the *dimensionless maximum contact width* ξ_{max}— i.e. the maximum diameter of the droplet *directly in contact* with the surface D_{max}, divided by its initial diameter D_0. While technically, ξ_{max} is slightly different from S_{max} as shown in **Figure 2.4**, the two parameters are obviously still highly correlated. It can thus reasonably be expected that ξ_{max} will follow the relationship presented if and only if S_{max} does *in general*.

Figure 2.4. Difference between S_{max} and ξ_{max} of a droplet at maximum spreading state.

2.3.4 Rebound Droplet Dynamics

After spreading and retraction, a droplet may rebound depending on the exact combination of initial kinetic energy and surface wettability. It is intuitive that the rebound of the droplet typically occurs when it has undergone retraction beforehand— as the latter event allows the accumulation of kinetic energy from the surface energy temporarily stored during deformation. This accumulated

kinetic energy can also be moderated by viscous dissipation however, which ultimately results in a decreased rebound behavior of the droplet. As another remark, it must be stressed that the converse of the earlier statement is not always true: a droplet may still not rebound despite undergoing retraction.

The presence of surface roughness complicates its rebound behavior, particularly because the droplet may exhibit one of the two scenarios upon impacting: (1) to remain floating on top on the roughness elements (as in Cassie-Baxter state); or (2) to fill the cavities by pushing out the trapped air, essentially "sticking" to the solid surface (as in Wenzel state). In the former case, the droplet can still completely rebound without fragmentation as it ignores the structures underneath. On the contrary, a fraction of the droplet contact width becomes stuck on these roughness structures in the latter case— effectively dissipating energy and thus, diminishing the rebound behavior. Therefore, the droplet only partially rebounds, following a droplet break-up as shown in **Figure 2.5**.

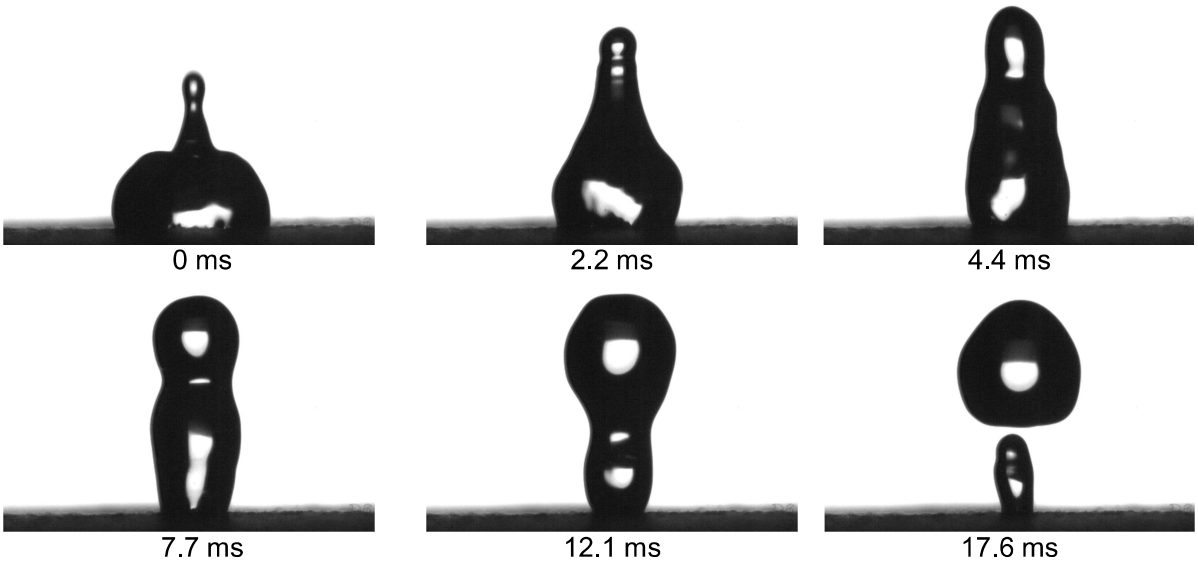

Figure 2.5. Millisecond image sequences showing partial rebound of water droplet. The bottom part of the droplet sticks to the surface near the impact area— leaving a smaller droplet during its lift-off.

An impacting droplet can transition from Cassie-Baxter to "sticky" Wenzel state given specific conditions. Such transition is governed by the balance between (1) the dynamic pressure ($\sim\rho V^2$), which promotes the wetting of surface, and (2) the capillary pressure for liquid/vapor interface deformation, which opposes this wetting tendency. Therefore, the droplet can attain this sticky behavior once it has a sufficiently large impact speed. Reyssat et al. solved for this critical impact speed for sticking phenomenon, V_{stick}, for micro-structured surfaces. They found that: $V_{stick} = (\sigma H/\rho L^2)^{1/2}$, where H is the height of the micro-roughness posts, and L is the distance between two posts. [7] Bobinski et al. found a similar relation too, as they noticed that complete rebound behavior occurs only when the spacing-to-width ratio of the micro-posts is sufficiently low. [21] This dependence of V_{stick} on the geometric parameters of micro-patterned surfaces has also been confirmed by the work of Jung and Bhusban. In addition, their group has also made the connection between static wettability and rebound behavior: they verified through experiments that though decreasing L tends to increase V_{stick}, it leads to the decrease of static contact angle θ too unfortunately. [25] This second result should not be surprising, as it simply links the main theoretical findings discussed up until now in this chapter. Overall, to prevent the sticking behavior of droplet (i.e., to keep its full rebound behavior for a larger *We* range), it is essential to have a surface where the roughness posts are tall (high H) and close with each other (low L) to impart a larger capillary

pressure. [7] This aspect already reveals how *surface topography* can affect the final droplet impact behavior by itself. Furthermore, at the extreme case, the cavities can be completely filled by the droplet fluid and the sticking behavior becomes complete droplet pinning: by effectively "pinning" the droplet on the surface, its bouncing tendency becomes fully suppressed. By extension from droplet sticking (i.e. partial rebound), droplet pinning is thus mainly dictated by the balance of the mentioned wetting and anti-wetting forces. [14]

Summing up, the rebound behavior of the droplet passes through several regimes for *increasing We,* as summarized by Malla et al.: (1) absence of bouncing due to insufficient energy; (2) complete bouncing; (3) partial bouncing with droplet break-up, as the onset of "sticky" behavior; and finally, (4) absence of bouncing due to pinning, with the latter two being the consequence of the transition from Cassie-Baxter to Wenzel state. [4] [14] It is worth-mentioning that this sequence of events is only one of the typical possibilities, and a droplet may just as well deposit on the surface for the entire *We* range given a highly wettable substrate.

As final information, recent studies showed that at certain impacting conditions, a droplet may also exhibit *pancake rebound* or *jetting* in rare occasions. During pancake rebound, the droplet rebounds shortly after it has reached its maximum spreading but before it completes its retraction, allowing it to keep its flat "pancake" shape even mid-air. [20] In contrast, during jetting, the bottom portion of the droplet gets pushed into the surface as the droplet "jets" quickly upwards. The droplet thus keeps its contact with the surface the whole time during its rebound. This phenomenon of jetting has been observed to occur in surfaces where the spacing-to-width ratio of the roughness micro-posts is sufficiently low. [21] While pancake rebound was not observed in this work, jetting was seen occasionally in some samples.

2.4 *Machine Learning*

As mentioned previously, there are three machine learning algorithms used in this work: Artificial Neural Network *(ANN),* Random Forest *(RF)* and Principal Component Analysis *(PCA).*

2.4.1 Artificial Neural Network (*ANN*)

ANN is a supervised-learning technique typically used for regression tasks. An *ANN* model is based on several nodes (called *neurons)* which are specifically arranged in several layers for a *multi-layer perceptron architecture*. As illustrated in **Figure 2.6**, there are always at least three main layers in this architecture: (1) the input layer, which contains the features of the samples; (2) the hidden layer, which determines how the input features are complexly related to each other; and (3) the output layer, which contains the desired information. If there are multiple hidden layers, the output of the neurons from one layer will simply serve as the input for the subsequent layer. Finally, the connections between neurons contain specific *weights*, which capture the strength of influence of one neuron to another.

Figure 2.7 shows in greater detail the computation occurring inside a neuron. The weighted inputs (from the neurons of the previous layer) and a constant term called *bias* together form a sum, which then passes through a non-linear *activation function* to determine the final output of this specific neuron. The most common activation function is the *Rectified Linear Unit (ReLU)*, which takes the form $\varphi(A_i) = max(0,A_i)$ (where A_i is the input prior to activation). Essentially, *ReLU* transforms all the negative input values into zeroes but keeps the positive ones. This activation

step is what ultimately allows *ANN*, unlike linear regression techniques, to capture and predict complex nonlinear relationships between specific features and a target parameter.

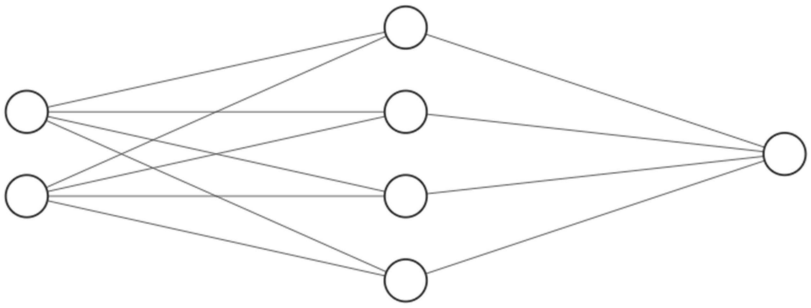

Figure 2.6. A typical *ANN* multi-layer perceptron architecture. The first (input) layer consists of two neurons, which typically represents the number of features. The intermediate (hidden) layer consists of four neurons, whereas the final layer contains the single output neuron. In this case, all the neurons in one layer are connected to all the neurons in the *next* layer, in a fully-connected (*dense*) fashion. The nodes corresponding to *bias* terms are not included. The schematic architecture was generated using an open-source tool [30].

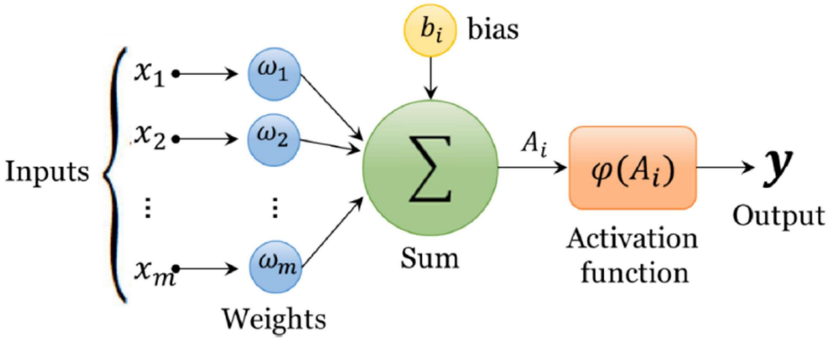

Figure 2.7 Calculation inside an artificial neuron. The sum of weighted inputs and a bias term first passes through a non-linear activation function before the final output is determined. Figure taken from [14].

To obtain a good accuracy for an *ANN* model, the initially-selected network parameters (i.e., the weights and biases) are updated *iteratively* in such a way that the residual error between the actual and predicted target value gets minimized. This error is encapsulated in the *loss* function, which can take the familiar form of *mean squared error (MSE)* for regression tasks, as shown below:

$$L = \frac{1}{N}\sum_{i=1}^{N}(y_{i,pred} - y_{i,act})^2 \qquad \textbf{Equation 2.4}$$

where *N* is the total number of samples in the training set. The adjustment of network parameters is typically accomplished by using a *back-propagation* algorithm, which employs a *gradient descent* principle. Put simplistically, each parameter is updated based on how the loss function varies when the magnitude of such parameter is changed, for a given *learning rate.* The task of minimizing the loss through gradient descent is normally optimized by changing the learning rate and using the concept of *momentum* (factoring in the previous update to the next update) throughout several iterations. This is carried out using specific loss optimizers, with *Adaptive Moment Estimation (Adam)* being one of the most common ones. [14]

Finally, it must be emphasized that creating a predictive model based on *ANN* typically requires tuning several hyperparameters to create the final architecture— such as the number of neurons in each layer, the number of hidden layers, and the nature of the activation and loss functions, among others.

2.4.2 Random Forest (*RF*)

RF is a supervised-learning technique used for both regression and classification tasks. It is an *ensemble* of decision trees, where the latter are made of *nodes* and *branches:* each node addresses specific features, while the branches split the dataset according to a specific rule about those features. There are three kinds of nodes in each decision tree, as illustrated in **Figure 2.8**. These are: (1) the *root* node which contains the *entire* dataset; (2) the *internal* node, which consists of a *subset* of samples satisfying a requirement on particular features; and (3) the *terminal* node or *leaf*, which represents the final outcome. Different parameters are used for selecting a feature as criterion for splitting— such as information gain and entropy for classification, and mean squared error for regression. The splitting process for each decision tree occurs recursively until there are only a certain number of samples left in each leaf or a specific condition is met. Intuitively, the prediction of a new sample will pass through several branches where rules are observed and decisions are made— starting from the root node and until the final leaf is reached. For a regression task, the final output will be the mean of the target parameter values of the samples present in the concerned leaf. [14]

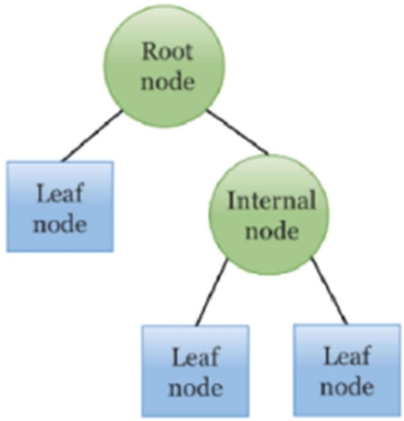

Figure 2.8. A typical decision tree architecture. The root and internal nodes (green) contain the initial dataset and intermediate subset, respectively. On the other hand, the leaf nodes (blue) contain the final subsets of samples generated by deciding whether their features satisfy the specific criteria or not. Figure taken from [14].

In the context of *RF,* each decision tree is trained to work only on a random subset of samples and a random subset of features— mainly to address the issue of overfitting that using decision trees conventionally faces. These subset-based trees are then finally combined to create the whole forest. This randomization and aggregation approach enables *RF* to have a performance better than that of single decision trees.

In *ANN, RF,* or any *ML* algorithm used for prediction, it is useful to have a measure of the relative importance of the features in terms of predicting a target parameter. One tool to accomplish such task is *Permutation Importance*— which evaluates the decrease in model accuracy when the values of a specific feature are shuffled randomly. In other words, the dependence of the model on a specific feature is probed by breaking the relationship between this feature and the target parameter. As a final note, it is obvious that such estimation of feature importance is only sensible when the accuracy of the developed model is good enough.

2.4.3 Principal Component Analysis (*PCA*)

PCA is an unsupervised learning technique used for reducing the number of dimensions of a dataset containing a *huge number of features*. Originally, each data point can be positioned in *n*-dimensional space given *n* number of features, where each dimension corresponds to one specific feature. However, representing a dataset visually in *n*-dimensional space is an impossible task, particularly for n≥4. Through *PCA* nonetheless, the number of features in the original dataset can be reduced by finding a new set of parameters as *linear* combinations of the initial *basis* features—ultimately enabling the dataset to be projected into a lower-dimensional space with minimal loss of information. These new parameters, called *principal components,* capture the amount of variance (i.e., information being represented by spread of data) in the initial dataset, while also being uncorrelated (*orthogonal*) unlike the old features. These principal components are formed such that the *first component* contains the highest amount of variance in the dataset; the *second component* contains the next highest variance while remaining perpendicular to the *first component,* and so on. Therefore, besides giving a visual representation of a dataset, *PCA* also enables extraction of information and patterns, which could otherwise be difficult to see in the original complex dataset. Finally, it must be stressed that *PCA* simply applies a rotation of the data space; thus, the relative positions of the points are kept the same. [26]

Experimental

The experimental work performed for this study will be presented chronologically— starting from the preparation of coated fabrics and study of droplet impact dynamics, up to the analysis of videos and development of machine learning models. This chapter will end with some of the limitations encountered during the experimental work, framing the results presented in the next chapter in a defined context.

3.1 *Preparation of Coated Fabrics*

Seven rough woven polyester fabrics were used for this study, which were supplied by Decathlon and Centexbel. While six of them have plain weave pattern (Fabric 1 to Fabric 6), the remaining one has twill weave pattern with two different faces (Fabric7A and Fabric7B). Hence, there are eight unique fabric (surface) samples in total, each having a specific roughness. To decrease the wettability of these fabrics, three commercial hydrophobic coatings were used— with their relevant description shown in **Table 3.1**. From hereon, only their abbreviated names will be used.

Table 3.1. Characteristics of commercial hydrophobic coatings

Commercial Name	**Composition**	**Weight % Solid**	**Abbreviated Name**
Phobotex RSH [*]	Water-based modified resin	N.A.	PhobRSH
3M™ PM 900	Water-based emulsion of C4-fluoropolymer (perfluorobutyl-modified polyurethane)	~30	C4F
Wacker HC303	Water-based silicone emulsion	~17	PDMS

[*] Unlike C4F and PDMS, PhobRSH requires a separate crosslinker formulation (*Phobol Extender XAN*) to fully function as hydrophobic coating. Since information on its % weight solid is not available, the procedure provided in its technical data sheet is adapted to a laboratory setting.

To prepare the coated fabrics, the general procedure drafted by Jonas, Glinel et al. was adopted. [12] First, PhobRSH was diluted with acidified water of pH 4.0 – 5.0 by a factor of 25, using Milli-Q water (resistivity 18.2 MΩ-cm) during its preparation. A crosslinker formulation (*Phobol Extender XAN*) was then added to the acidified diluted PhobRSH suspension in a ratio of 1:250 by mass. On the other hand, the C4F and PDMS suspensions were simply diluted until a final concentration of 1.5 wt. % solid is obtained. Next, the fabric samples were dip-coated in these diluted coating suspensions for 3 minutes. After being suspended in air for few seconds, they were placed on a hot plate at 150˚C for certain duration (5 minutes for PhobRSH, and 3 minutes for C4F and PDMS formulations) to dry and crosslink the polymer of the coating. Finally, after cooling, the coated fabrics were fixed on glass substrates to minimize their deformation during droplet impact studies.

Moreover, flat samples were prepared by spin-coating of silicon wafers at 3000 rpm for 30 seconds, and then annealing at 150˚C for 2 minutes. These flat samples were coated with (1) undiluted PDMS suspension, (2) C4F suspension diluted by a factor 2, or (3) prepared PhobRSH mixture diluted by a factor 2. The flat samples were used simply to establish a baseline as smooth hydrophobic surfaces, i.e. without the influence of roughness, on static contact angle.

3.2 *Physical Characteristics of the Fabrics*

Given that this study builds on the initial work of Jonas, Glinel et al., [12] the fabric samples have already been characterized extensively. **Table 3.2** summarizes all the information obtained for the fabrics. The experimental roughness *r* is defined as the ratio of the actual (probed) area to the projected area of the fabric surface (*r ≥ 1)*, as in the initial work. In addition to the previously-obtained physical parameters, the defect count classification of each fabric sample has also been determined (see **Supplementary S.3.1**).

Table 3.2. Physical characteristics of fabric samples

Fabric Sample	**Experimental Roughness *r***	**Fiber Diameter (μm)** *[*]*	**Unit Cell Length (μm)** *[*] [**]*	**Defect Count Classification** *[***]*
Fabric1	1.19	10 / 20	600 / 400	Low (≤12)
Fabric2	1.27	14 / 25	750 / 600	Low (≤12)
Fabric3	1.46	22 / 20	340 / 550	Low (≤12)
Fabric4	1.47	22 / 18	310 / 680	High (≥ 24)
Fabric5	1.77	16 / 18	730 / 810	Intermediate (> 12 but < 24)
Fabric6	1.77	20 / 16	540 / 350	High (≥ 24)
Fabric7A	1.71	12 / 14	330 / 450	Intermediate (> 12 but < 24)
Fabric7B	1.67	16 / 12	540 / 550	Intermediate (> 12 but < 24)

[*] Fiber diameter and unit cell length have two values each as chosen by the textile manufacturers for weaving.
[**] Unit cell adopts the same definition as in crystallography. The two values represent the length of the two different sides making up rectangular unit cells of small size (not necessarily primitive).
[***] The average defect count per *8.5 mm^2 fabric area* is the value enclosed in parentheses. See **Supplementary S.3.1** for full description of classification of fabric samples based on their defect count.

With the abundance of literature on the effect of surface roughness on the dynamic behavior of the droplet, as previously presented in **Theoretical Framework**, it is not difficult to see why the roughness *r* of the textiles is the most interesting parameter to investigate among the given physical parameters. The huge amount of research work on the topic of roughness also gives an opportunity to compare our results with similar studies and put our work in a larger context. Nevertheless, hypotheses can still be made based on physical arguments regarding the potential influence of other fabric parameters on the droplet behavior. Finally, as operating definition in this work, the term *fabric samples with high roughness* will refer to Fabric 3 to Fabric 7 (with *r > 1.4*), while that with *low roughness* will include Fabric 1 and Fabric 2 only.

3.3 *Contact and Roll-Off Angle Measurements*

The contact angle measurements were conducted by gently depositing 10.0-μL water droplet on fabric surfaces (known as *sessile drop method*) and performing *ellipse-fitting*. Roll-off angle measurements of 10.0-μL water droplet were also performed: the droplet is initially deposited on the fabric, and subsequently allowed to roll-off by progressively tilting the sample stage at a rate of less than 3.0˚/s. Both measurements were performed using OCA 20 goniometer from Dataphysics. Each fabric sample was evaluated in at least six different positions for contact angle measurements, and in at least four different positions for roll-off angle measurements.

3.4 *Droplet Impact Dynamics Studies*

The droplet impact behavior on the different fabrics samples was surveyed by recording numerous videos with a high-speed camera at a frequency of ~900 frames-per-second (fps) and an optical resolution of ~16.7 µm-per-pixel. The water droplets were dispensed at a flow rate of 5 µL/s from a 500-µL Hamilton syringe pump of the same goniometer, with the experimental setup shown in **Figure 3.1**. Two sizes of needles were used (0.30-mm and 0.52-mm diameter) to generate two narrow range of droplet diameters (~1.9 mm and ~2.7 mm), respectively. Upon release, the droplets impact the fabric surfaces at a *normal* angle. During its fall, it was assumed that the droplet volume did not change (i.e., no significant evaporation) in the analysis of all the videos obtained. This is a reasonable assumption for a liquid droplet such as water, which is less volatile than common organic solvents (e.g. ethanol or acetone). Another important assumption made is that the droplet has kept its spherical shape from its time of release, allowing to neglect the effect of droplet shape (i.e. asymmetry and ellipticity) prior to impact. [3]

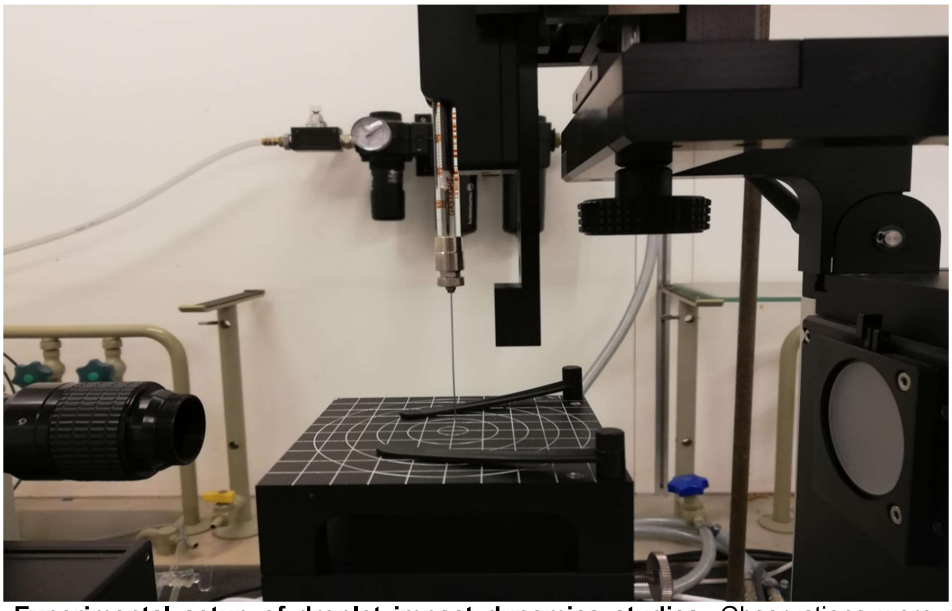

Figure 3.1. Experimental setup of droplet impact dynamics studies. Observations were made using OCA 20 goniometer from Dataphysics. Initially, the syringe (at the middle) dispenses water droplets of specific volume through its needle from a selected dropping height. Shortly after, the droplets impact the surface placed in the sample stage. The camera (on the left) records the dynamic behavior of the droplet for a certain duration, with the lamp (on the right) being used for illumination.

A wide range of dropping height was considered— from around 5 mm to 200 mm— to capture a range of droplet dynamic behavior for different impact speed (thus Weber number *We*). The exact height values were obtained by analyzing specific images using *Matlab* and/or measuring with a ruler. To calculate *We,* the droplet impact speed was manually determined for every dropping height (shown in the next section) instead of being approximated by free-fall formula (See **Supplementary S.3.2**). Based on this computation, the observed *We* range for our experimental setup is around $1 < We < 120$.

3.5 *Analysis of Videos and Extraction of Relevant Parameters*

The first part of this work involves analyzing the videos using the routine developed by Prof. Jonas on *Wavemetrics Igor Pro*. This procedure extracts the number of droplets, the center of mass (as

weighted-average if multiple droplets are present) and the contact width values of the droplet for every frame of the video— outputting a text file for each video or *observation*.

The second part involves processing all the text files at once using *Python* and extracting the relevant parameters from each observation (video), which have been organized in **Table 3.4.1**. This analysis generated the final dataset where each row represents an observation and each column represents a specific parameter.

Only the most interesting scatter plots obtained from the dataset were presented in **Results and Discussion**. Unless explicitly mentioned otherwise: (1) each point represents one observation of given dropping height and droplet volume for a specific fabric sample with a given coating; and (2) if each point represents an average, the assigned error bar is the corresponding *standard error of the mean* for its corresponding set of observations (which was computed using the formula $\sigma/\sqrt{n}$, where σ is the standard deviation and n is the number of observations). The uncertainty of the values reported in tables in **Results and Discussion** is also computed as standard error of the mean.

Table 3.3. Relevant video output parameters for droplet impact dynamics studies

Parameter	***Intermediate* Working Definition**	***Final* Physical Units**
Average number of droplets	Number of droplets averaged over a chosen number of frames N (Note: N = 80 frames)	None
Rebound height [**]	Maximum difference of number of pixels between the center of mass of droplet at time t and its center of mass at rest with a specific threshold value, solely along the vertical direction (Note: N = 80 frames)	m
Non-contact time	Number of frames where the droplet is mid-air and considered to be at "bounce"	s
Maximum contact width [*]	Maximum number of pixels of the droplet directly in contact with the fabric surface	m
Maximum spreading rate	Maximum increase in contact width of the droplet between two consecutive frames	m/s
Maximum receding rate	Maximum decrease in contact width of the droplet between two consecutive frames	m/s
Equilibrium contact width	Contact width of the droplet at rest (after several oscillations)	m
Maximum spreading time	Number of frames until the droplet reaches its maximum contact width starting from its impact as $t = 0$	s
Impact speed	Decrease in center of mass of droplet along the vertical direction between two consecutive frames right before impact, divided by the timeframe	m/s
Weber number [***]	Given by the formula: $\rho V^2 D_o / \sigma$, where D_0 is the initial droplet diameter, V is the impact speed described above, and ρ and σ are the literature values of density and surface tension of water, respectively	None
Restitution coefficient [**] [****]	Given by the formula: V_{Af} / V_{Bf}, where V_{Bf} is simply the impact speed V described above and V_{Af} is the speed "after impact" (i.e., towards the end of its rebound flight, right before it impacts the surface *again*)	None

[*] Dimensionless equivalent corresponds to maximum contact width divided by initial droplet diameter.

[**] The rebound behavior, quantified through the parameters rebound height and restitution coefficient, is described as the movement of center of mass of the droplet or collection of droplets solely along the vertical direction. The droplet is considered to be at "bounce" if the current height of its center of mass exceeds a specific threshold relative to the one at rest. This threshold value is set by visual inspection and analysis of the videos where the droplets did not bounce (30 pixels for ~1.9 mm droplet and 42 pixels ~2.7 mm droplet). The contact width was not chosen as the criterion for bouncing due to several cases of partial rebound (where a smaller droplet remained on the surface as the main droplet lifted off) and a few cases of jetting (where the droplet kept a large area of contact with the fabric despite reaching a high center of mass) observed during the course of data-gathering. Finally, it is highly encouraged for the reader to remember this operating definition well and visualize these different possibilities when the term *rebound* is mentioned in **Results and Discussion**.

[***] The initial droplet diameter is taken from the input volume in OCA20 software linked to goniometer used for impact studies, assuming the droplet has a perfectly spherical shape.

[****] The computation of restitution coefficient requires determining the impact speed of the droplet after rebound. Given that the typical rebound height is less than 3 mm, the effect of air resistance can be neglected. This claim is supported by **Supplementary S.3.3**, which shows that classical kinematics can be applied on this rebound behavior in general. As such, the "after impact" speed V_{AI} can simply be approximated by the free-fall equation: $V_{AI} = \sqrt{(2gH_B)}$, where H_B is the corresponding rebound height of the droplet.

3.6. *Machine Learning*

All the machine learning (*ML*)-based analyses were performed using *Python* open-source packages: *TensorFlow* and *Scikit-learn.* Characterizing the droplet behavior requires predicting two parameters: (1) the dimensionless maximum contact width ξ_{max} to account for its spreading dynamics, and (2) the restitution coefficient R_C to account for its rebound dynamics. While the prediction of ξ_{max} was based on the Artificial Neural Network (*ANN*) algorithm, the prediction of R_C was based on the Random Forest (*RF)* algorithm. The target parameters and the respective size of dataset for the two models, together with a common set of input features, are summarized in **Table 3.4.**

Table 3.4. Input features and target parameters for *ANN* and *RF* models

Model	Input Features	Target Parameter	Size of Initial Dataset	Train/Validation/Test Data Split Ratio
Artificial Neural Network (ANN)	▪ Droplet diameter ▪ Droplet impact speed ▪ Fabric roughness ▪ Fiber diameter 1 ▪ Fiber diameter 2 ▪ Unit cell length 1 ▪ Unit cell length 2 ▪ Defect count	Dimensionless Maximum Contact Width ξ_{max}	290 samples	70:10:20
Random Forest (RF)		Restitution Coefficient R_C	136 samples	80:0:20

For both models, all the values in the dataset part of the input feature space were standardized and scaled into a mean value of 0 and a standard deviation of 1 prior to training and testing. This pre-treatment of data was performed in order to remove the influence of the actual magnitude of values obtained. Then, each dataset was split according to **Table 3.4**.

The developed *ANN* model for predicting ξ_{max} has an architecture described as follows. The input layer consists of 8 neurons, corresponding to the number of input features in this work. There are three hidden layers: while the first and third hidden layers contain 8 neurons each, the second hidden layer contains 16 neurons. Finally, there is a single neuron for the output layer. Moreover,

this network architecture is composed of *dense* fully-connected layers. Rectified Linear Unit (*ReLU*) activation functions were used *only* for the input and hidden layers. The loss function was based on the Mean Squared Error (*MSE),* using Adaptive Moment Estimation (*Adam*) for optimization.

On the other hand, the developed *RF* model for predicting R_C uses the *MSE* as the criterion for splitting. The number of estimators (decision trees) is set at 100. The maximum tree depth has not been specified, i.e. the tree is allowed to expand until the contents of each leaf become *pure* (obtain low error). Nevertheless, its optimum value is estimated to be between 5 and 10 based on its evolution with *MSE* (See **Supplementary S.3.4**).

The performance metric for both *ANN* and *RF* models is the Mean Absolute Error (*MAE*). Each model has been tested using several random seeds to confirm the reproducibility of the obtained results. Additionally, *Permutation Importance* was used to evaluate the relevance of each feature for the two predictive models. The *importances* were computed using the *test set alone* to identify which features provide the largest contribution to how well the predictive model can generalize.

Finally, certain parameters from the obtained videos (given in **Table 3.3**) were studied using Principal Component Analysis (*PCA).* The selection of parameters involved two screening stages. First, the impact speed and Weber number *We*— which are characteristics of the droplet *prior* to impact— were excluded, since the primary aim of this task is to differentiate the fabric samples based on how they influence the droplet behavior. Secondly, from the remaining 9 parameters, 4 other parameters were removed as they were found to have high Pearson correlation values (>0.80) with others. By the end, there were *five features* examined using *PCA*: (1) restitution coefficient R_C, (2) average number of droplets, (3) dimensionless maximum contact width ξ_{max}, (4) equilibrium contact width and (5) maximum receding rate. Similar to *ANN* and *RF*, the 5 input features were also standardized to eliminate the effect of actual magnitude of values. Finally, data visualization of 136 points (observations which show the droplet behavior on different fabric samples and *We*) was accomplished by plotting the first two principal components. The physical characteristics and wettability characteristics of the fabrics (roughness, contact angle θ and roll-off angle θ_{RO}) were used as colormap to distinguish the points from each other and identify possible clusters or trends. As a final note, *all ML*-related analyses were performed using observations *only from PhobRSH-coated fabric samples* as datasets.

3.7 *Experimental Limitations of the Study*

The general experimental setup has imposed some limitations on the study, which must be kept in mind when understanding the results and conclusions. These are the following:

Number and nature of fabric samples: All the fabrics are made of polyester. More importantly, however, these fabrics have physical properties already set by the supplying textile manufacturer. Thus, the investigation of how a specific output varies with a specific fabric physical property was inherently difficult— especially that there are only eight unique fabric samples in total. Nonetheless, hypotheses can still be developed in explaining the phenomena observed based on physical arguments. While these can be used for making suggestions to textile manufacturers, they must still be taken with reasonable skepticism. An exception to this is the study of the effect of their roughness, which can be performed because of the abundant literature available related on this subject— allowing a comparison of observed trends among different types of samples. Moreover,

the establishment of the baseline as the droplet-fabric interface was quite difficult, particularly in some samples with inherently rough surfaces, resulting in some uncertainty. This issue is particularly relevant for the determination of contact angle and establishment of (maximum) contact width. Finally, the number of tested fabric samples also put the obtained predictive accuracy of the developed *ML* models in a limited context.

Camera settings: Tradeoffs were made in selecting the appropriate pixel size (field of view) and frame rate, considering that both length and time measurements must be obtained from the videos taken. The maximum field of view of the camera has certainly limited the amount of information which can be captured— particularly in some cases when tiny droplets are ejected far from the main droplet during splashing or partial rebound, and a few cases when the height of droplet rebound is much larger than the ones typically observed.

Dropping height: The maximum attainable dropping height was limited to around 210 mm by the setup. A larger dropping height would have been useful (1) to see the (potential) splashing behavior in other fabrics, and (2) to check whether the water droplets can penetrate all the fabrics at very high impact speed. (The specific details of these concerns will be provided in **Sections 4.2** and **4.7**, respectively.)

Video analysis: Only the translational motion of the droplet has been considered, as reflected by the chosen video output parameters. In other words, the vibrational motion (i.e., oscillations when moving along a specific direction) and occasional rotational motion of droplet are both not part of the analysis in this work.

Results and Discussion

Before delving into the results of droplet impact studies, it will be established first that the coated fabrics are truly hydrophobic, i.e. with low static wettability. Then, the main results of this work will be delivered in this chapter— which will focus on determining the influence of fabric characteristics (mainly roughness) and droplet properties (mainly impact speed) on the droplet dynamic behavior. Splashing, spreading and rebound dynamics of the droplet impacting on textiles will be tackled in this exact order. Different explanations will be offered to discuss the underlying phenomena behind the observed trends and relationships. Afterwards, a more thorough investigation of water repellency of *PhobRSH-coated* fabrics will be conducted— in which hypotheses will be offered concerning the possible factors creating the wide range of behavior. Next, the developed machine learning models will be used to predict the spreading and rebound behavior, as well as to describe the general dynamics of impacting droplet. In addition, they will also solidify some key observations made in the previous sections of this chapter. This chapter will end with a more complete perspective on the water repellency of textiles and the observed dynamic behavior of droplet on these substrates.

Despite being obvious, it is still important to raise as caveat that the image sequences provided in this chapter are not exactly the same for the given set of fabric samples and impact conditions being considered. For example, as will be seen later, the rebound behavior of the droplet can take many forms, and the illustrated cases in this account are clearly non-exhaustive. Nevertheless, our best attempts were made to cover a wide range of scenarios as much as possible in order to provide a more complete picture of this work.

4.1 *Contact Angle and Roll-Off Angle of Coated Fabrics*

The obtained contact angle and roll-off angle values for different coated fabrics are presented in **Tables 4.1** and **4.2**. **Figure 4.1** provides a better visualization of these results.

Table 4.1. Contact angle for different coated fabrics

Fabric Sample	Roughness *r*	Coating		
		PhobRSH	C4F	PDMS
Flat	1.00	105.4˚ ± 0.7	107.3˚ ± 1.2	107.6˚ ± 0.4
Fabric1	1.19	129.4˚ ± 0.8	128.1˚ ± 0.6	131.6˚ ± 0.6
Fabric2	1.27	130.7˚ ± 0.6	126.1˚ ± 0.8	124.2˚ ± 0.6
Fabric3	1.46	136.1˚ ± 0.5	136.0˚ ± 0.3	135.4˚ ± 0.6
Fabric4	1.47	131.7˚ ± 0.6	135.2˚ ± 0.7	133.5˚ ± 0.7
Fabric5	1.77	138.8˚ ± 0.6	137.9˚ ± 0.5	138.1˚ ± 0.7
Fabric6	1.77	139.7˚ ± 0.6	138.0˚ ± 0.6	142.8˚ ± 1.1
Fabric7A	1.71	137.2˚ ± 1.8	137.7˚ ± 0.6	138.8˚ ± 0.2
Fabric7B	1.67	138.6˚ ± 0.2	137.6˚ ± 0.5	138.9˚ ± 0.6

Table 4.2. Roll-off angle for different coated fabrics

Fabric Sample	Roughness *r*	Coating		
		PhobRSH	C4F	PDMS
Flat	1.00	> 90˚	> 90˚	> 90˚
Fabric1	1.19	> 90˚	> 90˚	> 90˚
Fabric2	1.27	> 90˚	> 90˚	> 90˚

Fabric3	1.46	32.9˚ ± 1.6	> 90˚	> 90˚
Fabric4	1.47	55.8˚ ± 4.1	> 90˚	> 90˚
Fabric5	1.77	42.8˚ ± 2.2	> 90˚	> 90˚
Fabric6	1.77	27.0˚ ± 0.9	> 90˚	35.0˚ ± 2.7
Fabric7A	1.71	26.4˚ ± 1.8	> 90˚	42.8˚ ± 1.9
Fabric7B	1.67	37.1˚ ± 1.4	> 90˚	51.7˚ ± 2.2

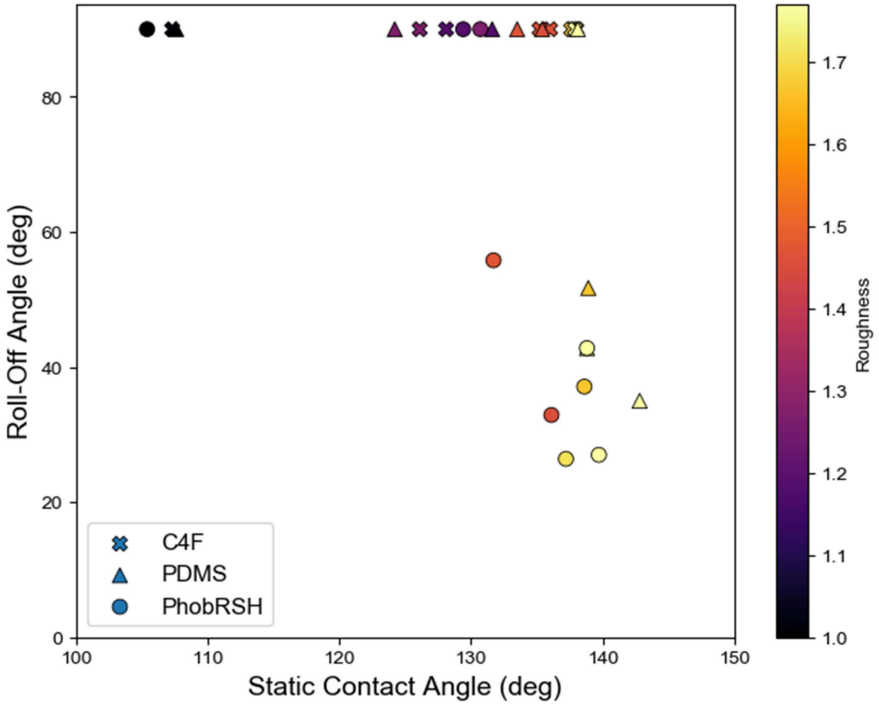

Figure 4.1. Contact angle θ and roll-off angle θ_{RO} values as function of fabric roughness *r* and coating type. The displayed contact angle is average of at least six values, while the displayed roll-off angle is average of at least four values, for each coated fabric. Error bars have been purposely removed for clarity, but an equivalent figure containing them is also presented (see **Supplementary S.4.1**). The influence of fabric roughness on contact angle can be easily checked by seeing how the colormap matches almost completely the contact angle range by going from left to right. In essence, having *both* higher contact angles and lower roll-off angles could only be observed for *some* fabrics with high roughness (*r >1.4)*, with *PhobRSH* giving better roll-off properties than the other two coatings.

Similar to its original work [12], **Figure 4.1** also shows the same two key observations in the coated fabrics used for this study: (1) higher contact angles θ were observed in fabric samples possessing high roughness (*r>1.4*), with minimal effect of the nature of coating; and (2) roll-off angles θ_{RO} less than 90˚ were observed only in samples with high roughness, and mostly in samples with *PhobRSH* coating. It has been argued in the original work that the influence of roughness on θ can be understood as that: the fabrics with low roughness (*r < 1.4*) tend to be in *partially-impregnated state,* whereas the ones with high roughness tend to be in *superficially wet state.* The former case is analogous to Wenzel state— where the water droplet partially fills the upper part of fabric surface containing the roughness elements. Similarly, the latter case is analogous to Cassie-Baxter state— where the water droplet simply sits on top of these roughness elements containing trapped air pockets. It is through this difference in wetting states that such improvement (increase) of θ for rougher fabrics can be rationalized. [12]

The influence of roughness on θ_{RO}, on the other hand, is not as straightforward. It is evident in **Figure 4.1** that there is no trend between fabric roughness or θ and θ_{RO}. While it is true that lower θ_{RO} values were mostly attained by having high roughness and *PhobRSH* coating, fabric samples

of similar roughness and/or θ have shown varying results. For example, *Fabric5* and *Fabric6* exhibited a vast difference in their θ_{RO}, despite having equal roughness. Also, *Fabric5* showed lower θ_{RO} than either *Fabric7A* or *Fabric7B*, despite the latter two having slightly lower roughness and all three having very close θ. Such difference could be attributed perhaps to the presence of surface roughness heterogeneities. [14] As θ_{RO} is related largely with the contact angle hysteresis $\Delta\theta$, a droplet may find it easier to roll off in a fabric with higher uniformity (i.e., lower variability) in roughness, compared to a fabric with the same roughness but higher variability. The same argument on the observed improvement (decrease) of θ_{RO} when using *PhobRSH* coating is proposed— i.e. that *PhobRSH* creates less $\Delta\theta$ too, similar to the original work. [12] It has been suggested in the original work that fabric defects, such as loops and protrusions, could "pin" the droplet and thereby increase θ_{RO} as well. Overall, θ_{RO} appears to be affected by the precise surface topography and quality of the fabric samples, in contrast with θ.

4.2 *Splashing Behavior of Droplet on Coated Fabrics*

In this work, splashing refers to events which lead to the detachment of smaller droplets from the main droplet only during impact (instantaneous), spreading (outward motion) or retraction (inward motion); it does not include the case where a tiny droplet is ejected from or left by the main droplet during rebound. An example of droplet splashing is shown in the bottom image sequence of **Figure 4.2**, where small secondary droplets are produced as the main droplet spreads and recedes on a rougher fabric for a given large dropping height.

(1)

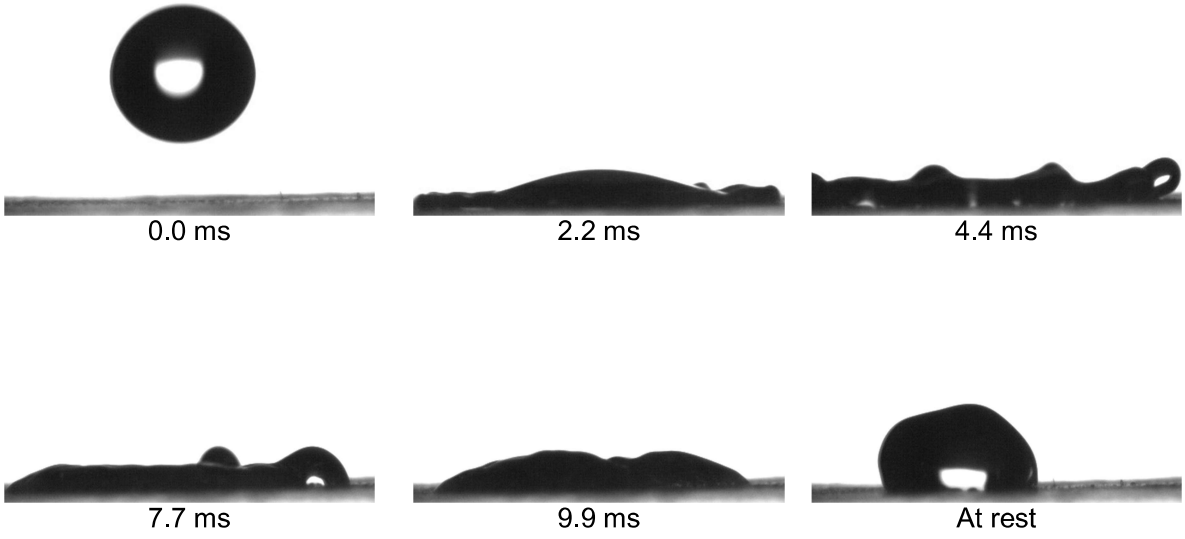

(2)

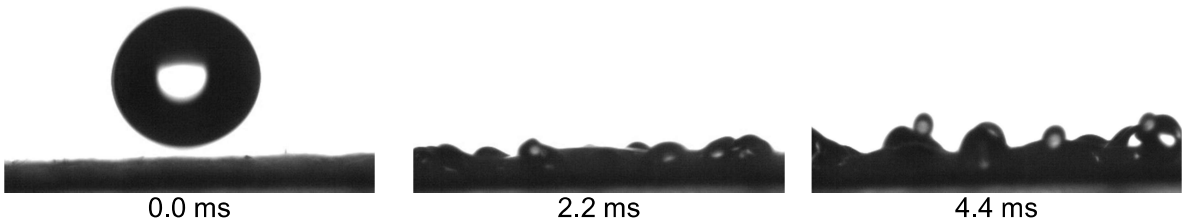

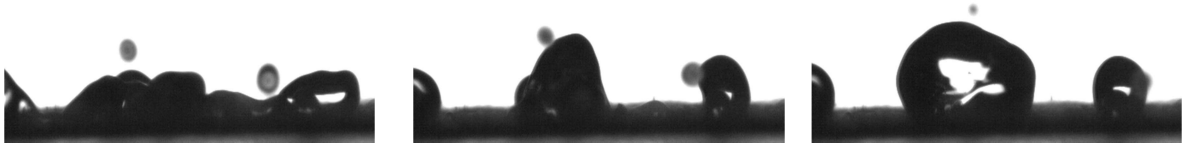

Figure 4.2. Comparison between a droplet exhibiting (1) non-splashing (*Fabric1*, *r = 1.19*) and (2) splashing behavior (*Fabric5*, *r = 1.77*) on *PhobRSH*-coated fabric samples at *We = 90.8 (D = 2.7 mm, V = 1.6 m/s).* Whereas the droplet remains intact the whole time after impact on the fabric with low roughness (*r < 1.4*), it breaks into smaller volumes during spreading and retraction on the fabric with high roughness.

Figure 4.3 gives a global account of splashing observed in some fabric samples for specific impact conditions. As established in **Theoretical Framework**, a droplet will only splash if it has sufficiently high kinetic energy in the first place; it is thus trivial that splashing is only observed in samples with high Weber number *We*. A more interesting observation in **Figure 4.3** is that the samples which exhibited splashing all come from fabrics with high roughness *(Fabric3* to *Fabric7, r > 1.4*). This result is consistent with the findings of Santiago et al., Tang et al. and other research groups working on solid surfaces. [1] [3] [19] In general, fabric surfaces with high roughness create larger perturbations in the dynamics of the droplet, resulting in its disintegration. It was proposed that for prompt splashing (mainly during impact and early-phase spreading), the edges of the droplet are destabilized by surface asperities which hamper its motion. This destabilization is promoted by higher fluid momentum and taller asperities, and eventually results in fragmentation of smaller droplets. [27] For the case of receding break-up, the origin of droplet fragmentation is the destabilization of formed *fingers* (i.e. long cylindrical edges)— which can be seen starting from the maximum spreading state of the droplet in **Figure 4.2** (i.e. ~4.4 ms and beyond).

The presence of fabric defects (loops and protrusions) could have amplified this splashing behavior of droplet too. This hypothesis is derived from the work of Josserand et al., which found that protrusions in solid surfaces can trigger splashing of impacting droplets. [20] In this work, it is *posited* that fabric defects cause droplet break-up by acting either as (1) obstacles which destabilize droplet's edges or (2) pinning points which compete with the pull from droplet's retraction. In both cases, the overall motion of the droplet is perturbed, such that a huge gradient of velocities within the droplet (parallel to the surface) is created. This huge difference in velocities between the upper and lower extremities of the droplet (with contact width still close to the maximum value) finally elicits the separation of fingers from the main droplet to form the secondary droplets. Unfortunately, it is difficult to identify which of the two— surface roughness or defect count— is more relevant in dictating the splashing behavior observed in this work. This complication mainly arises from the limitation in the nature of samples obtained, i.e. that the fabrics with high roughness are mostly the ones with intermediate to high defect count too.

As a caution, it is worth-mentioning that there are occasional absences of splashing on rougher samples despite the droplets having sufficiently high *We*. This can be traced back in **Figure 4.3**, focusing on how the proportion of splashing events in rougher fabrics is sometimes less than 1 at high *We*. This absence could simply be the result of the intrinsic variability of fabrics, whether in roughness or presence of defects. Therefore, the interaction of droplet with rougher fabrics does not always result in its splashing even when having a high *We*— simply showing how splashing depends on the exact *local* characteristics of the fabric area which the droplet covers. As additional caution, it is possible that droplet splashing might also occur on fabrics with low roughness (*r<1.4*),

albeit for much higher *We* outside the range considered. An inference can still be drawn nonetheless after taking these two complications into account: that splashing is less likely to occur on fabric surface which has *both* low roughness and low defect count.

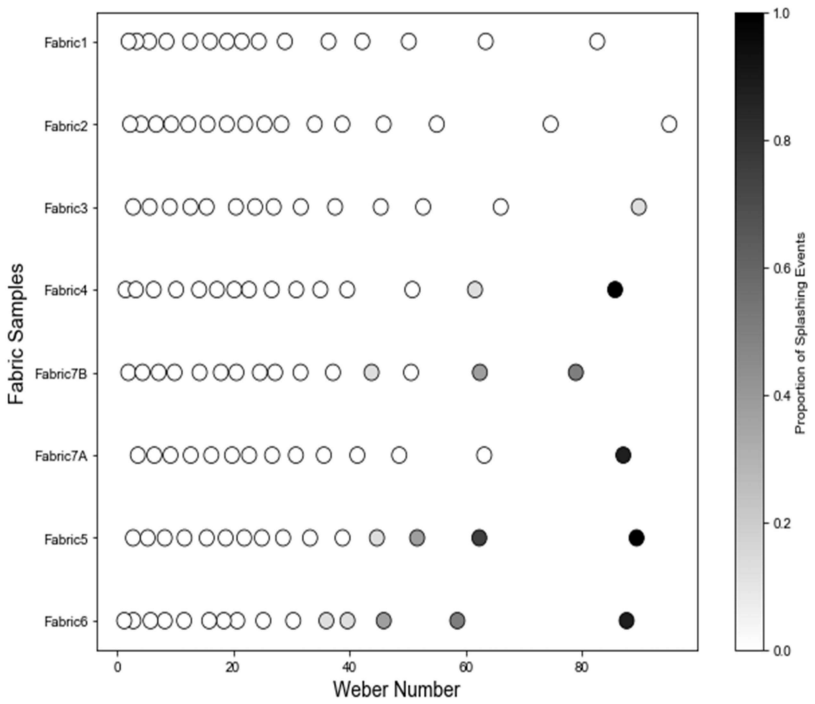

Figure 4.3. Splashing behavior of droplet on different fabrics over a range of Weber number *We*. Each point represents an average of eight observations. Fabrics are arranged in order of increasing roughness from top to bottom part of the y-axis. The colormap denotes the proportion of splashing events for each point, i.e. the number of observations which exhibited splashing divided by the total number of observations (eight). For clarification, the point with highest *We* for *Fabric 3* is light gray. All three coatings are used to create this plot. The classification for splashing was established based on non-integral time-average number of droplets. The choice of such parameter gives a better resolution by excluding the cases where a small droplet was ejected/left but rejoined the main droplet shortly after rebound (potential false positive). Unfortunately, this also excludes samples exhibiting mild splashing (false negative). Splashing is more likely to occur in fabrics with high roughness (*Fabric3* to *Fabric 7)* compared to the ones with low roughness (*Fabric1* and *Fabric2*) at sufficiently high *We.*

4.3 *Spreading Behavior of Droplet on Coated Fabrics*

The spreading behavior will be characterized by the maximum *contact* width of the droplet, $D_{max,}$ in this work, as established in **Theoretical Framework**. **Figure 4.4** shows the maximum spreading state of the droplet on two fabric samples with different roughness *r*, over a range of Weber number *We.* The observed similarity of D_{max} for the two fabric samples for every given *We* is consistent with the scaling relationship proposed in previous studies [2] [8] [9] [21] — revealing that the maximum spreading characteristic mainly depends on droplet properties, i.e. its kinetic energy through *We* in this case.

Figure 4.5 gives a global account of the *increase* of dimensionless maximum contact width ξ_{max} (thus contact area) of the droplet with *We.* The obtained plot is not completely linear, which could be explained by the two regimes of maximum spreading behavior presented in **Theoretical Framework**. A *capillary regime* exists at low *We*, where the kinetic energy of the droplet is

balanced by its surface energy. On the other hand, a *viscous regime* exists at higher *We*, where its kinetic energy is mainly dissipated by viscous forces.

(1)

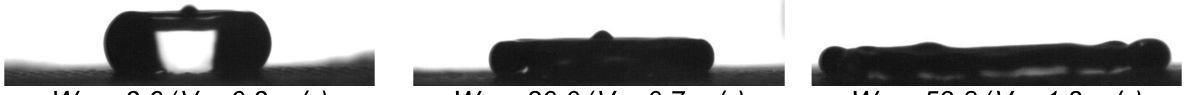

We = 3.6 (V = 0.3 m/s) *We = 20.0 (V = 0.7 m/s)* *We = 59.8 (V = 1.3 m/s)*

(2)

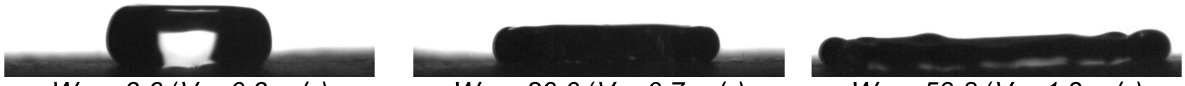

We = 3.6 (V = 0.3 m/s) *We = 20.0 (V = 0.7 m/s)* *We = 59.8 (V = 1.3 m/s)*

Figure 4.4. Comparison of maximum *contact* width D_{max} of the droplet between (1) *Fabric2* (*r = 1.27*) and (2) *Fabric7A* (*r = 1.71*) of *PhobRSH* coating at different Weber number *We* (*D = 2.7 mm*). Visual inspection suggests that D_{max} of droplet in the two fabrics of highly different roughness is indeed very similar with each other for a given *We*. The variation of D_{max} with *We* (horizontal comparison) is much stronger than the variation of D_{max} with fabric roughness (vertical comparison).

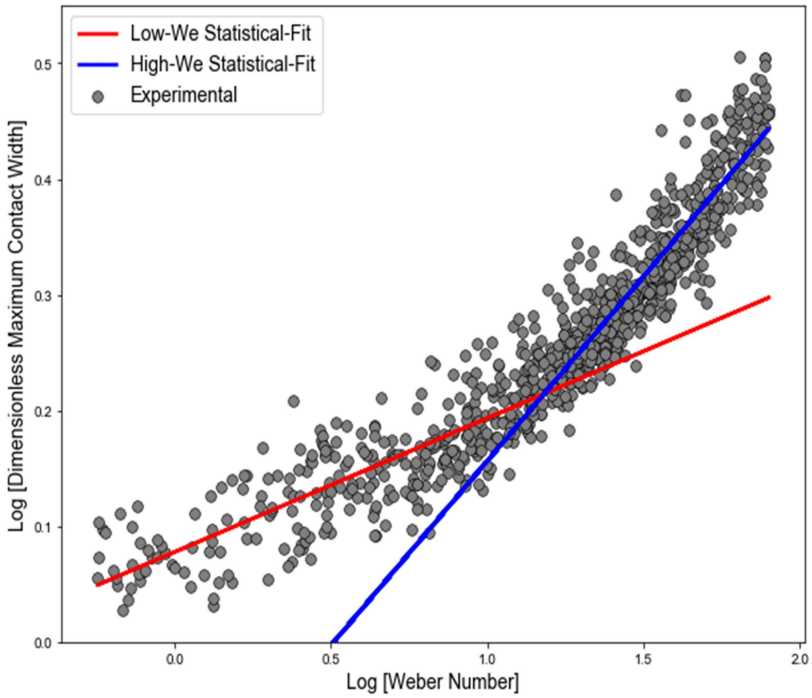

Figure 4.5. Global variation of (logarithm of) dimensionless maximum contact width ξ_{max} with (logarithm of) Weber number *We*. Each point represents one observation. All three coatings are used to create this plot. Plotting ξ_{max} against *We* resolves the two different droplet diameters used in this work into a single master curve containing all the points. Our results followed the proposed scaling law $\xi_{max} \propto We^{B}$ at low *We* values (more strictly, *We* > *1* based on the condition of Clanet et al. in their scaling law [8]). Due to having two regimes (*capillary* and *viscous*) for droplet behavior, a non-linear evolution of ξ_{max} with *We* exists. In

consequence, the break in linear trend had to be determined (using *Piecewise Linear Fit* function of *Python*). The linear part at *low We* (red line) was found to observe the relationship: $\xi_{max} = 1.20We^{0.12}$, with $R^2 = 0.68$. In contrast, the linear part at *high We* (blue line) followed: $\xi_{max} = 0.69We^{0.32}$, with $R^2 = 0.82$.

Figure 4.6 shows how ξ_{max} varies across fabric samples of different roughness over a given *We* range— illustrating that fabric roughness has minimal influence on the maximum spreading of droplet. This result is in slight agreement with the work of Santiago et al., which stated that such observation is typically found when the impacting droplet is in Cassie-Baxter state and the roughness structures are ignored by the "floating" droplet during spreading. [1] However, as will be seen shortly, droplet pinning was observed for some fabric samples when its impact speed (thus *We*) is sufficiently high. As presented in **Theoretical Framework**, this pinning behavior signifies the transition from Cassie-Baxter to Wenzel state of the impacting droplet. Interestingly, **Figure 4.6** has not been influenced by such events by and large; in other words, the pinning of a droplet near the impact point does not affect its maximum spreading, despite pinning being able to influence its rebound behavior. The same observation was made by Antonini et al. when they investigated the spreading behavior of water droplet on two different superhydrophobic surfaces. [9] These results tie beautifully with the fact that the fabrics with low roughness ($r<1.4$), despite *always* being in partially-impregnated (Wenzel) state, also give values of ξ_{max} similar to those of fabrics with high roughness. Putting all things together, it is thus *proposed* that in this specific work, the maximum spreading state of the droplet is indifferent to whether its impact has resulted in Cassie-Baxter state or Wenzel state— thus extending the findings of Santiago et al. to include Wenzel state as well.

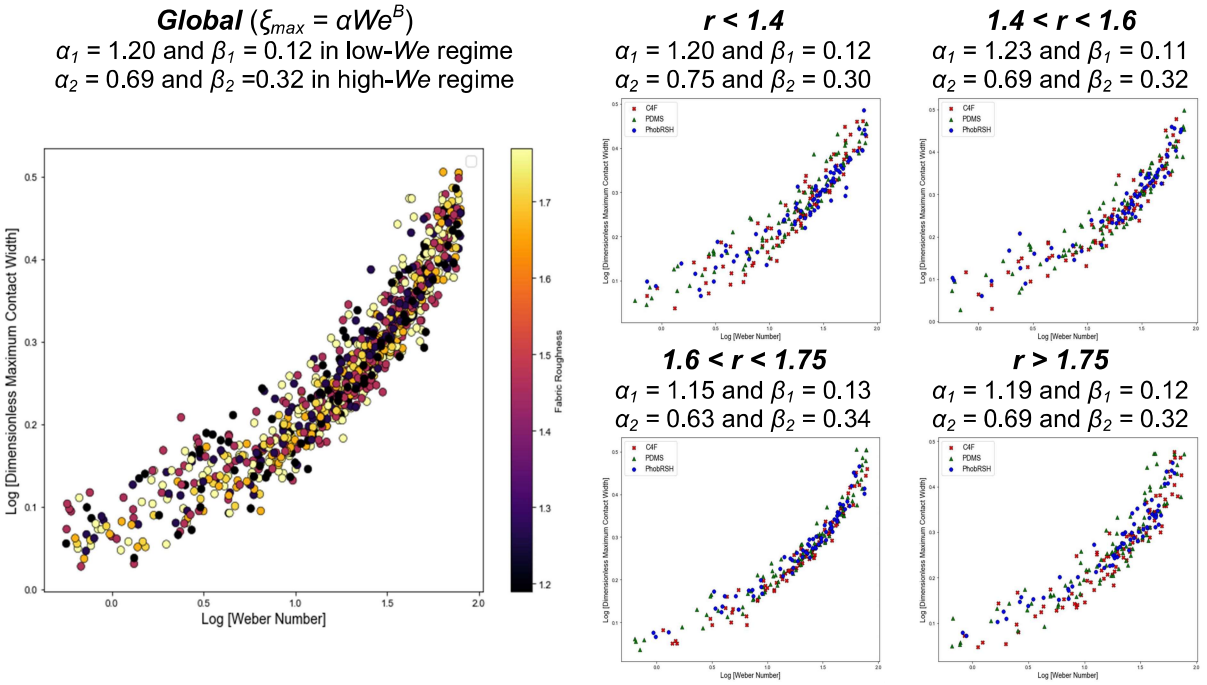

Figure 4.6. Variation of (logarithm of) dimensionless maximum contact width ξ_{max} with (logarithm of) Weber number *We*, *highlighting different fabrics* (left). This figure was created using the same dataset for Figure 4.5, but focusing on fabric roughness. The ξ_{max} of the droplet is only affected minimally by the roughness of the fabric on which it spreads over— given the strong overlapping of several colors. Finally, different pairs of fabrics (grouped according to roughness *r*) are used to create the different plots on the right, with coating as color code. These plots only serve as reference for the reader *for the moment.* The fit parameters α_1 and β_1 for low *We,* and α_2 and β_2 for high *We,* were also provided for comparison.

Figure 4.7, on the other hand, reveals the effect of the chemical nature of coating on ξ_{max}. It can be inferred that the coating composition also has minimal influence on the maximum spreading state of the droplet. This result is again consistent with the findings of previous work on solid surfaces. [8] [9] [21] As a caution however, this only applies to *hydrophobic* coatings which give the rough fabrics contact angle values mostly between 125° and 140°. As a consequence, the result of this work cannot be used to generalize and include the spreading behavior on *hydrophilic* and perhaps even *superhydrophobic* fabric surfaces.

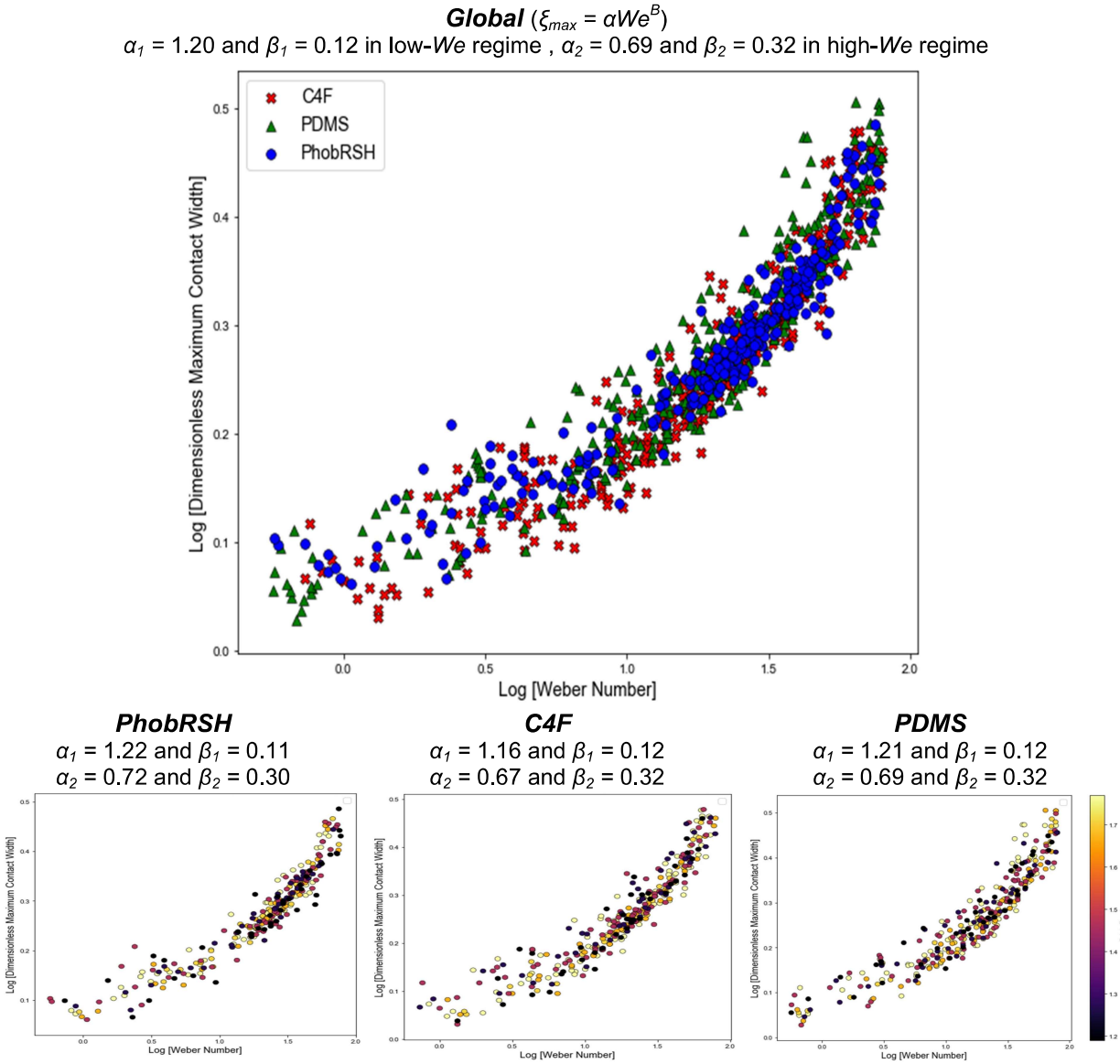

Figure 4.7. Variation of (logarithm of) dimensionless maximum contact width ξ_{max} with (logarithm of) Weber number *We*, *highlighting different coatings*. This figure was created using the same dataset for Figure 4.5, but focusing on the three types of coatings. The ξ_{max} of the droplet is also affected minimally by the nature of *hydrophobic* coating on which it spreads over— given the strong overlapping of several colors. The fit parameters α_1, β_1, α_2, and β_2 were again provided for qualitative comparison.

However, despite the observed trend in the evolution of ξ_{max} with *We*, the data points in **Figures 4.6** and **4.7** have noticeable breadth (range and variance). Comparing this to the obtained results of similar studies on solid surfaces, it is *suggested* that this is due to the complications presented by having textiles as subject. One factor has already been mentioned in **Experimental** section: the

contact line of fabric/droplet interface is difficult to establish, particularly in some rough samples. This has introduced a degree of uncertainty on obtained maximum contact width D_{max}, and thus ξ_{max}— resulting in the significant spread of data for a given *We*.

Moreover, another interesting parameter to investigate is the time required to reach maximum spreading, t_{ms}. As illustrated in **Figure 4.8**, the droplet reaches its maximum contact width D_{max} in all the fabric samples at the same time for the given *We*— with t_{ms} being in the order of milliseconds similar to previous experiments. [14] This result solidifies further that the maximum spreading characteristics of the droplet is indeed independent of the fabric roughness.

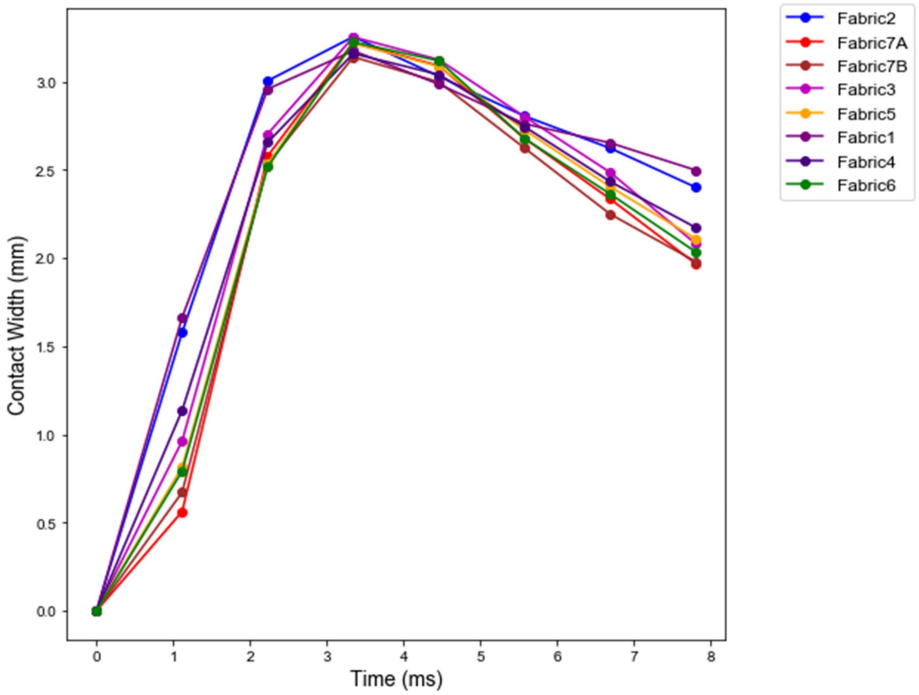

Figure 4.8. Evolution of droplet contact width with time for different *PhobRSH*-coated fabric samples for *We* ≈ 14.0 *(D = 1.99 mm)*. Each point represents an average of around 6 observations. All the curves follow the same trend: beginning from its impact *(t = 0)*, the contact width increases until it reaches a maximum value during spreading, and then it decreases as the droplet recedes. In all the fabric samples, the maximum contact width is reached at around 3.3 ms—showing that fabric roughness does not play a huge role in the maximum spreading time of droplet as well, at least in the order of a millisecond.

One may certainly argue that, because of the limited frame rate of camera used in this work (i.e. timescale of one frame is ~1.1 ms), our setup is not simply capable of identifying the possibly significant differences in maximum spreading characteristics (both ξ_{max} and t_{ms}) among fabrics of different roughness. There are at least two counter-arguments to such concern: one from a state-of-the-art standpoint concerning results of similar studies, and another from a physical standpoint concerning energy and time. First, previous work on rough solid surfaces also found the same conclusion that roughness does not affect droplet spreading behavior. [1] [21] Secondly, given that the kinetic energy of droplet is at its lowest at maximum spreading, there is a larger window of time to capture such state. Thus, it is expected that the obtained contact width will tend to cluster very close to, if not at, its maximum value when a specific timeframe is sampled. This is what was observed when different frame rates were surveyed to justify the validity of the chosen frame rate (See **Supplementary S.4.2**). Besides, it still depends on the actual application whether the observed range of variation of ξ_{max} and t_{ms} may be acceptable or not.

Altogether, the maximum spreading behavior of droplet is unaffected by fabric roughness and indifferent to its wetting state (whether partially-impregnated or superficially-wet). It can thus be inferred that the rebound behavior of droplet cannot be deduced from its spreading behavior on these fabrics. Taking it a step further, this means that the droplet spreading behavior does not provide any information on the overall wettability of each fabric sample and thus, observing the spreading dynamics alone cannot contribute to distinguishing the fabrics according to water repellency *in this particular work.*

4.4 *Rebound Behavior of Droplet on Coated Fabrics*

There are three general scenarios which can occur after impact and retraction of droplet, as outlined previously. [21] The droplet can either (1) directly oscillate without bouncing, keeping in contact with the surface the whole time, or (2) rebound off the surface. Other than having (2.1) a complete rebound, the droplet may also exhibit (2.2) partial rebound or (2.3) jetting depending on the exact conditions. These were all illustrated in **Figures 4.9** and **4.10**, where majority of the observed rebound activity occurred in fabrics with high roughness (r > 1.4). These scenarios were witnessed multiple times in the study, except for jetting which occurred only in rare occasions. For the specific case of partial rebound, it has been seen only after a specific Weber number *We* is reached. This observation is consistent with the discussed transition from Cassie-Baxter state to "sticky" Wenzel state in **Theoretical Framework**: the droplet with low *We* (thus kinetic energy) can completely rebound after impact, while the one with sufficiently high *We* may stick into the surface. [2] [4] [7] [28] This transition marks the onset of partial wetting of fabric surfaces, where a fraction of the previously "floating" droplet becomes trapped in the roughness elements (cavities).

While the two previous figures show some possible events at *low to moderate We,* **Figure 4.11** gives an example of the changes in droplet rebound behavior at *(very) high We.* In this regime, majority of the observed droplets have lost their rebound capacity— signifying the existence of droplet pinning. This scenario marks the complete wetting of fabric surfaces, with the fraction of droplet filling in and getting impaled in the cavities.

(1)

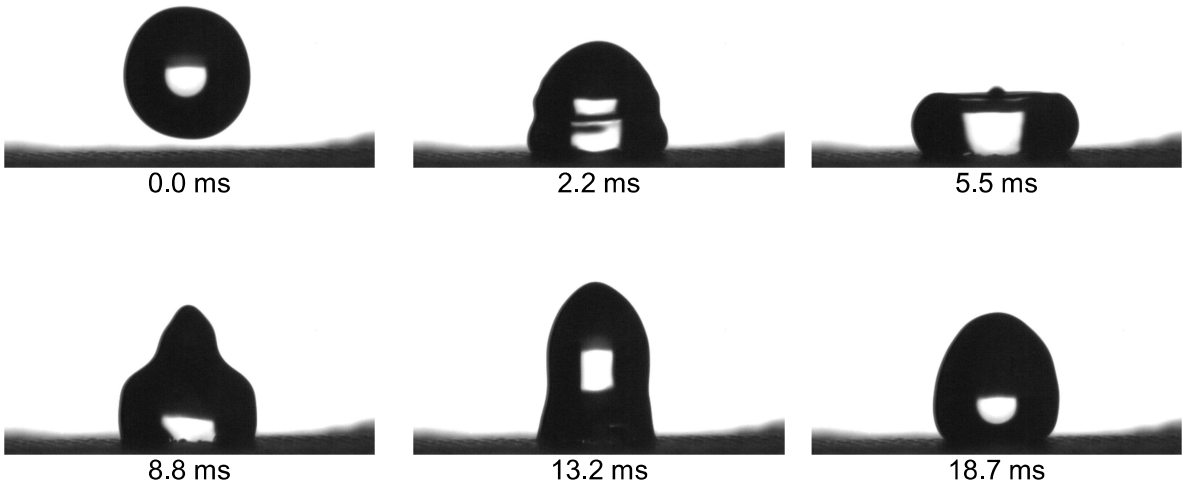

(2.1)

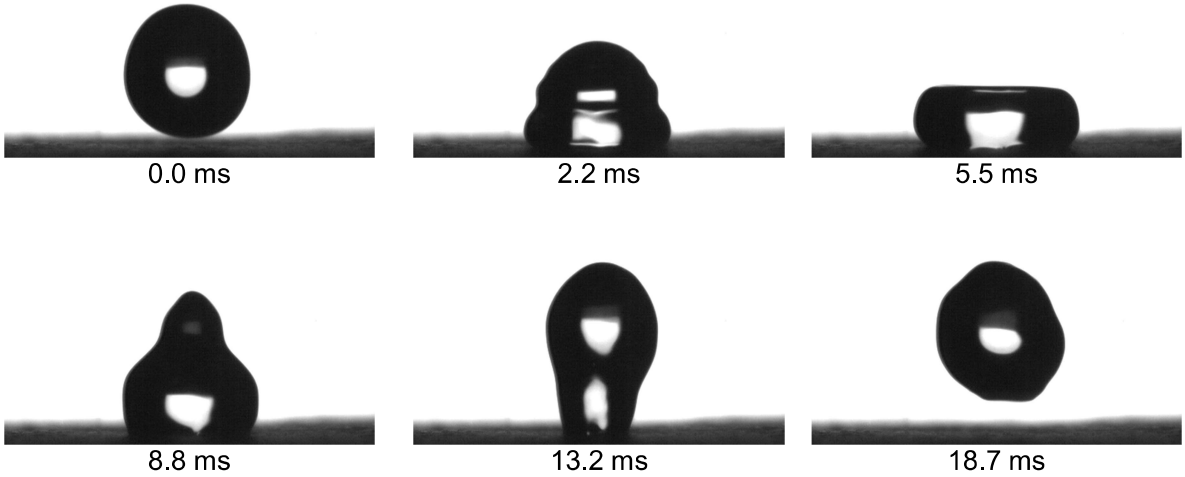

Figure 4.9. Comparison between a droplet (1) not rebounding (*Fabric2*, *r = 1.27*) and (2) rebounding off completely the surface (*Fabric7A*, *r = 1.71*) of *PhobRSH*-coated fabrics at *low We* (*We = 3.6, D = 2.7 mm, V = 0.3 m/s*). The two image sequences are very similar until 8.8 ms. At ~13.2 ms, the center of mass of droplet along the vertical direction in the second case (rougher fabric) is already higher than the one in the first case. Eventually, one droplet successfully rebounds while the other does not at ~18.7 ms.

(2.2)

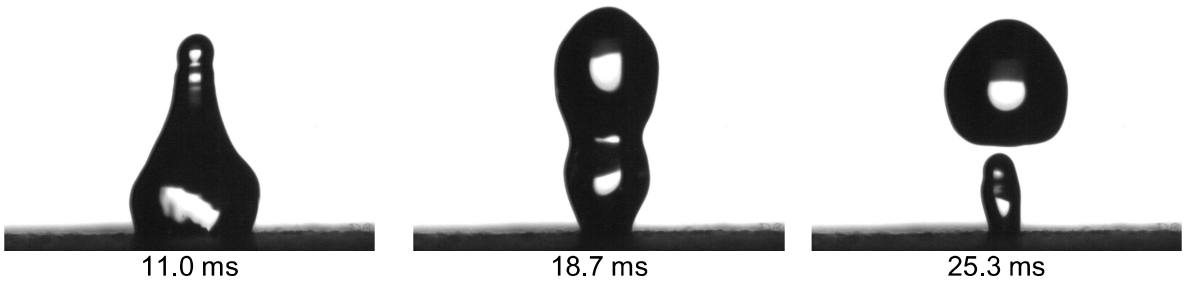

(2.3)

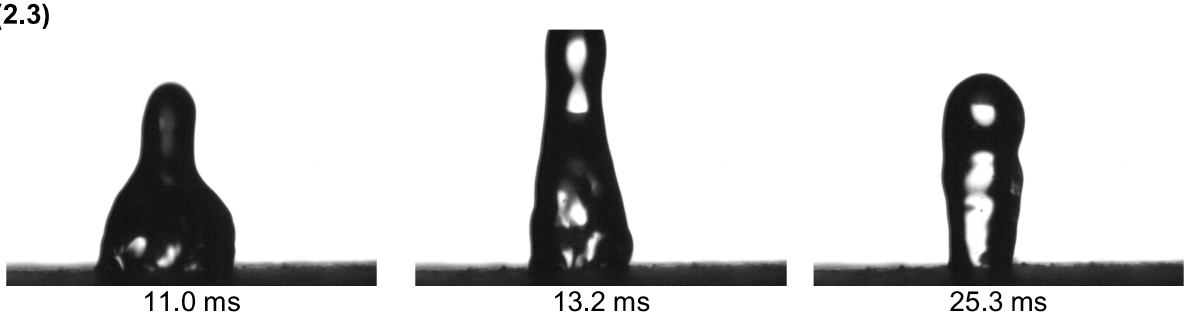

Figure 4.10. Comparison between a droplet exhibiting (1) partial rebound (*We = 17.1, V = 0.7 m/s*) and (2) jetting (*We = 59.8, V = 1.3 m/s*) off the surface of *PhobRSH*-coated *Fabric7A* (*r = 1.71)* at *low We* (*D = 2.7 mm*). The first three image sequences before 11.0 ms were omitted already since they are similar to the first three images of the bottom sequence (2.1) of Figure 4.9. Partial rebound occurs when a smaller droplet is left on the fabric as the main droplet lifts off. On the other hand, jetting occurs when a deformed droplet keeps its contact with the surface during the whole process of rebound. As a consequence of defining rebound properties based on center of mass, both cases are considered to be part of general rebound behavior in this work.

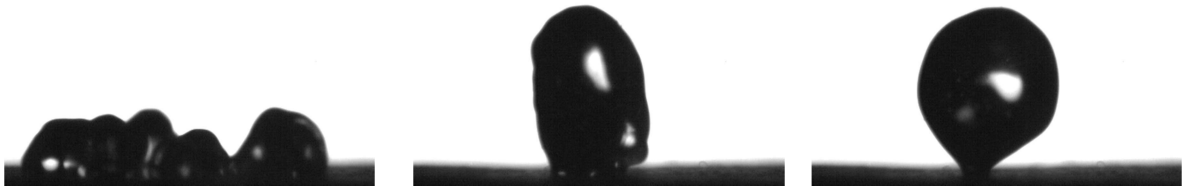

Figure 4.11. Complete pinning of droplet on *PhobRSH*-coated *Fabric 7A* (*r = 1.71)* at *high We* (*We = 98.2, D = 2.7 mm, V = 1.6 m/s*). Only the informative images which describe the phenomenon of pinning were included. Pinning occurs when the droplet becomes stuck on fabric as it (sometimes) *attempts* to rebound, all while keeping its contact with the fabric.

Figure 4.12 gives a global account of how the droplet rebound behavior varies across fabric samples of different roughness over a given *We* range. By and large, better rebound properties can be achieved using fabrics with high roughness (*r>1.4*), as characterized by their high restitution coefficient R_C (R_C > *0.2*). This observation can be explained *in general* as follows. First, as discussed in the previous section, the maximum contact width of the droplet is almost the same for every fabric sample at a given *We.* Secondly, by Cassie-Baxter definition, rougher surfaces create smaller ratio of actual solid-liquid contact area to (total) projected contact area. Combining these two pieces of information, the droplet is thus in contact with larger fraction of air pockets at its maximum spreading on high-roughness fabrics. As generally, the liquid droplet has larger interfacial energy when in contact with air than with hydrophobic substrate, it stores even higher surface energy from its *initial* kinetic energy when there are more air pockets. During retraction, the droplet can then recover higher kinetic energy from this stored surface energy— ultimately allowing it to reach a larger height during its rebound for surfaces with high roughness. Extending this analysis to this *specific* work, as the rougher fabrics tend to be in superficially wet state, there are air pockets available to increase further the surface energy of the droplet at maximum spreading. In contrast, being in partially-impregnated state, the low-roughness fabrics do not have these air pockets. The difference in observed rebound behavior between these two sets of fabrics hence mainly lies on the (un)availability of air pockets. While this explains how better rebound behavior is achieved in fabrics with high roughness relative to the ones with low roughness *in general*, one must keep in mind that there are still other factors which can differentiate one coated fabric sample from another: this includes the coating type (to be discussed shortly) or the precise surface topography (to be discussed in the next section), for example. Finally, looking at **Figure 4.12** again, the observed difference in rebound behavior between fabrics of high and low roughness diminishes with increasing *We* unfortunately. This is simply a consequence of the general trend of R_C to decrease— which will again be explained shortly. Therefore, the higher rebound properties achievable on most high-roughness fabric samples are mainly observed *at low We* only.

Figure 4.13, on the other hand, illustrates the influence of chemical nature of coating on R_C of the droplet**.** In general, better rebound properties can be achieved using *PhobRSH* instead of either *C4F* or *PDMS* coatings. As seen previously, *PhobRSH* is also the coating which tends to give lower roll-off angles θ_{RO}. It is thus reasonable to hypothesize that the *proposed* lower contact angle hysteresis $\Delta\theta$ for this coating also plays a role on the observed better rebound behavior on *PhobRSH*-coated fabrics. Extending this observation further, the coated fabrics with better rebound properties are in fact mostly the ones with better roll-off properties as well. These specific samples come from the fabrics with *high roughness* (*r>1.4*) and *PhobRSH coating*. This observation already hints that the surface characteristics influencing θ_{RO} of the droplet also play a role on determining its rebound behavior in droplet impact tests. This will be probed more in detail in the coming

sections. **Figure 4.14** provides a clear visual summary of the influence of fabric roughness and coating type on the droplet rebound behavior.

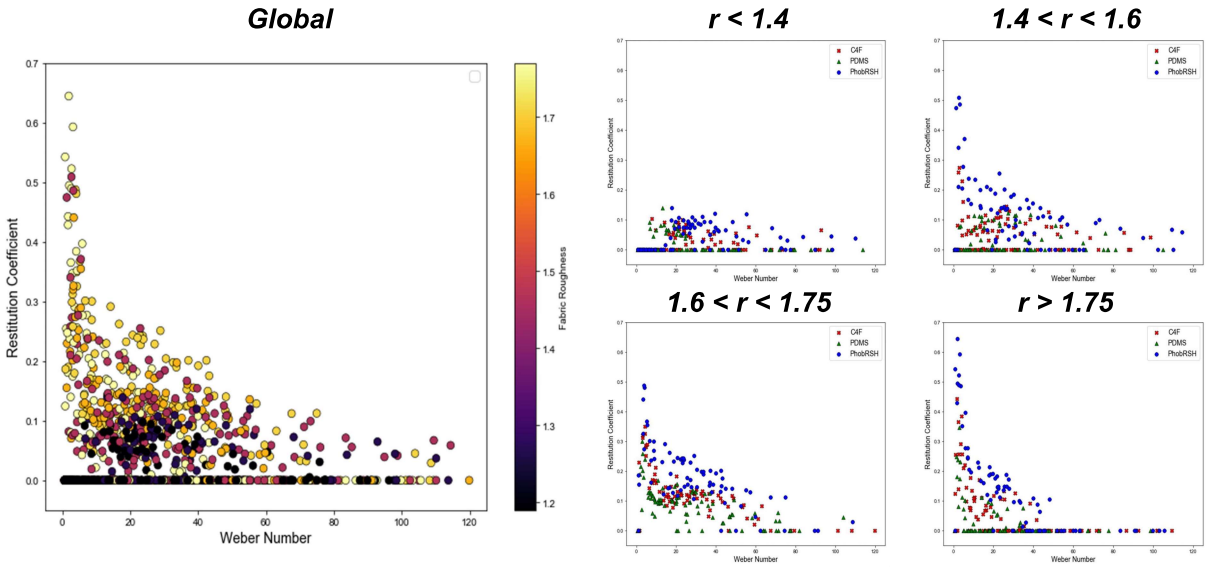

Figure 4.12. Variation of restitution coefficient R_C with Weber number *We, highlighting different fabrics (left).* Each point represents one observation. All three coatings are used to create this plot. Higher rebound behavior (R_C > *0.2*) was observed more frequently in fabrics with high roughness (*r > 1.4)* at *low We*. The presence of low-roughness fabrics (black points) giving higher R_C than the high-roughness fabrics (purple/orange/yellow points) at *low We* is due to the intrinsic variability and precise surface topography of the fabrics, as well as the interference of coating type. These factors will be explained more in detail shortly. Finally, different pairs of fabrics (grouped according to roughness *r*) are used to create the different plots on the right, with coating as color code. These plots only serve as reference for the reader *for the moment.*

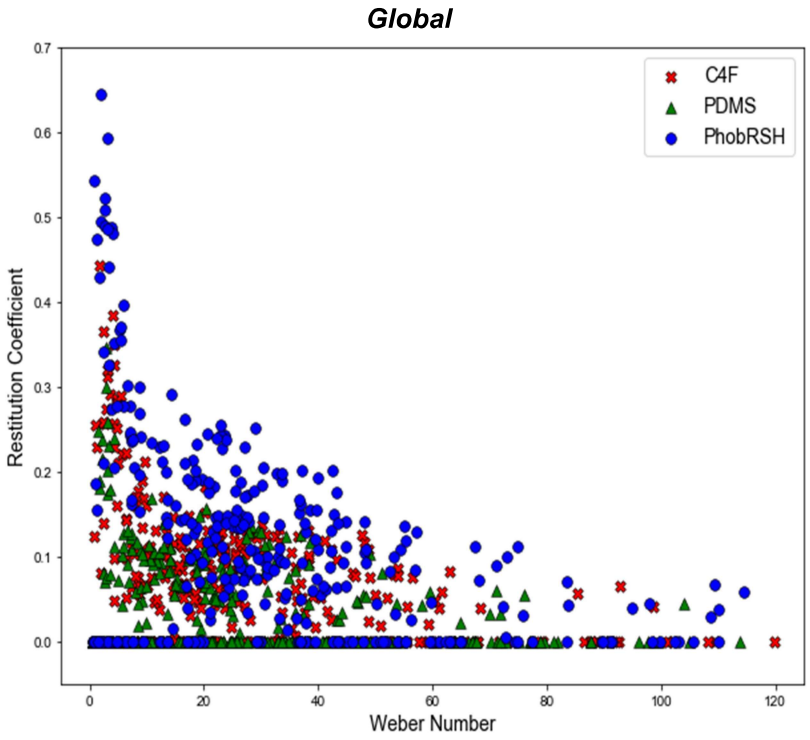

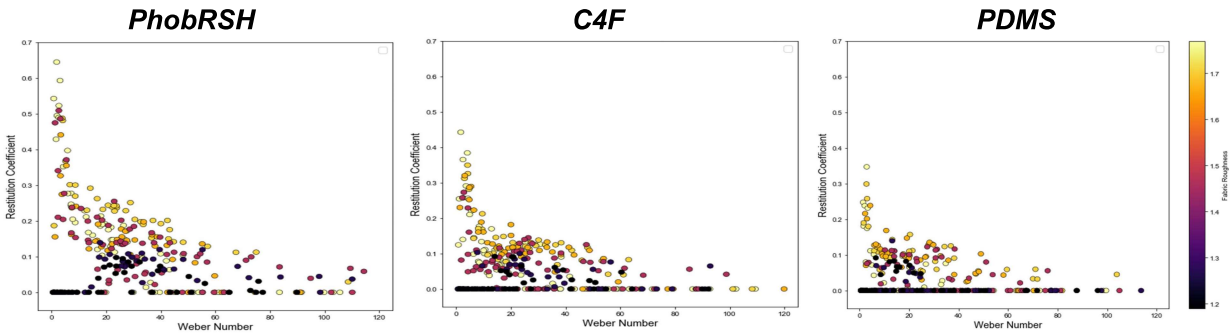

Figure 4.13. Variation of restitution coefficient R_C with Weber number *We, highlighting different coatings*. This figure was created using the same dataset for Figure 4.12, but focusing on the three types of coatings. Higher rebound behavior was observed more frequently in *PhobRSH*-coated fabrics than either *C4F*-coated or *PDMS*-coated fabrics.

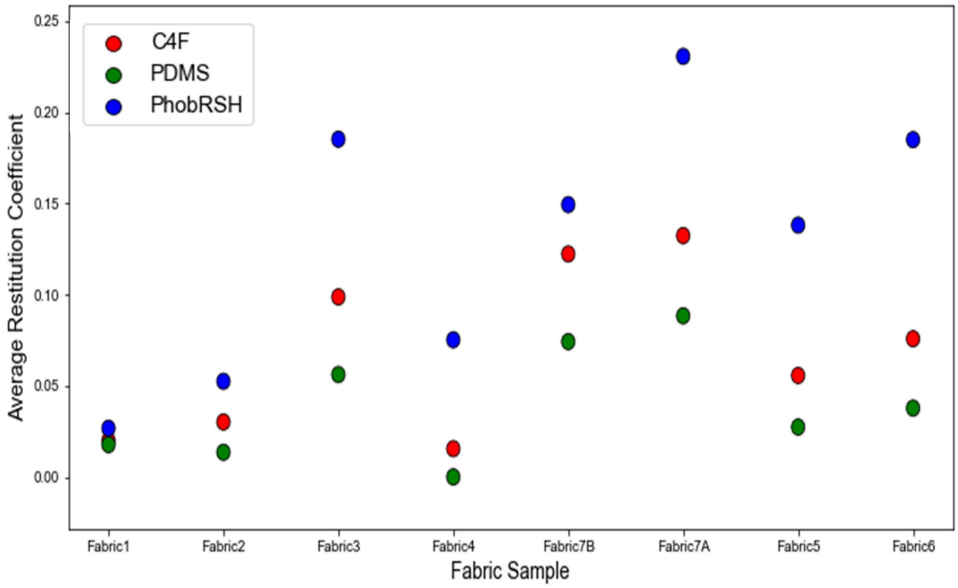

Figure 4.14. Average restitution coefficient R_C for different coated fabrics for a specific Weber number *We* range. This figure was created using the points in Figure 4.12 with *We* < 80. Each point represents an average of around 30 to 40 observations, with an average *We* between 24 and 30. Fabrics are arranged in order of increasing roughness from left to right of the x-axis, starting from the least rough sample (*Fabric 1*). In general, higher average R_C can be achieved using fabrics with high roughness (*Fabric 3* to *Fabric 6* in x-axis). PhobRSH coating has consistently given the highest average R_C across several fabric samples.

A final observation to be made in **Figures 4.12** and **4.13** is that R_C generally decreases with increasing *We*, as hinted several times. One explanation for this trend is the onset of droplet sticking (i.e. partial rebound) and the eventual complete pinning— which are two phenomena exclusive to *rough surfaces*. As discussed earlier, these two are simply the consequence of transition to "sticky" Wenzel state: the pinning of a fraction of the droplet acts against its tendency to rebound, which dissipates its energy and lowers its achievable rebound height. Ultimately, the bouncing behavior becomes fully suppressed for a sufficiently high impact speed (high *We*). Moreover, the fabric defects (whether loops or protrusions) might have augmented this pinning tendency and energy dissipation. The increasing droplet-fabric contact area with *We* makes this interaction highly probable— which supports this observed decrease of R_C with *We*.

Another explanation of this trend of decreasing R_C is the loss of kinetic energy through turbulent motion inside the droplet (viscous dissipation)— which is applicable to *both smooth and rough*

surfaces. Durickovic et al. argued that, despite the droplets having larger initial kinetic energy in the regime of high *We*, a much larger fraction of this energy would also be dissipated due to this internal motion. [6] Based on their numerical simulations on drop energetics, Sharma et al. postulated that the kinetic energy loss can occur either when the droplet is in contact with the surface or at mid-air during its rebound flight— with the former being more dominant at higher *We*. [29] As an example for the *latter* case, oscillations during rebound may lower R_C by inducing dissipative motions inside the droplet, as in the experiment of Richard et al. on drop bouncing on superhydrophobic surfaces. [10] These turbulences due to vibrational motion, and even rotational motion, of droplet at higher *We* have not been accounted for in this work unfortunately. On the other hand, the dissipation mechanism for a droplet in contact with the surface was already seen previously: it is related on how the spreading behavior transitions from capillary regime to viscous regime (see **Figure 4.5** if needed). More specifically, the increase of vigorous internal motion is rooted on how the increase of *We* causes the droplet to spread and retract *more quickly.* The higher spreading and receding rate is simply the manifestation of a large-scale deformation of the droplet at a higher rate against its viscosity, which requires a larger amount of force to be *spent*. Additionally, the increase of *We* might also increase the tendency of *vortical* motions *within* the droplet. [8] Ultimately, any of these mechanisms yields to larger energy dissipation for the droplet at higher *We*. Overall, these results are consistent with the findings of studies on superhydrophobic surfaces, where they also observed that the restitution coefficient of the bouncing water droplet would indeed decrease with increasing *We*. [6] [10]

Finally, before evaluating the water repellency of each fabric sample, it must be noted first that: unlike its spreading behavior, the rebound behavior of droplet is highly sensitive to the fabric surface and its local characteristics. This can only be partially seen in **Figure 4.12** unfortunately— the points of the same fabric sample (same color) only form a "general" trend, and there are sometimes huge variations between two points of consecutive *We.* This observation is simply the consequence of having different kind of driving forces between these two phenomena. Whereas droplet spreading is driven by its kinetic energy, droplet rebound is driven by its surface energy and interaction with the fabric. With the influence of fabric's intrinsic variability, a range of rebound behavior is observed instead— similar to an issue faced in one research work on solid surfaces. [2] To circumvent this problem, multiple observations need to be averaged for each fabric sample in line with the investigation of its water repellency behavior. This will be tackled in the next section.

4.5 *Water Repellency of PhobRSH-Coated Fabrics*

For the remainder of this chapter, only *PhobRSH*-coated fabrics will be covered: they will be used in thorough evaluation of water repellency behavior and application of machine learning (*ML*). This is still in line with the primary objective to differentiate the water repellency of these coated textiles mainly based on the physical characteristics of the fabric, with the chemical composition of coating being only of secondary importance. Besides, the global trend required for comparison of fabrics of different coatings has already been established in the previous sections.

Figure 4.15 shows the different restitution coefficient R_C curves representing the different fabric samples, over a given Weber number *We* range. Although each curve is different from the rest, there are two general trends which can be observed. (1) For samples *with low roughness* (*Fabric1* and *Fabric 2*, $r < 1.4$), R_C reaches a maximum value at *low-intermediate We* ($15<We<20$). (2) On the other hand, for samples with *high roughness* (*Fabric 3* to *Fabric 7*), R_C starts from a high value at very low *We* ($We < 5$) and continuously decreases with *We*— either reaching zero or stopping at

an “intermediate” plateau. It is expected that the fabrics which have reached plateau until *We* ≈ 30 in **Figure 4.15** will also reach close to zero eventually as *We* increases, due to the observed (onset of) droplet pinning for most fabrics at very high *We*. Moreover, it is also worth-mentioning that the fabric samples with larger error bars *and* more kinks in the curve in **Figure 4.15** are the ones which have *very* high roughness (*r > 1.7)* and/or high defect count. This notion reflects the cause of the observed *range* of rebound behavior in the fabrics: it is posited to be related to the very high yet *irregular* surface roughness and/or the abundance of defects.

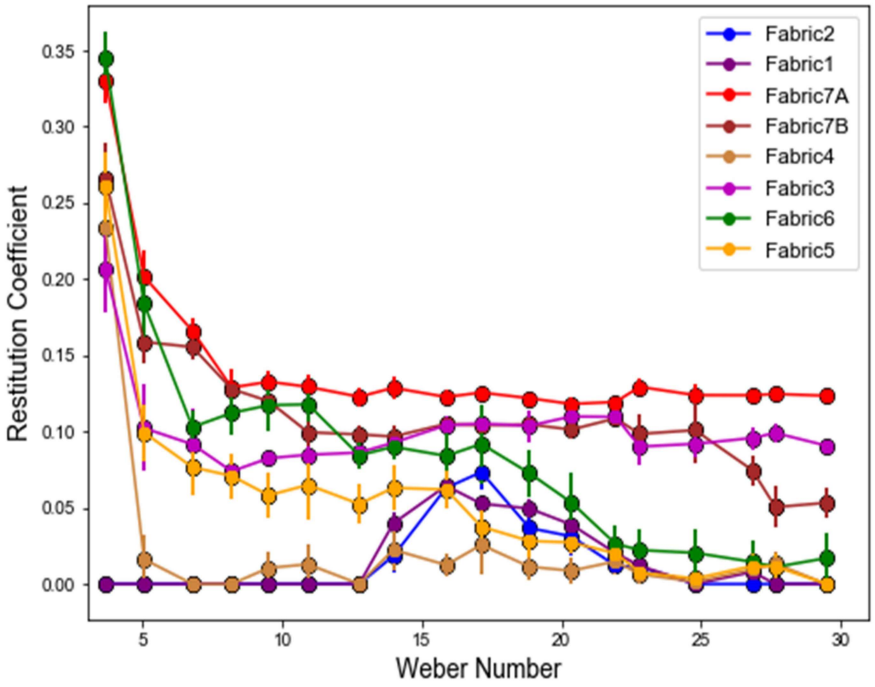

Figure 4.15. In-depth comparison of restitution coefficient R_C of the fabric samples for a small Weber number *We* range. *D = 1.99 mm.* Each point is an average of around 6 observations, in order to minimize the noise created by the sensitivity of rebound behavior on local characteristics of fabric surface. Although the used *We* range is narrower than that used previously, the different fabric samples can still be sufficiently distinguished from each other given the uniqueness of each curve and the variety of trends observed. Whereas the samples with high roughness (*Fabric 3* to *Fabric 7*, *r > 1.4*) show a decreasing R_c with increasing *We*, the samples with low roughness (*Fabric 1* and *Fabric 2*) show a maximum R_c at low-intermediate optimum *We.*

Unfortunately, there is currently no research available to explain such stark difference in behavior of R_C with *We* of fabrics with *low roughness* from the ones with high roughness. Still, a hypothesis can be proposed by considering the energy balance for this unique droplet behavior on fabrics with *low roughness*: the absence of rebound behavior *could* be due to insufficient contact width to store surface energy at *low We*, and viscous dissipation at *high We.* As a reminder, rebound only occurs when the droplet has recovered enough kinetic energy during retraction, and in turn, this kinetic energy is limited by the maximum contact width of the droplet during spreading. At very low *We* (5 < *We* < 13) in **Figure 4.15**, there seems to be insufficient surface area and contact width for the droplet to store as much energy as it needed to rebound in these low-roughness fabrics. In other words, *to compensate for the lack of air pockets*, these fabrics would have to wait for the droplet to achieve a sufficiently large surface area and contact width on them by having higher *We*. Once low-intermediate *We* is reached (13 < *We* < 25), enough kinetic energy can now be provided to let the droplet rebound. However, further increase of *We* (past *We > 25*) in **Figure 4.15** would cause viscous dissipation to become significant as well— mainly as turbulent motion of droplet during

spreading or retraction. Hence, an optimum contact width (thus *We*) exists for fabrics with *low roughness*— which provides the best compromise between (1) the need for sufficient stored surface energy and (2) the need for tolerable degree of viscous dissipation.

On the other hand, each fabric sample with *high roughness* gives a *unique* curve in **Figure 4.15**. To explain such observation, one must first look back at the physical parameters of these fabrics— which are shown again below in **Table 4.3**, but with the additional information of R_C averaged over relevant range of *We* (expressed *as* $\langle R_C \rangle_{We}$) from **Figure 4.15** for approximate comparison. By comparing the values of *r* and $\langle R_C \rangle_{We}$ and inspecting the relevant curves in **Figure 4.15**, it is immediate that fabric roughness alone does not determine the average rebound behavior of droplet. If fabric roughness *was* the sole determinant, both *Fabric 5* and *Fabric 6* should have had the highest $\langle R_C \rangle_{We}$— but that is obviously not the case here. This only means that, although high water repellency behavior is observed mostly in fabrics with high roughness at *low We*, the converse may not be true: in other words, using a fabric with higher roughness does not necessarily guarantee higher water-repellency behavior. This seeming conflict can be addressed by the two other possible factors influencing the rebound behavior of fabric samples with *high roughness*: (1) the presence of defects, which was covered in the previous section; and (2) the precise surface topography creating the roughness, which will now be covered.

.

Table 4.3. Physical characteristics of fabric samples

Fabric Sample	Experimental Roughness *r*	Fiber Diameter (μm)	Unit Cell Length (μm)	Defect Count Classification (Average Defect Count per 8.5 mm^2 fabric area)	Average R_C over *We* range [*]
Fabric1	1.19	10 / 20	600 / 400	Low (≤12)	0.012
Fabric2	1.27	14 / 25	750 / 600	Low (≤12)	0.013
Fabric3	1.46	22 / 20	340 / 550	Low (≤12)	0.100
Fabric4	1.47	22 / 18	310 / 680	High (≥ 24)	0.033
Fabric5	1.77	16 / 18	730 / 810	Intermediate (> 12 but < 24)	0.053
Fabric6	1.77	20 / 16	540 / 350	High (≥ 24)	0.118
Fabric7A	1.71	12 / 14	330 / 450	Intermediate (> 12 but < 24)	0.150
Fabric7B	1.67	16 / 12	540 / 550	Intermediate (> 12 but < 24)	0.113

[*] The relevant *We* range used for averaging R_C is $3 < We < 30$.

It is *suggested* that the influence of surface topography is largely rooted on its effect on the pinning tendency of droplet for increasing *We*, i.e. its transition from Cassie-Baxter to "sticky" Wenzel state. To recall, it was found in previous studies that the critical impact speed for sticking V_{stick} is *inversely* proportional to the distance between the roughness micro-posts (spacing) for structured surfaces: smaller spacing leads to a larger capillary pressure, which has to be offset by the dynamic pressure from droplet impact. [7] [21] [25] In other words, smaller spacing *preserves* the complete rebound behavior of droplet *until a larger We* and thus *over a wider range*, but not necessarily gives the highest rebound for all the given *We*. Taking a *simplistic* view in this work, the spacing between the roughness elements on a fabric may be considered to be in the *order of magnitude* of *mean* fiber diameter $\langle d_f \rangle$. Using this proposition, *Fabric7A* should have the highest R_C at $We \approx 30$ in **Figure 4.15** given that it has the smallest $\langle d_f \rangle$ in **Table 4.3**— which is what has been observed in this work. Given a sufficiently large range of *We*, it is not surprising that the $\langle R_C \rangle_{We}$ of *Fabric7A*

is also the highest. Interestingly, based on **Figure 4.15**, *Fabric3* has the second highest R_C at $We \approx 30$ and not *Fabric7B* (which has the second smallest $\langle d_f \rangle$). It can be argued that such deviation is due to the interference of the influence of defect count: as fabric defects also promote pinning tendency, the lower defect count in *Fabric3* enables it to have higher R_C than *Fabric7B*. However, it must be stressed again that this line of reasoning is only a *simplistic* take on understanding the observed range of rebound behavior of fabrics with *high roughness* in **Figure 4.15**. Unfortunately, due to several limitations (number of fabric samples, time and amount of literature on this specific topic), it has not been possible to support this argument more convincingly. Thus, it must be received with reasonable skepticism until (1) a more complete investigation has been performed; and (2) similar studies on textiles have confirmed such results. Nevertheless, *Fabric7A, Fabric3* and *Fabric7B* can still be practically regarded as the most water-repellent fabric samples (in decreasing order) based on the high value of (1) R_C up to $We \approx 30$ in **Figure 4.15** *and* (2) $\langle R_C \rangle_{We}$ at **Table 4.3**. Further investigation of their physical characteristics might thus be interesting for understanding water repellency and designing appropriate textiles.

As a final point, it would not be correct to state that the fabrics with high roughness always provide better droplet rebound than the ones with low roughness *for all given We.* As an example from **Figure 4.15**, *Fabric4* and *Fabric5* (the latter only to a slight extent) have actually given lower R_C than *Fabric1* and *Fabric2* ($r < 1.4$) at low-intermediate *We* ($15 < We < 20$). This simply shows that even low-roughness fabrics can perform better than high-roughness fabrics at certain range of *We.* It is not surprising however that *Fabric4* and *Fabric5* have the highest roll-off angle θ_{RO} (poorest performance) *among the fabrics with high roughness* (see **Table 4.2** if needed). More precisely, it is *suggested* that such observation is due to the huge amount of defects in *Fabric4* and prevalent surface heterogeneities in *Fabric5.* Going back to the main point, it means that the actual rebound behavior of droplet (thus water repellency of surface) is highly influenced by *We* as well. Put differently, identifying the useful range of *We* might be crucial for some applications, especially when one is not expecting to use them for an extremely wide range of *We.* This last point however may not be applicable to textiles since they must cater to a wide range of activities and phenomena.

4.6 *Application of Machine Learning*

As discussed previously, there are three machine learning (*ML*)-based analyses developed to describe the droplet dynamic behavior on textiles. While the first model was based on Artificial Neural Network *(ANN)* to predict the dimensionless maximum contact width ξ_{max}, the second model was based on Random Forest *(RF)* to predict the restitution coefficient R_C. The third analysis was performed using Principal Component Analysis (*PCA*), which has two aims in this work: (1) to generate a 2D visual representation of the dataset; and (2) to gain more information about the droplet dynamic behavior by identifying parameters which can potentially separate the data space into defined clusters.

Before looking at the accuracy of the first two predictive models, it is necessary to reiterate the context of the obtained results. As hinted in **Experimental 3.7**, a limited number of fabric samples entails a limited amount of data available to distinguish the fabrics, which in turn limits the ability of these models. Hence, it is natural that their predictive power will be better when working at new droplet properties (specifically its impact speed), than when working at new unseen fabric samples in most cases.

First, to estimate its performance accuracy, the developed *ANN* model was used to predict ξ_{max} values from the dataset— as illustrated in **Figure 4.16**. It was found that the corresponding *mean absolute error (MAE)* of ξ_{max} is 0.07 for both the *whole* dataset and the *test* set, for an average ξ_{max} value equal to 1.94. The relatively small error (< 5%) in the *whole* dataset signifies that *ANN* can predict the maximum spreading behavior of droplet with *high* accuracy for these fabric samples. Secondly, the comparable small error (< 5%) in the *test* set demonstrates that the *ANN* model can generalize its good prediction to unseen data— especially to the observations with new droplet impact speed. Finally, based on the permutation importance given in **Figure 4.17**, the *ANN* model confirms that the Weber number *We* of the droplet (through its kinetic energy/impact speed) mainly dictates this spreading behavior.

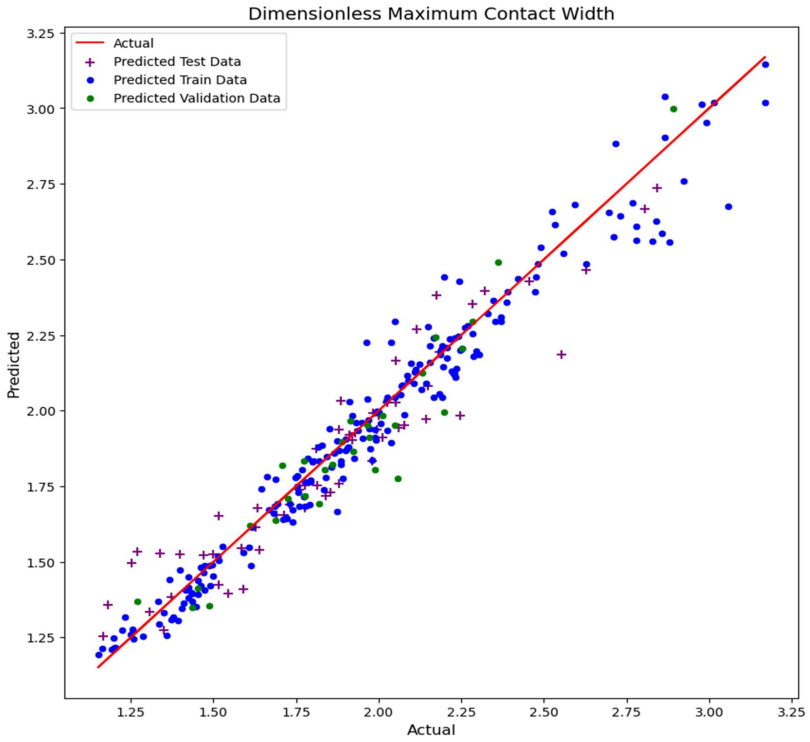

Figure 4.16. Prediction of dimensionless maximum contact width ξ_{max} of the droplet based on Artificial Neural Network *(ANN).* Each point is plotted using actual ξ_{max} as its x-coordinate and predicted ξ_{max} as its y-coordinate. Essentially, the closer the points are to the line $y=x$, the better the prediction is (i.e., a perfect model is where all the points lie along the line). The dataset is based on **Figure 4.7**, but only using *PhobRSH*-coated fabrics.

The same treatment was performed on the developed *RF* model in predicting R_C values of the dataset— as illustrated in **Figure 4.18**. It was found that the corresponding *MAE* is 0.005 for the *whole* dataset and 0.010 for the *test* set, for an average R_C value equal to 0.060. In contrast with the *ANN* model, the developed *RF* model can predict the rebound behavior of the droplet only with *reasonable* accuracy, given the slightly higher error (< 10%) observed for the *whole* dataset. Nevertheless, the *RF* model can still generalize to unseen data fairly well based on the *tolerable* error in *test* set— but again limited to the observations with new droplet impact speed. Finally, based on permutation importance given in **Figure 4.19**, the *RF* model confirms that the precise topography of fabric roughness— rather than simply the roughness itself— contributes the most to determining the actual droplet rebound behavior.

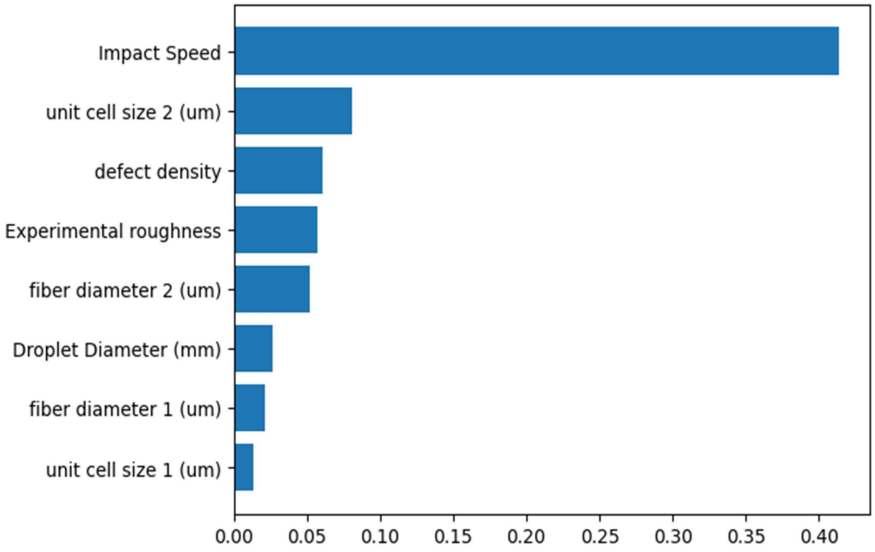

Figure 4.17. Ranking of relevance of each feature in the prediction of dimensionless maximum contact width ξ_{max} using *permutation importance.* The impact speed of the droplet is the most relevant parameter in predicting its ξ_{max} using this model.

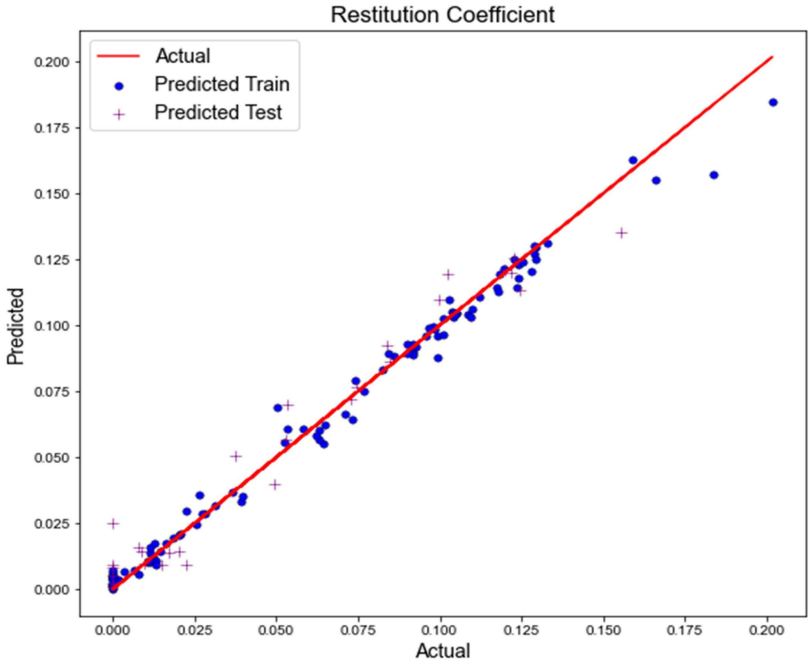

Figure 4.18. Prediction of restitution coefficient R_C of the droplet based on Random Forest (*RF*). *D = 1.99 mm.* Each point is plotted using actual R_C as its x-coordinate and predicted R_C as its y-coordinate. The dataset is based on **Figure 4.15**, with *We > 4.*

Finally, using *PCA,* the dynamic behavior of droplets in the fabric samples was visualized— as shown in **Figure 4.20**. From the caption in **Figure 4.20,** the breakdown of the first and second principal components (*PC1* and *PC2,* respectively) can be interpreted as follows based on the previous results. *PC1* includes splashing (represented by average number of droplets) and rebound (represented by restitution coefficient R_C) — both of which are more likely to occur in fabrics with high roughness ($r > 1.4$). The equilibrium contact width, which represents the final wetting state of the sample similar to contact angle θ, is also included in *PC1.* Because of the expected *lower* equilibrium contact width for high-roughness fabrics (due to having higher θ), this

parameter takes a negative sign in *PC1.* On the other hand, *PC2* includes the spreading behavior (represented by dimensionless maximum contact width ξ_{max}), which is mostly dictated by the Weber number *We*. In addition, varying *We* will affect the deformation rate of the droplet, and thus its maximum receding rate.

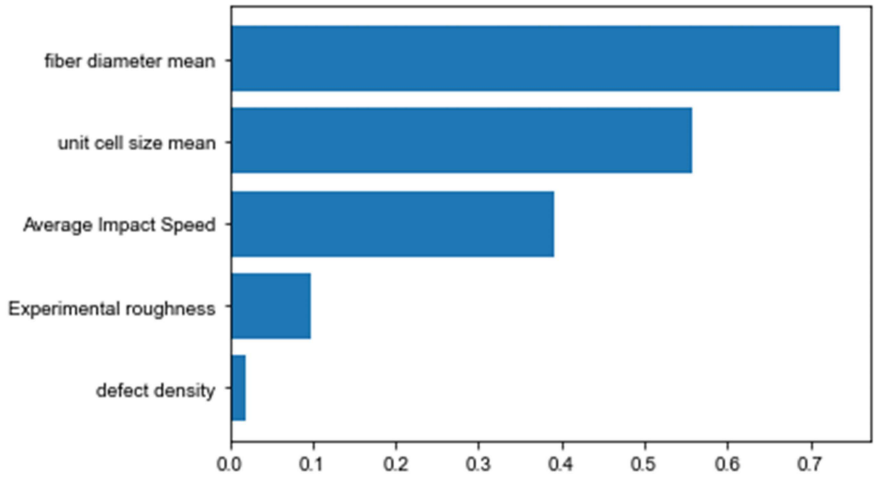

Figure 4.19. Ranking of relevance of each feature in the prediction of restitution coefficient R_C using *permutation importance.* In contrast with the result in spreading behavior, the mean fiber diameter and mean unit cell length of the fabrics are the two most relevant parameters in predicting the R_C of the droplet using this model.

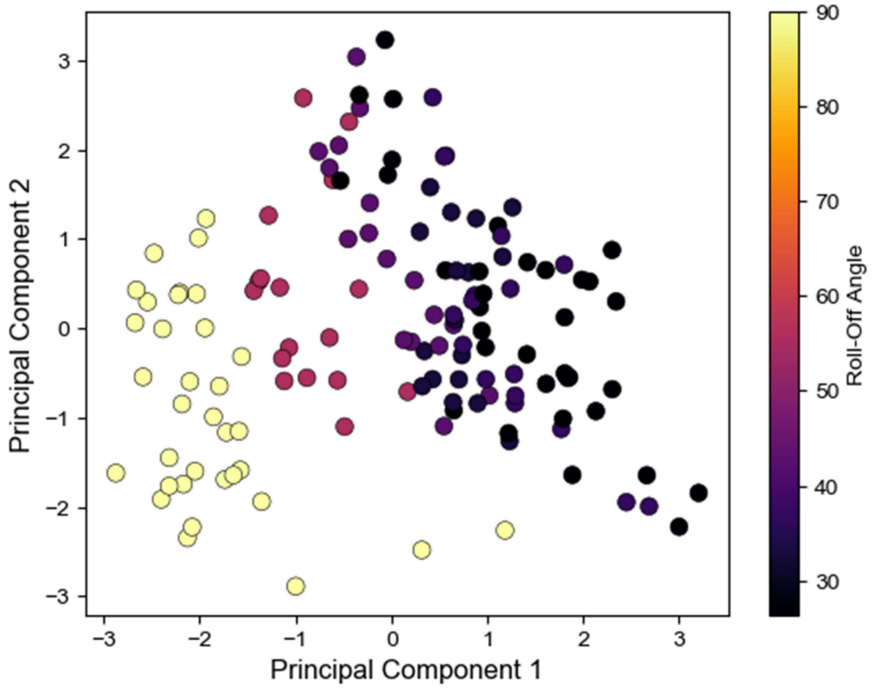

Figure 4.20. Visual representation of droplet dynamic behavior in different fabrics at low *We* (*We* < 30) based on the first two principal components of *PCA*, with roll-off angle θ_{RO} of fabrics as colormap. The principal components are combinations of the relevant parameters extracted from the observations (videos). More specifically, the 1st principal component *(PC1)* is based on *59.8 restitution coefficient, -55.7 equilibrium contact width* and *45.5 average number of droplets*. On the other hand, the 2nd principal component *(PC2)* is based on *66.3 maximum receding rate* and *64.2 dimensionless maximum contact width.* The coefficients of the parameters (i.e., *59.8, -55.7, etc.*) forming each principal component are simply the elements from the component's corresponding eigenvector. In this analysis, only the sign of the coefficients is given attention since their magnitudes are relatively close to one another. Based on the distribution of important parameters between the two principal components, *PC1* can be related to the fabric

physical characteristics, while *PC2* can be related to the droplet physical properties. The dataset is based on **Figure 4.15**, with *We > 4.*

Therefore, a high *PC1* indicates higher rebound, more frequent splashing and lower equilibrium contact width of the droplet— all of which are *desirable* characteristics of a water-repellent surface (to be developed more fully in the next section). A high *PC2,* on the other hand, *generally* indicates high spreading and receding characteristic of the droplet due to high *We.* More generally, *PC1* can be associated with the influence of fabric physical characteristics, while *PC2* can be associated with the influence of droplet physical properties, on the overall droplet-fabric interaction. Finally, it is worth-mentioning that the seeming decrease of *PC1* with increasing *PC2* for a given fabric sample (particularly the black and violet points) is simply a consequence of *We* acting as a *confounding variable*. To demonstrate this effect, *We* was also used as a colormap for this kind of plot (See **Supplementary S.4.3** for full details).

Different physical and wetting characteristics of fabrics were used to establish a good separation of color-coded clusters in **Figure 4.20**. By the end, using roll-off angle θ_{RO} as colormap provided the most effective resolution in distinguishing the droplet dynamic behavior in different fabrics. This result should not be surprising, as it has been emphasized in the previous sections that the surface *quality* of the fabric is reflected on the dynamic behavior of an impacting droplet and the roll-off tendency of a static droplet, and not much on the contact angle θ. There are two important conclusions to draw from this result: one is about the experimental aspect, and the other is about understanding the underlying phenomenon. First, θ_{RO} can distinguish the different fabrics based on the behavior of impacting droplet. That is, for a given *We* (linked to droplet properties as *PC2*), the θ_{RO} of a fabric may be able to provide an *approximate* description of how the fabric will interact with the droplet in an impact test. Thus, in this work, it *appears* that the evaluation of θ_{RO} is not only a simple *screening* step; rather, it is an *effective* method, if not a *sufficient* one by itself, in establishing the water repellency of coated fabrics. As a caveat however, given the number of fabric samples studied, further work is certainly necessary to confirm such findings. Indeed, if evaluating θ_{RO} is as reliable as performing several drop impact tests on determining the water repellency of fabrics, a significant amount of time and resources might be saved when doing quality control. It would be very interesting to see how this result compares with the observations of long-running textile manufacturers.

Secondly, the fabrics with lower θ_{RO} (black and violet points) almost always have higher *PC1* than the rest of the fabrics for any given *PC2* based on **Figure 4.20**. In other words, the fabrics with lower θ_{RO} are also the ones which give better water repellency behavior based on our drop impact studies. This simply shows that the underlying mechanisms which prevent the droplet from rolling off easily also play a role in preventing the droplet from rebounding well. These unwanted mechanisms might be brought by improper topography, heterogeneities, defects or other unseen parameters related to surface quality of the fabric.

4.7 *Global Perspective on Droplet Behavior and Water Repellency of Textiles*

Through drop impact tests, the dynamic behavior of water droplet on the rough coated fabric samples has been studied. It was found that splashing is more likely to occur on fabrics with high roughness (*r > 1.4)* at sufficiently high Weber number *We.* On the contrary, spreading is only affected minimally by the fabric roughness, although it also becomes more dominant at higher *We*. Better rebound behavior can be achieved using most fabrics with high roughness in general, but only at low *We*. The actual fabric nature also plays an important role in both splashing and

rebound. While fabric defects are expected to promote splashing, they may also act as pinning sites which dissipate energy and suppress rebound tendency. On the other hand, fabric surface topography is mainly linked to the transition from complete rebound to partial rebound and ultimately to complete pinning. **Table 4.4** summarizes the influence of different parameters on the three main droplet behaviors considered in this work.

Table 4.4. Influence of different physical parameters on droplet dynamic behavior

Parameter	***We***	**Fabric roughness**	**Coating type**	**Fabric physical parameters**
Splashing	Requires high *We*	Splashing observed in fabrics with high roughness	Not determined in this work	Splashing promoted by defects
Spreading	Increases with *We*	Spreading affected minimally by roughness	Spreading affected minimally by coating	Spreading affected minimally by fabric nature
Rebound	Decreases with *We*	Higher rebound can be achieved using fabrics with high roughness	Higher rebound can be achieved using PhobRSH	Affected heavily by topography; Diminished by defects

Distinction has also been made between fabrics of high roughness ($r > 1.4$) and low roughness. The fabrics which exhibited *both* substantial splashing and rebound behaviors *come from* the ones with high roughness. This is not surprising, as frequent splashing and high rebound behavior may occur when there is minimal (unfavorable) interaction of water droplet with fabric surface. [6] On the other hand, spreading is not influenced by the fabric-droplet interaction — given that it is indifferent to fabric roughness and its possible wetting states (whether partially-impregnated or superficially wet). Thus, whereas splashing and rebound behavior of the droplet can differentiate and reveal the water repellency of fabrics, spreading unfortunately does not provide any information on such. As a caution however, splashing may help revealing the water repellency of fabrics *only because* imparting roughness is a method used to decrease their wettability, and rough surfaces inadvertently promote splashing. Furthermore, it was found that the droplet has *lower* maximum receding rate in fabrics with *low roughness* compared to the ones with high roughness, as shown in **Figure 4.21**. This result is rooted on how droplet retraction is influenced by surface characteristics of the fabrics as well, unlike spreading. As higher interfacial energy is achieved when there are (more) air pockets underneath a droplet in its maximum contact width, the droplet can retract much faster. This result must be treated with some reservations however, given that the measurable maximum rate is limited by the available frame rate. Nevertheless, it might be interesting to verify if this trend can be observed in droplet impact studies for *rough solid* surfaces as well once this parameter has been largely studied. Finally, it was also found that these two sets of fabrics give different equilibrium contact width of the impacting droplet (See **Supplementary S.4.4**).

It has been well-established already at this point that the water repellency of fabrics depends largely on the fabric physical characteristics, and not on roughness alone. However, it must also be emphasized again that the exact rebound behavior of droplet is still influenced by *We.* As a consequence of the latter, some low-roughness fabrics might provide better rebound than the high-roughness fabrics depending on the actual *We*. As employed in one previous section, there is: (1) *average* water repellency, which applies to a large range of *We*; and (2) *specific* water repellency, which only accounts for the relevant *We* (in the context of rain refers to the highest *We* possible). Respecting these two requirements in this work, *Fabric7A, Fabric3* and *Fabric7B* appear to be most water-repellent fabric samples (in decreasing order).

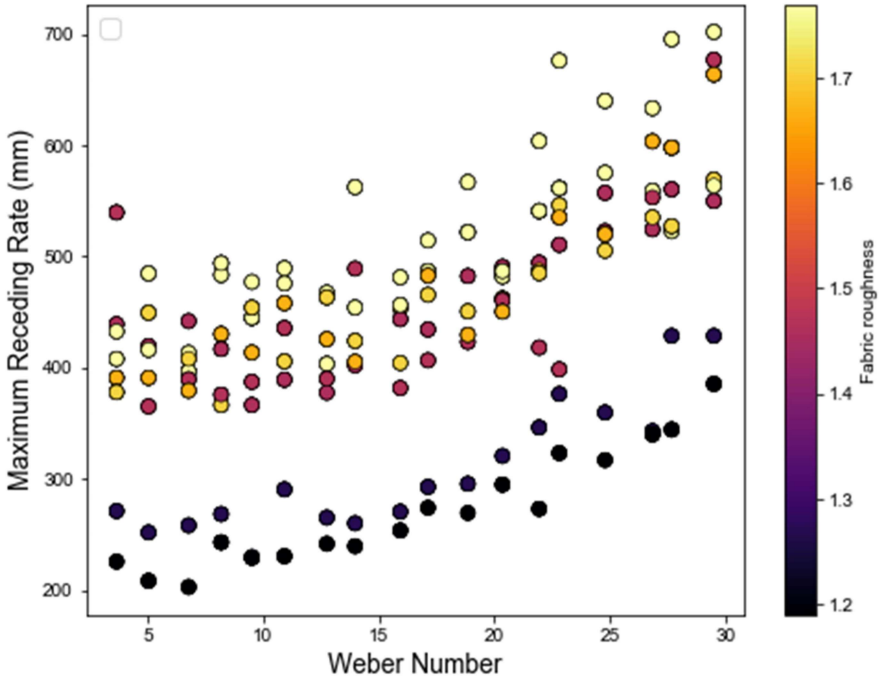

Figure 4.21. In-depth comparison of maximum receding rate in different fabrics for a small *We* range. *D = 1.99 mm.* Each point is an average of 6 observations. Averaging of values has been necessary since the retraction of droplet is affected by the local characteristics of the fabric surface, given that this process is driven by the interfacial tension of droplet with the fabric. Lower maximum receding rate was observed for fabric samples with low roughness (black points, *r < 1.4)*.

One remaining important concept to discuss is that, unlike solid surfaces, fabrics might be penetrated by the water droplets. An impacting droplet with sufficiently high kinetic energy may start pushing itself through the pores of a fabric. Penetration occurs with the dissipation of the droplet's kinetic energy by viscous forces, as the liquid flows through the pores of the fabric and forces a way to reside in the *solid-fabric* interfacial region. [11] This simply means that the absence of penetration is another characteristic of high water repellency, because: (1) penetration could cause fractions of droplet to reside in the pores of the fabric; but also (2) penetration could reduce the available energy of the droplet, thereby suppressing its rebound tendency. It was found that the critical impact speed for penetration V_{pen} of fabrics depends on both the pore size and wettability of the fabrics. Fabrics which have smaller pores and/or lower wettability would require higher V_{pen}. [2] [11] In this specific work, droplet penetration appears to be not relevant except at high Weber number *We* (*We* ≈ 80) and for some *C4F*-coated and *PDMS*-coated fabric samples.

Given all the information provided, a global understanding on the water repellency of textiles can now be established from three different perspectives: (1) practical, (2) theoretical and (3) design. First, from a practical standpoint, water repellency favors specific outcomes when droplets impact on textiles. For instance, splashing and rebound are both desirable for water-repellent fabrics. On one hand, splashing *may* facilitate the reduction of volume of a droplet residing on a fabric by fragmentation of smaller droplets. On the other hand, rebound *may* also offer an opportunity for elimination of a large volume of droplet during its flight, such as when hitting the fabric at an inclined orientation far from normal angle. The removal of droplet is likely, since the fabrics which let it rebound well typically also let it roll off easily, as established in the previous section. In contrast, pinning and penetration are both undesirable as they cause the droplet to stick to the fabric surface at the very least— which could make the droplet harder to remove.

Secondly, from a theoretical standpoint, water repellency measures the resistance of the fabric from an impacting droplet. Coming from a specific dropping height, a droplet will exert a dynamic pressure related to its kinetic energy on the fabric surface. Depending on its exact geometry and its chemical wettability, the fabric surface might possess sufficiently high capillary pressure (a) between its roughness elements to resist droplet pinning and (b) within its pores to resist droplet penetration. This can be addressed by having (a) optimal surface topography and (b) minimal pore size, respectively. That is, finely-structured fabrics could have high water repellency behavior— resisting pinning or penetration for a wider range of droplet impact speed (dropping height).

Finally, from a design standpoint, a few suggestions can be offered to the textile manufacturers in the design of water-repellent textiles based on the *most relevant results of this work* and *findings from related literature*. These are the following:

Topography of surface: Based on the trends observed and physical arguments made in this work, it *appears* that manufacturing the fabrics using fibers with smaller diameter may offer higher water repellency. It was posited that the small diameter of fibers would translate to small spacing between roughness elements— which would provide large capillary pressure needed to resist droplet pinning, similar to the findings for micro-structured surfaces. [7] [21] [25] This is the hypothesis developed in this work regarding why *Fabric7A* has the highest water repellency among the given fabrics. However, it is encouraged again to keep reasonable skepticism with regard to this result until further investigation and validation experiments on a larger set of textiles have been performed.

Presence of defects: The amount of defects must be reduced for a given fabric. While they can improve the tendency for splashing, these fabric defects might also pin the droplets (dissipate their energy and ultimately suppress their rebound behavior), similar to a previous work on solid surfaces. [10] This is the suggested explanation in this work regarding why *Fabric 3* has kept better water repellency than *Fabric7B* at higher *We.*

Quality of surface: While introducing roughness is necessary to achieve high droplet rebound, surface heterogeneities and inconsistencies might be imparted unintentionally as well. In solid surfaces, it was found that the lack of uniformity in roughness may act against the droplet's roll-off tendency by increasing the contact angle hysteresis $\Delta\theta$. [14] This principle is expected to hold true for the case of fabrics as well. Thus, one must carefully design and structure the fibers to obtain a widely-uniform roughness as much as possible; otherwise, the whole task would be ineffective, if not futile.

Size of pores: The fabric pore size must be kept as small as possible. [2] Smaller pores offer higher capillary pressure which can match a larger dynamic pressure exerted by the droplet's kinetic energy, as discussed earlier. [11]

Nature of coating: The coating must be chosen such that the contact angle hysteresis $\Delta\theta$, which determines roll-off angle θ_{RO}, is very small. [12] $\Delta\theta$ can act as a source of energy dissipation, [10] which can lead to a decrease in roll-off or rebound tendency.

Summary, Conclusions and Future Work

This work has investigated the droplet impact dynamics on rough woven textiles coated with hydrophobic formulations and fixed on glass substrates. The influence of different parameters— Weber number *We,* fabric roughness, coating type and specific fabric physical characteristics— was identified. The results obtained for these textiles are largely in good agreement with previous studies performed on solid surfaces. Moreover, this work has conducted an evaluation of water repellency of the fabric samples, first solely based on rebound behavior and later globally. Practical, theoretical and design perspectives were also offered to provide a richer understanding of the subject of water repellency of textiles. Furthermore, this work has demonstrated that machine learning can be integrated into this field of research: predictive models of droplet behavior with reasonable to high accuracy can be developed. Through machine learning, the most significant parameters in spreading and rebound behavior of droplet were identified and found to be consistent with the physical arguments presented. A visual representation of relevant parameters describing droplet behavior was also provided — which showed that the droplet's dynamic behavior during impact test is strongly linked to its roll-off tendency during roll-off test.

Fabrics with high roughness show some significant differences from the ones with low roughness in terms of the actual dynamic behavior of the impacting droplet. Splashing is more likely to occur on rougher fabrics at sufficiently high Weber number, whereas spreading appears to be indifferent between the two sets of fabrics despite their different wetting states. Even though higher rebound behavior is observed for most fabrics with high roughness, a more in-depth investigation of each fabric revealed that increasing its roughness alone does not guarantee higher water repellency. Other fabric physical characteristics (such as defect count and surface topography) together influence the rebound tendency of the droplet as well.

There are several directions this research work could take in the future. One major limitation faced in our setup is the limited number of available fabrics. Thus, it would be interesting to have more fabric samples in the future— to create better models in evaluating the relative contribution of each of the physical parameters of woven fabrics in their water repellency behavior. If however, that is not possible, a more in-depth investigation of the available fabrics is proposed. For example, it might be possible to confirm if the spacing between the roughness elements of the fabrics is truly in the order of fiber diameter *in general.* The relationship of this spacing with the critical impact speed for sticking V_{stick} could be established specific for fabrics, once a more systematic account of defects has been performed. Moreover, the physical and chemical durability of these coated fabrics might be worth-examining, especially in relation with understanding if and how their water-repellency behavior changes with time. Finally, it might be interesting to construct a phase diagram even though it seems ambitious: the diagram will show the different regimes of droplet rebound behavior (complete rebound, partial rebound and pinning), which can potentially overlap with the regimes of splashing and penetration. The phase diagram will be created based on textiles and coating compositions of wide range of properties using machine learning.

Indeed, this work is only one step among many others in the future towards understanding the water repellency of textiles. According to National Aeronautics and Space Administration (*NASA*), a raindrop can reach a terminal impact speed as high as 10 m/s in *still air*. Once the exact link between fabric characteristics and their water repellency has been unraveled, addressing the issue of a fast raindrop through appropriate textile design will be the next practical step.

References

[1] "The effect of surface roughness on the contact line and splashing dynamics of impacting droplets". Miguel Quetzeri-Santiago, Alfonso Castrejon-Pita & Rafael Castrejon-Pita. *Nature* **9**, 15030 (2019)

[2] "Droplet impact dynamics on textiles". Gannian Zhang et al. *Soft Matter* **14**, 8182 (2018)

[3] "An introduction of droplet impact dynamics to engineering students". Sara Moghtadernejad, Christian Lee and Mehdi Jadidi. *Fluids* **5**, 107 (2020)

[4] "Droplet bouncing and breakup during impact on microgrooved surface". Laxman Malla et al. *Langmuir* **33**, 9620-9631 (2017)

[5] "Dynamic hydrophobic behavior of water droplets impact on the cotton fabrics coated with POSS block copolymer". Que Kong et al. *Cellulose* **27**, 1705-1716 (2020)

[6] "Between bouncing and splashing: water drops on a solid surface". Bojan Durickovic and Kathleen Varland. University of Arizona: Tucson, AZ, USA (2005)

[7] "Bouncing transitions on microtextured materials". M. Reyssat et al. *Europhys. Lett.* **74**, 2 (2006)

[8] "Maximum deformation of an impacting drop". C. Clanet, D. Richard et al. *J Fluid Mech.* **517**, 119-208 (2004)

[9] "Drop impact and wettability: From hydrophilic to superhydrophobic surfaces". Carlo Antonini, Alidad Amirfazli and Marco Marengo. *Physics of Fluids* **24**, 102104 (2012)

[10] "Bouncing water drops". D. Richard et al. *Europhys. Lett.* **50**, 6 (2000)

[11] "Droplet impact of Newtonian fluids and blood on simple fabrics: effect of fabric pore size and underlying substrate". T.C. de Goede et al. *Physics of Fluids* **33**, 033308 (2021)

[12] "How roughness controls the water repellency of woven fabrics". Alain Jonas, Karine Glinel et al. *Materials and Design* **187**, 108389 (2020)

[13] "Machine learning for molecular and materials science". Keith Butler et al. *Nature* **559**, 547 (2018)

[14] "Investigation of experimental analysis and machine learning to predict drop behavior on superhydrophobic surfaces". A. Azimi Yancheshme et al. *Chemical Engineering Journal* **417**, 127898 (2021)

[15] "Using neural networks to predict icephobic performance". Rahul Ramachandran. University of Nevada: Reno, NV, USA (2020)

[16] "Data mining and machine learning in textile industry". Pelin Yildirim, Derya Birant and Tuba Alpyildiz. *WIREs Data Mining Knowl Discov* **8**, 1228 (2018)

[17] "Procedures for the characterization of wettability and surface free energy of textiles – use, abuse, misuse and proper use: a critical review". Thomas Bahners and Jochen Gutmann. *Rev. Adhesion Adhesives* **7**, 3 (2019)

[18] "Adherence and bouncing of liquid droplets impacting on dry surfaces". D. Caviezel, C. Narayanan and D. Lakehal. *Microfluid Nanofluid* **5**, 469-478 (2008)

[19] "Outcomes from a drop impact on solid surfaces". R. Rioboo, C. Tropea and M. Marengo. *Atomization and Sprays* **11**, 155-165 (2001)

[20] "Drop impact on a solid surface". C Josserand and S Thoroddsen. *Annual Review of Fluid Mechanics* **48**, 365-391 (2016)

[21] "Droplet bouncing on the surface with microstructure". T. Bobinski et al. *Arch. Mech.* **69**, 2 (2017)

[22] "Dynamics of droplet impact on solid surface with different roughness". Tang et al. *Int. J. Multiph. Flow* **96**, 56-69 (2017)

[23] "Maximum spreading of liquid drops impacting on groove-textured surfaces: effect of surface texture". Vaikuntanathan, V. & Sivakumar, D. *Langmuir*, **32**, 2399–2409 (2016)

[24] "Revealing how architecture of surface microstructures alters capillary spreading". Lee, Y. et al. *Sci. Reports* **9**, 7787 (2019)

[25] "Dynamic effects of bouncing water droplets on superhydrophobic surfaces". Yong Chae Jung and Bharat Bhushan". *Langmuir* **24**, 6262-6269 (2008)

[26] "Principal Components Analysis". Steven M. Holland. University of Georgia: Athens, GA, USA

(2019)
[27] “Splashing of liquids: Interplay of surface roughness with surrounding gas”. L. Xu, L. Barcos and S. R. Nagel. *Phys. Rev. E* **76**, 066311 (2007)
[28] “A study on the dynamic behaviors of water droplets impacting nanostructured surfaces”. Geunjae Kwak et al. *AIP Advances* **1**, 042139 (2011)
[29] “Energetics of a bouncing drop: Coefficient of restitution, bubble entrapment and escape”. Praveen K. Sharma and Harish N. Dixit. *Physics of Fluids* **32**, 112107 (2020)
[30] <http://alexlenail.me/NN-SVG/index.html> (Last accessed: 05/21)
[31] “Drop dynamics after impact on a solid wall: Theory and simulations”. Jens Eggers et al. *Physics of Fluids* **22**, 062101 (2010)

Supplementary

This section of the report contains the other parts of research work deemed not significant to be part of the main discussion. It was created to document other results and to provide additional information to the reviewers.

S.3.1 *Determination of Defect Count from Optical Microscope Images of Fabrics*

Figure S.3.1 shows some optical microscope images of the eight fabric samples, which were used for counting defects. The number of defects per fabric sample given in **Table S.3.1A** is reported as average of at least four values. The computation of standard error of values was deemed unnecessary due to the qualitative and subjective nature of this task. Besides, only estimates are needed— as the fabric samples will be classified based on a *range* of number of observed defects. During the exercise, different types of fabric defects were identified: (1) loose and displaced protruding fibers with significantly higher elevation than the surrounding fibers; (2) both small and large fiber loops with high curvature; and (3) aggregate defect consisting of three or more fibers forming either of the two defects mentioned above. From the reported average defect count, each fabric sample was classified using the criteria on **Table S.3.1B**. The boundaries of such classification criteria were selected such that there will be (almost) equal distribution of fabric samples across the three categories.

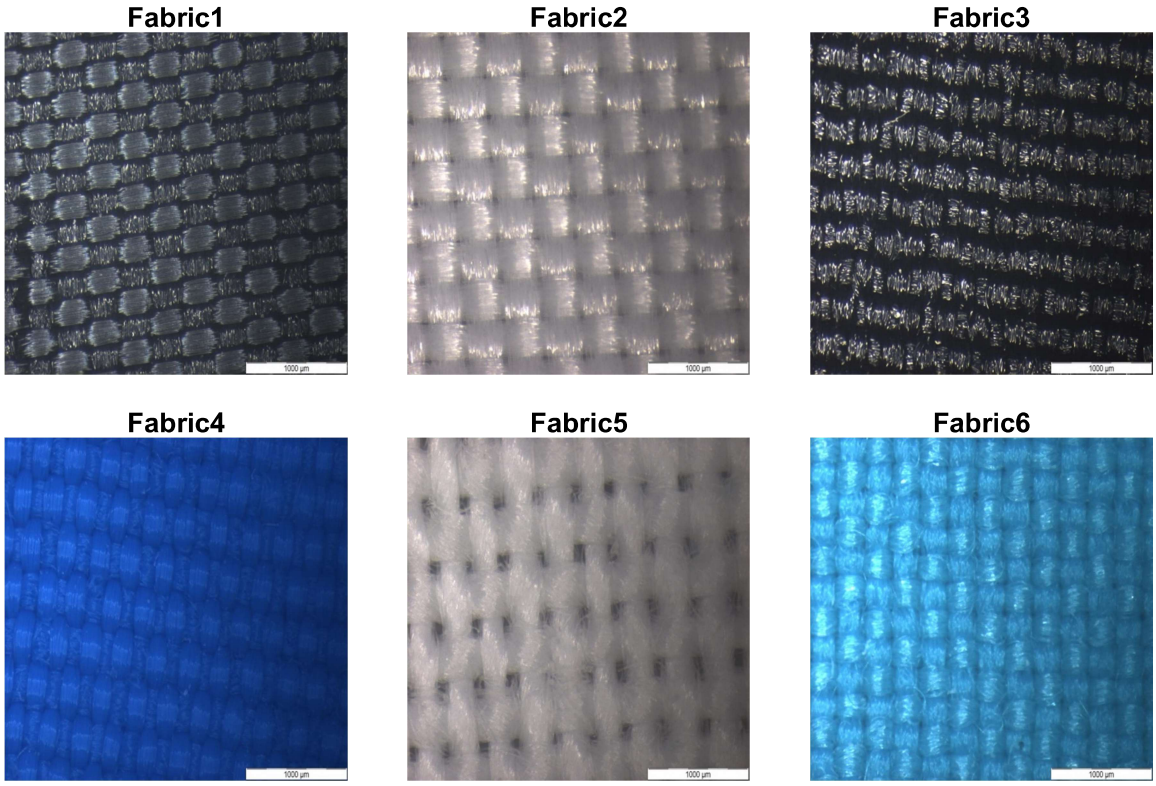

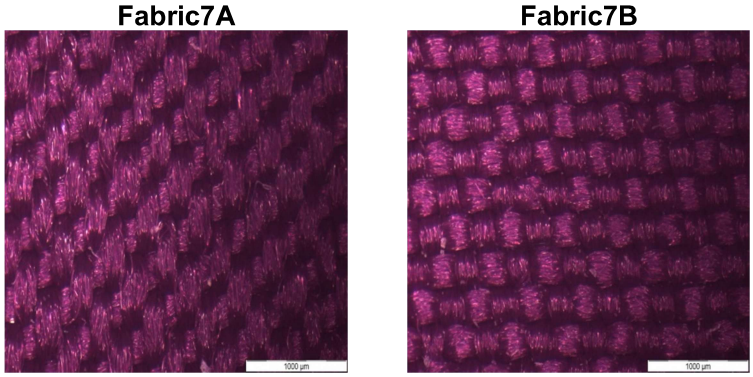

Figure S.3.1. Optical microscope images of the fabric samples. All the images are from PhobRSH-coated fabric samples— taken at a magnification of 25x. Scale bars are given at 1000 µm.

Table S.3.1A. Classification of fabrics based on defect count

Fabric Sample	Average Number of Defects per Image	Classification of Defect Count
Fabric1	3	Low
Fabric2	2	Low
Fabric3	9	Low
Fabric4	30	High
Fabric5	16	Intermediate
Fabric6	26	High
Fabric7A	19	Intermediate
Fabric7B	17	Intermediate

Table S.3.1B. Classification criteria for fabric defect fount

Average Defect Count per 8.5 mm^2 fabric area	Classification of Defect Count
≤12	Low
> 12 but < 24	Intermediate
≥ 24	High

S.3.2 *Relation between Dropping Height and Impact Speed of Droplet*

Figure S.3.2 shows the variation of droplet speed *V* during initial impact with the corresponding measured dropping height *H*. The difference between the two curves is potentially caused by: (1) the (systematic) error on measurement of *H*; and perhaps (2) the effect of air resistance on dampening *V*. It is immediate that the actual *V* (blue curve) nevertheless still scales as square root of *H*.

S.3.3 *Description of Rebound Behavior using Classical Kinematics*

Figure S.3.3 shows the linear dependence of rebound height H_B with square of non-contact time t_{NC}^2. The fair agreement between theoretical fit and actual values shows (1) the general validity of the experimental design and (2) how the rebound behavior can be approximated using classical kinematics, especially *when the observed rebound height is relatively small.* It is suspected that the deviation of some t_{NC}^2 values is due to any of the three factors: (1) a rebound behavior which is not

completely *normal* to the fabric surface; (2) significant vibration or rotation of the droplet during its rebound; and/or (3) the limit on maximum vertical field of view of camera. By using H_B for the computation of after-impact droplet speed V_{AI} for restitution coefficient R_C nonetheless, the difficulty of estimating V_{AI} for droplets of high degree of deformation (such as during partial rebound or jetting) can be circumvented.

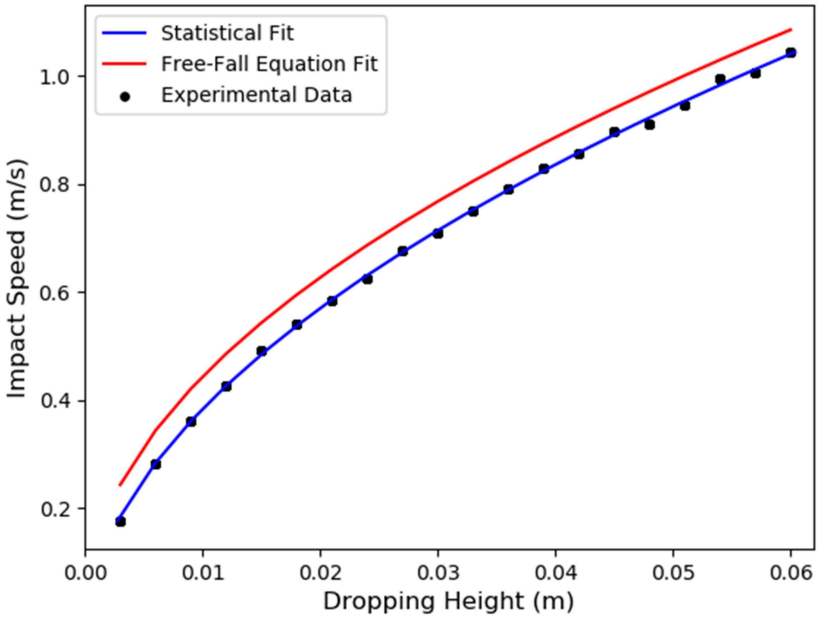

Figure S.3.2. Impact speed *V* as a function of dropping height of the droplet *H*. Each point is an average of at least 20 observations. The red curve corresponds to the fit of experimental data using the free-fall formula: $V = \sqrt{(2gH)}$, where g is the constant equal to 9.81 m/s^2. The blue curve corresponds to the statistical *inverse quadratic* fit, having an equation $H = 0.0476V^2 + 0.0083V - 0.0002$ with $R^2 = 0.999$. Finally, the curves shown here only contain observations where D = 1.99 mm.

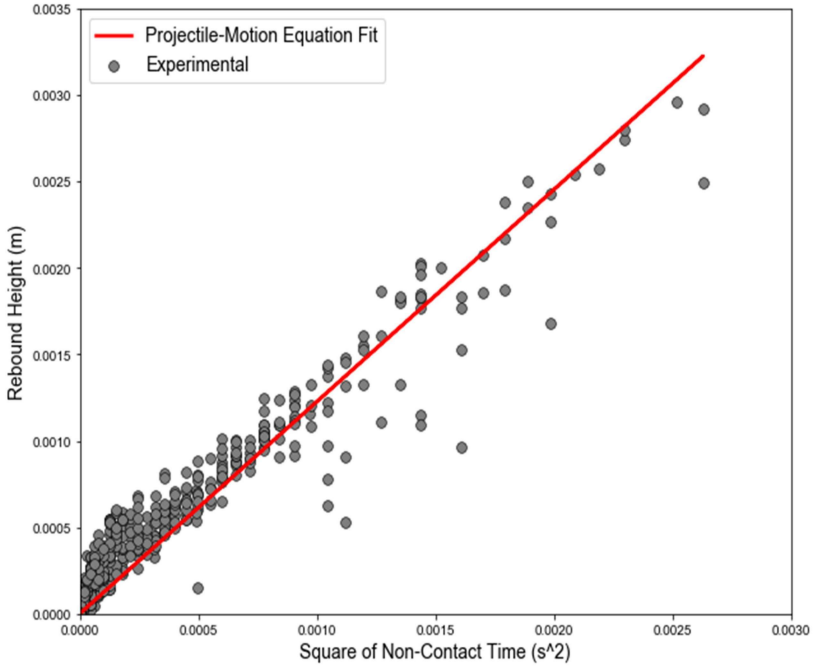

Figure S.3.3. Rebound height H_B as a function of square of non-contact time t_{NC}^2. Each point corresponds to one observation. The red line corresponds to the theoretical-fit of experimental data using the projectile-motion formula: $H_B = gt_{NC}^2/8$, where g is again equal to 9.81 m/s^2, with $R^2 = 0.92$.

S.3.4 *Selection of Maximum Tree Depth for Random Forest (RF) Implementation*

Figure S.3.4 shows the variation of mean squared error *(MSE)* with maximum depth of tree in the Random Forest (*RF*) model. The figure reveals that the optimum value for maximum tree depth is between 5 and 10, slightly past the elbow region of the curves; there is sufficiently low error already in this region and no significant decrease can be observed beyond it, given the flattening of the curves.

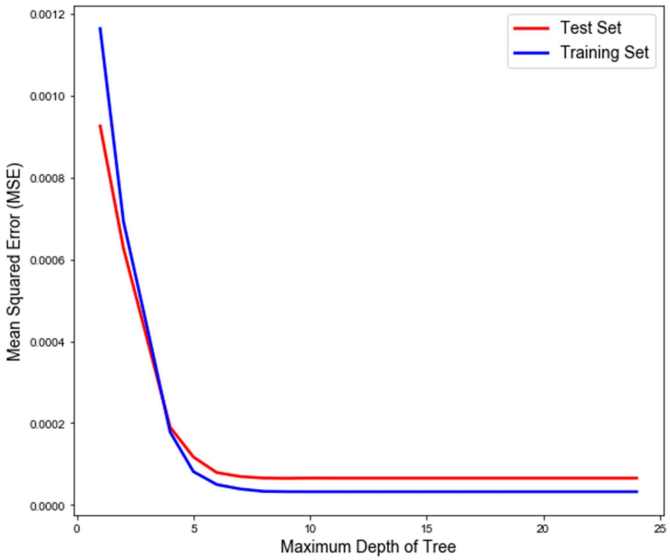

Figure S.3.4. Mean squared error *(MSE)* as a function of maximum tree depth.

S.4.1 *Contact Angle and Roll-Off Angle Measurements with Standard Error*

Figure S.4.1 shows the magnitude of standard error associated with each contact angle (horizontal bar) and roll-off angle (vertical bar) measurement. Generally, the error bars are negligible relative to the trends covered in **Results and Discussion**.

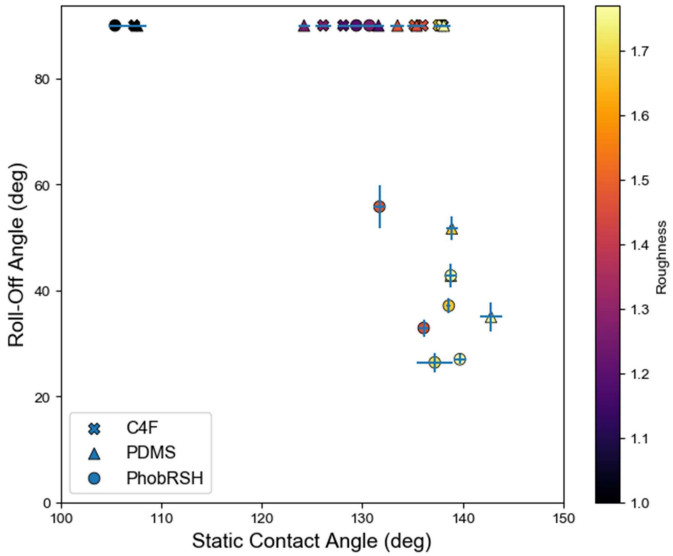

Figure S.4.1. Contact angle and roll-off angle values for different coated fabrics (with error bars).

S.4.2 *Effect of Frame Rate on Measured Maximum Contact Width*

Table S.4.1 shows that the maximum contact width of the droplet does not vary significantly with frame rate for the two different fabrics at a given *We (We = 30.4, D = 2.7 mm, V = 0.9 m/s*). This shows that the choice of frame rate of 900 fps has not influenced the dimensionless maximum contact width ξ_{max} values presented in the report. Moreover, it is interesting that even the associated uncertainty is also almost consistent among the three frame rates. More importantly however, each uncertainty is very small with respect to the corresponding mean value— meaning that, the value obtained from a single observation is not significantly far from the expected average value of multiple observations for characterizing *spreading behavior.*

Table S.4.1. Comparison of the effect of frame rate using two different fabrics

Frame rate (fps)	Maximum contact width (mm)	
	Fabric2 (r = 1.27)	***Fabric7A (r = 1.71)***
600	5.32 ± 0.02	5.30 ± 0.03
900	5.29 ± 0.02	5.19 ± 0.03
2000	5.30 ± 0.01	5.24 ± 0.03

S.4.3 *Principal Component Analysis using Weber Number as Colormap*

Figure S.4.2 shows the obtained plot from *PCA* when Weber number *We* is highlighted with different colors. The *general* trend of increasing *We* is toward the upper-left corner of the plot. Given this information, the decrease of *PC1* with the corresponding increase of *PC2* for a given fabric sample (shown in the original figure in **Results and Discussion**) can now be interpreted as follows. With increasing *We* in **Figure S.4.2**, *PC1* decreases due to the observed trend of decreasing restitution coefficient R_C with *We.* In contrast, *PC2* increases due to the increase of dimensionless maximum contact width ξ_{max} with *We.* The seeming relationship between *PC1* and *PC2* is thus simply due to *We* acting as *confounding* variable.

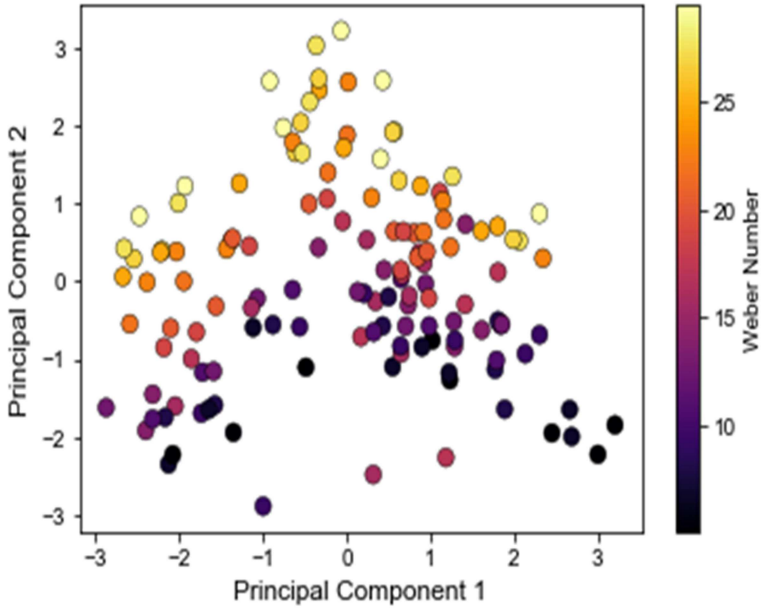

Figure S.4.2. Visual representation of droplet dynamic behavior in different fabrics at low *We* (*We*<30) based on the first two principal components of *PCA*, with *We* of droplet as colormap.

S.4.4 *Equilibrium Contact Width of Low-Roughness Fabric Samples*

Apart from the different rebound behavior given by restitution coefficient R_C, it was also found that the droplet has *higher* equilibrium contact width on fabrics with low roughness ($r < 1.4$) relative to the ones with high roughness— as given in **Figure S.4.3**. Given that it is analogous to the *equilibrium* contact angle in the absence of splashing (which is true at this low *We* range), the equilibrium contact width of the droplet is also related to the final wetting state of the fabric. The low-roughness fabrics give higher equilibrium contact width of the impacting droplet, making them more wetted than the high-roughness fabrics. To make its link to a *non-impacting* water droplet, this difference in wetting behavior has in fact been seen already in the observed lower *static* contact angle θ in low-roughness fabrics. Unfortunately, it is difficult to establish this result more conclusively since as mentioned previously, the contact width has some uncertainty due to difficulty in establishing the droplet-fabric interface baseline.

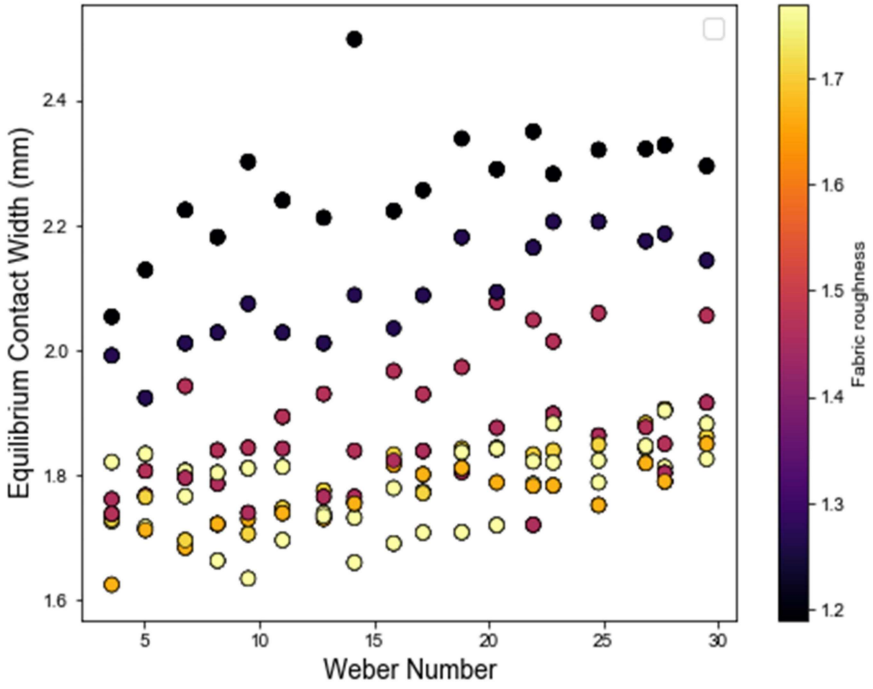

Figure S.4.3. In-depth comparison of equilibrium contact width in different fabrics for a small *We* range. *D = 1.99 mm.* Each point is an average of 6 observations. The equilibrium contact width— i.e., its contact width at rest after a series of oscillations— was observed to be higher for fabric samples with low roughness (black points, *r < 1.4)*.

UNIVERSITÉ CATHOLIQUE DE LOUVAIN
École polytechnique de Louvain
Rue Archimède, 1 bte L6.11.01, 1348 Louvain-la-Neuve, Belgique | **www.uclouvain.be/epl**